EPA 600/R-07/008 | November 2007 | www.epa.gov/ord

United States
Environmental Protection
Agency

In-situ Regeneration of Granular Activated Carbon (GAC) Using Fenton's Reagents

FINAL PROJECT REPORT

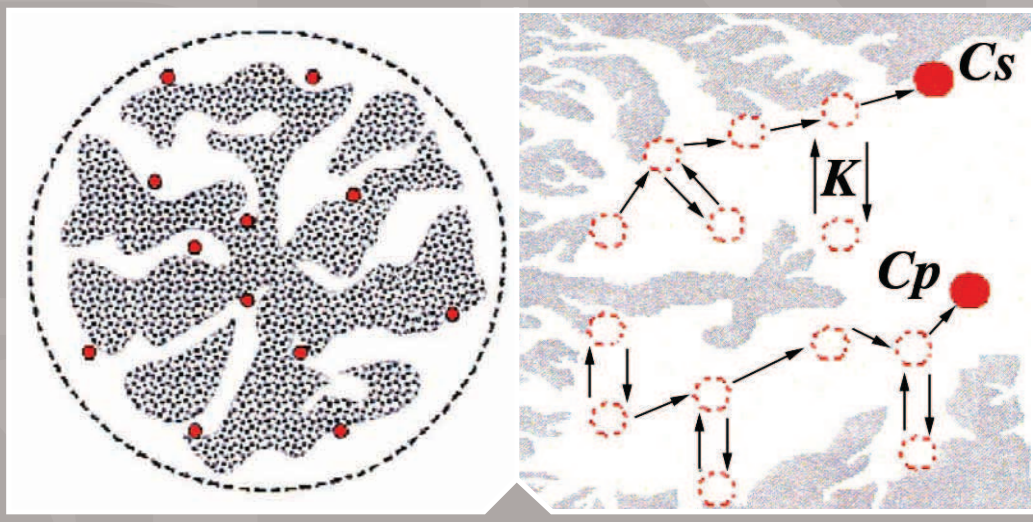

Office of Research and Development
National Risk Management Research Laboratory | Ground Water and Ecosystems Restoration Division

EPA/600/R-07/008
November 2007

In-situ Regeneration of Granular Activated Carbon (GAC) Using Fenton's Reagents

Final Project Report

Cooperative Agreement with the U.S. Environmental Protection Agency

Principal Investigator: Robert G. Arnold, Ph.D.
Co-Principal Investigator: Wendell P. Ela, Ph.D.
A. Eduardo Sáez, Ph.D.
Carla L. De Las Casas, M.S.
Chemical and Environmental Engineering Department
University of Arizona
Tucson, AZ 85721
rga@engr.arizona.edu
520-621-2410 520-621-6048 (fax)

Project Officer: Scott Huling
U.S. Environmental Protection Agency
Office of Research and Development
National Risk Management Research Laboratory
Ground Water and Ecosystems Restoration Division
Ada, OK 74820

U.S. ENVIRONMENTAL PROTECTION AGENCY
OFFICE OF RESEARCH AND DEVELOPMENT
NATIONAL RISK MANAGEMENT RESEARCH LABORATORY
CINCINNATI, OH 45268

Notice

The U.S. Environmental Protection Agency through its Office of Research and Development funded and managed the research described herein under Cooperative Agreement No. CR-829505 to the University of Arizona. It has been subjected to an administrative review but does not necessarily reflect the views of the Agency. No official endorsement should be inferred. EPA does not endorse the purchase or sale of any commercial products or services.

Foreword

The U.S. Environmental Protection Agency is charged by Congress with protecting the Nation's land, air, and water resources. Under a mandate of national environmental laws, the Agency strives to formulate and implement actions leading to a compatible balance between human activities and the ability of natural systems to support and nurture life. To meet these mandates, EPA's research program is providing data and technical support for solving environmental problems today and building a science knowledge base necessary to manage our ecological resources wisely, understand how pollutants affect our health, and prevent or reduce environmental risks in the future.

The National Risk Management Research Laboratory is the Agency's center for investigation of technological and management approaches for reducing risks from threats to human health and the environment. The focus of the Laboratory's research program is on methods for the prevention and control of pollution to air, land, water, and subsurface resources; protection of water quality in public water systems; remediation of contaminated sites and ground water; and prevention and control of indoor air pollution. The goal of this research effort is to catalyze development and implementation of innovative, cost-effective environmental technologies; develop scientific and engineering information needed by EPA to support regulatory and policy decisions; and provide technical support and information transfer to ensure effective implementation of environmental regulations and strategies.

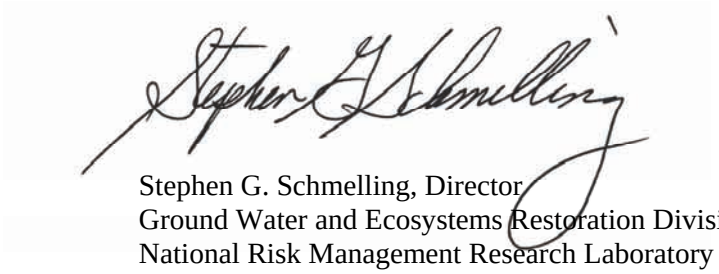

Stephen G. Schmelling, Director
Ground Water and Ecosystems Restoration Division
National Risk Management Research Laboratory

Table of Contents

List of Figures

List of Tables

Executive Summary

Fenton-dependent recovery of carbon initially saturated with one of several chlorinated aliphatic contaminants was studied in batch and continuous-flow reactors. A specialty carbon, URV-MOD 1 (Calgon) was employed to minimize non-productive H_2O_2 demand – that which does not yield hydroxyl or superoxide radicals. Because the reductive reaction of Fe(III) to Fe(II) limits the overall rate of radical generation via Fenton's mechanism, it was hypothesized that steps designed to increase the rate of ferrous iron generation would accelerate Fenton-dependent contaminant destruction, enhancing carbon recovery kinetics. Homogeneous-phase experiments were designed to establish the effects on PCE destruction kinetics of total iron concentration and additions of NH_2OH, various quinones or copper to the Fenton mixtures.

Up to almost the solubility limit of Fe(III), the pseudo-first-order rate constant for PCE disappearance was nearly proportional to the mass of iron added. At $Fe(III)_T$ = 2.0 mM, the half time for PCE disappearance was 19 minutes. Unfortunately, the limited solubility of ferric iron, even at pH 2.0, prevents further rate enhancement via this method.

As expected, the addition of hydroxylamine initially accelerated the destruction of PCE many fold, so that the half time for PCE disappearance was a few minutes. The effect of NH_2OH addition was rapidly lost, however, suggesting that hydroxylamine, initially provided at 0.01 M was approaching exhaustion after about 20 minutes. A second addition of 0.01 NH_2OH did not promote PCE transformation to the same degree. The observation is consistent with the hypothesis that time-dependent reduction in the specific rate of PCE loss was due to temporary accumulation of partial oxidation products derived from the initial reactions involving PCE.

Quinones are known to be electron shuttles in many environmental systems and, as such, were investigated as possible means to accelerate the iron reduction reaction in Fenton's system. Quinone addition increased the pseudo-first-order rate constant for PCE loss approximately three-fold. Above a 1,4-hydroquinone concentration of 0.2 mM, further addition of the compound had little effect on PCE loss. Unfortunately hydroquinone appears to have been quickly destroyed in mixtures containing iron and H_2O_2. After an hour, the initial, hydroquinone-dependent increase in the specific rate of PCE disappearance was completely lost. Reactors amended with 1,4-benzoquinone or 9,10-anthraquinone-2,6-disulfonic acid as electron shuttles provided similar results.

Only copper addition to the Fenton mixtures sustainably enhanced the specific rate of PCE loss. At a copper-to-iron ratio of 2 moles per mole, copper addition increased the pseudo-first-order rate constant for PCE transformation

by a factor of 4.3. It is apparent that the effect of copper addition on Fenton-dependent reaction rates is complex and involves a shift in chemical mechanism. The slopes of Arrhenius plots in copper-free and copper-amended solutions were significantly different suggesting that the overall rate limitation for PCE disappearance is derived from different steps in these two cases.

The effects of pH, chloride ion and other hydroxyl radical scavengers on the rate of Fenton-dependent compound degradation were evaluated. The PCE decomposition rate increased with pH in the range 0.9-3.0. PCE mineralization yields chloride ions, which accumulate in solution and inhibit the PCE degradation rate by scavenging •OH radicals. The PCE degradation rate decreased with increasing Cl^- concentration in the range of 0 to 0.058 M. Isopropanol, a known •OH radical scavenger, enhanced CT degradation in Fenton's reaction but inhibited PCE decomposition. The nature of the pathway for CT destruction was indicated by the presence of phosgene, CO_2 and chloride, which suggests that the superoxide radical ($O_2^{\bullet -}$), not •OH, is the species responsible for CT degradation (Smith et al., 2004).

A parallel experimental program was carried out to examine the sources of rate limitation when halogenated contaminants were initially adsorbed to activated carbon. Possibilities included rates of reaction between hydroxyl radicals and either the adsorbed or (bulk) aqueous-phase contaminant, the rate of contaminant desorption, the rate of diffusive transport of contaminants from the carbon interior, or some combination of these.

The feasibility of using Fenton's reagents for in-place recovery of spent granular activated carbon (GAC) was investigated in continuous-flow experiments. Fenton's reagents were cycled through spent GAC to degrade sorbed chlorinated hydrocarbons. Little carbon adsorption capacity was lost in the process. Seven chlorinated compounds were tested to determine compound-specific effectiveness for GAC regeneration. The contaminant with the weakest adsorption characteristics, methylene chloride, was 99% lost from the carbon surface during a 14-hour regeneration period. Results suggest that intraparticle mass transport generally limits carbon recovery kinetics, as opposed to the rate of oxidation of the target contaminants.

Mathematical models were developed to optimize Fenton-driven degradation of organic compounds in solution or adsorbed to GAC. Models can evaluate the effect of operational parameters ($[Fe(III)]_T$:$[H_2O_2]_o$ ratio, pH) on degradation kinetics. Computer modeling efforts were divided into homogeneous and heterogeneous simulations. The first model simulated experimental degradation of the organic target in a homogeneous Fenton-reaction system. This model was based on the system of reactions proposed by De Laat and Gallard (1999). The model was tested with experimental data for H_2O_2 disappearance and PCE degradation (pH 2), and verified against published data using non-halogenated organic targets (i.e. HCOOH). Although the model simulated the results well for simple Fenton's systems, it requires further refinement to closely simulate Fenton's systems in which reaction by-products (e.g., chloride, partially oxidized organics) play a significant role.

The second model simulated experimental GAC recovery, testing the hypothesis that intraparticle diffusion governs overall recovery kinetics. Analytical solutions were developed for mass transport-limited GAC recovery rates when contaminant adsorption is governed by a linear isotherm. A single fitting parameter (tortuosity) brought

simulations and data into reasonable agreement. However, a common tortuosity could not be obtained for all compounds, suggesting that desorption effects can also limit GAC recovery kinetics. More work is recommended in this area.

A pilot-scale reactor was designed for use in a field demonstration. The field site is among those on the state of Arizona Superfund list – the Park-Euclid site. Primary contaminants at that site include trichloroethylene, perchloroethylene and a mixture of volatile and semi-volatile hydrocarbons. Gases brought to land surface via soil vapor extraction (SVE) are treated via carbon adsorption and returned to the SVE collection system. In our study, carbon was regenerated periodically via Fenton's reaction and returned to service in order to establish process feasibility under field conditions. In the field, up to 95% of the sorbed TCE was removed from GAC during regeneration periods of 50-60 hours. Recovery of PCE was significantly slower. Although the process, as employed, was not cost-effective relative to thermal regeneration or carbon replacement, straightforward design and operational changes are likely to lower process costs significantly.

The field trials supported the bench-scale trial conclusions that the rate of GAC regeneration is compound specific. For the most soluble VOCs, with modest to low solid partitioning, the bulk radical reaction rate with the target compound can control the GAC recovery rate. For these cases, Fenton's based regeneration is a very attractive treatment option, from both economic and ease-of implementation perspectives. Less soluble, more reactive compounds like TCE are limited by desorption or intraparticle transport. The least soluble and most strongly partitioning compounds (e.g., PCE) are likely limited by the desorption reaction rate.

The field trials indicate that there is minimal loss of carbon adsorption capacity after Fenton-driven regeneration. The largest driver of Fenton system (operation and maintenance) costs is hydrogen peroxide (H_2O_2) usage. Its utilization rate can be optimized by: (i) using an optimal H_2O_2/iron concentration ratio, that which generates an optimum $[\bullet OH]_{ss}$ without scavenging most of the radicals by reaction with H_2O_2 itself, (ii) reducing the size of the reservoir, (iii) pulsed addition based on bulk VOC levels or injection of H_2O_2 before the GAC column for compounds that desorb rapidly, and (iv) employing iron-amended GAC, which can generate radicals near the surface of the carbon, thus reducing the use of H_2O_2. Activated carbons with more macroporous structures (and more frequent, shorter regeneration periods) may provide a means to reduce mass transfer limitations and increase overall system efficiency. Scoping-level cost estimates indicated that field use of Fenton regeneration is not cost effective without optimization and/or iron surface amendments, except in the case of the most soluble VOCs.

Background

Ten of the 25 most frequently detected hazardous contaminants at National Priority List (Superfund) sites are chlorinated volatile organic compounds (VOCs) (NRC, 1994). VOCs are commonly recovered from contaminated groundwater or soils using pump-and-treat, air stripping, and soil vapor extraction (SVE) methods. After the contaminated fluid is extracted from the subsurface, granular activated carbon (GAC) adsorption is often used to separate VOCs from liquid and gas streams derived from these recovery techniques. When the carbon is loaded to capacity, it must be regenerated or replaced. Advanced oxidation processes (AOPs) also can be employed for the remediation of the effluent of these fluid extraction processes (Kommineni et al., 2003; Prousek, 1995; Zoh and Stenstrom, 2002). AOPs can destroy VOC contaminants, leaving only mineralized products, but AOPs are relatively expensive for treatment of low-concentration pollutants.

In this project we explore the feasibility of using Fenton's reaction for regeneration of spent GAC that has been used to collect and concentrate VOCs. Fenton's reaction is an AOP process in which reaction of hydrogen peroxide (H_2O_2) with iron (Fe), generates two radical species (•OH, and $HO_2•/O_2•^-$). A very broad range of organics, including a variety of prominent contaminants, are oxidized by hydroxyl radicals, which are among the strongest and least specific oxidants known (Table I; Gallard and De Laat, 2000; Huling et al., 2000a; Duesterberg et al., 2005; Chen et al., 2001). Fenton-dependent processes can mineralize even heavily halogenated targets such as PCE and TCE (Teel et al., 2001). Rate limitations, potential rate acceleration strategies and process feasibility of Fenton-dependent regeneration of VOC-loaded GAC were investigated in a series of bench-scale experiments. Field-scale process feasibility was also examined at an Arizona State Superfund site, where GAC is being used to separate chlorinated VOCs and volatile hydrocarbons from an SVE gas stream. Carbon recoveries at bench and field scales were compared and evaluated.

The field site selected was the Park-Euclid (Tucson, Arizona) State Superfund site, where the primary vadose zone contaminants are PCE, TCE, dichloroethene isomers, and volatile components of diesel fuel. A SVE system with GAC treatment of the off-gas was installed at the site as an interim remediation scheme while the state Remedial Investigation at the Park-Euclid site was underway. There are four distinct zones of contamination -- the upper vadose zone, perched aquifer, lower vadose zone, and regional aquifer (Figure 1). Both the upper and lower vadose zones contain dry-cleaning-related contaminants (i.e. PCE, TCE, DCE isomers). The Park-Euclid SVE system draws

Table 1. Hydroxyl Radical (•OH) Reactivity with Organic Compounds

Target Compound	$k_{M, OH}$ (M^{-1} s^{-1})[a]
Trichloroethylene	2.90E+09
	(3.3-4.3) E+09[b]
Tetrachloroethylene	2.00E+09
1,1-Dichloroethane	7.90E+08
1,1,1-Trichloroethane	1.00E+08
1,1,2-Trichloroethane	3.00E+08[c]
Chloroform	5.00E+07[c]
Methylene Chloride	9.00E+07[c]
Carbon Tetrachloride	<1e6[c]
	1.90E+09[d]
1,4-Benzoquinone	1.2 E+09
Isopropanol	1.90E+09[d]
Atrazine	(1.2-3) E+09[e]
Formic Acid	6.50E+08[f]
H_2O_2	3.3 E+07[g]

Note: $k_{M,OH}$ is the second-order rate constant for the reaction of hydroxyl radical with the target organic compound.
Source: [a]Radiation Chemistry Data Center of the Notre Dame Radiation Laboratory, URL http://www.rcdc.nd.edu/ (Aug 2005) except [b]Trichloroethylene (Chen et al, 2001); [c]1,1,2-Trichloroethane, Chloroform, Methylene Chloride and CT (Haag and Yao, 1992); [d]CT and Isopropanol (Buxton et al., 1988); [e]Atrazine (Gallard and De Laat, 2000); [f]Formic Acid (Duesterberg, et al., 2005); [g]Hydrogen peroxide (De Laat and Gallard, 1999).

gases from the upper vadose zone. Chlorinated solvents (primarily PCE) are present in both free product (diesel fuel atop the perched aquifer (Figure 1)) and perched groundwater. The regional aquifer begins at about 200 ft below land surface. Diesel fuel has not contaminated the regional aquifer. However, a PCE plume with concentrations from 1-100 ppb extends more than 1,300 feet north-northeast from the origin of contamination, a well serving a former on-site dry cleaner (Miller Brooks, 2004). TCE and degradation by-products such as *cis*-1,2-dichloroethene are also present in the plume. Although there are no production wells in the immediate vicinity, the regional aquifer is relied upon to provide potable water within the Tucson basin. Maximum aqueous-phase contaminant concentrations in the regional aquifer are on the order of 10 and 100 ppb for TCE and PCE, respectively (Miller Brooks, 2004).

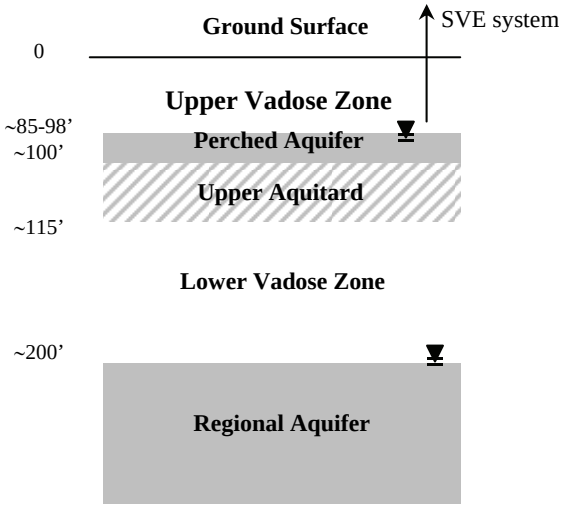

Figure 1. Cross-section of the Park-Euclid Arizona state Superfund site. PCE and TCE contamination is observed in the regional and perched aquifers and in both the lower and upper vadose zones. SVE gases are extracted from the upper vadose zone.

Fenton's Mechanism

In Fenton's mechanism, iron cycles between the Fe(II) and Fe(III) oxidation states due to reaction with H_2O_2. The oxidation of Fe(II) produces a highly aggressive hydroxyl radical (•OH) that is relied upon to attack organic environmental contaminants (Huling et al., 2000a; Teel et al., 2000). Reduction of Fe(III) to Fe(II) limits the overall rate of radical production under most circumstances (Chen and Pignatello, 1997; De Laat and Gallard, 1999; Teruya, 2000). Thus, iron speciation is a strong determinant of Fenton's kinetics (Gallard et al., 1999; De Laat and Gallard, 1999). The distribution of Fe(III) among free ferric ion and hydroxylated forms (predominantly Fe^{3+}, $FeOH^{2+}$, $Fe(OH)_2^{+}$, $Fe_2(OH)_2^{4+}$) depends primarily on solution pH. Furthermore, the insolubility of $Fe(OH)_3$ (s) (pK_{so} for $Fe(OH)_3$ (s, amorph) = 38.7; Stumm and Morgan, 1981) is expected to limit total iron solubility at all but very low pH values. At pH $\leq$ 2, the free ferric ion is the predominant Fe(III) species. Changes in iron speciation in the low pH range, however, can account for the dependence of Fenton reaction kinetics on pH. Fe(III)-hydroperoxyl complexation reactions are fast, and equilibrium conditions are generally satisfied on the timescale of Fenton applications. Complexation with peroxide ion precedes Fe(III) reductions.

The following mechanism for organic contaminant destruction is simplified from a more detailed Fenton's scheme proposed by De Laat and Gallard (1999):

Initiation reactions:

$$Fe(III) + H_2O_2 \rightarrow Fe(II) + HO_2\bullet + H^+ \quad (1)$$

$$Fe(II) + H_2O_2 \rightarrow Fe(III) + \bullet OH + OH^- \quad (2)$$

$$\bullet OH + R \rightarrow OH^- + \bullet R \quad (3)$$

Chain propagation:

$$\bullet R + Fe(III) \rightarrow R^+ + Fe(II) \quad (4)$$

(where Fe (II) reacts again with H_2O_2 to yield another hydroxyl radical)

The organic cation is consumed through a highly exothermic reaction as follows:

$$R^+ + H_2O \rightarrow ROH + H^+ \quad (5)$$

The dominant chain termination steps are:

$$\bullet R + \bullet R \rightarrow R\text{-}R \quad (6)$$

$$\bullet R + Fe(II) \rightarrow Fe(III) + R^- \quad (7)$$

The overall rate is limited normally by the rate of reduction of Fe(III) to Fe(II) by H_2O_2 (reaction 1). The hydroxyl radical produced from reaction 2 can oxidize the target organic compound (R), producing an organic radical (•R). These organic radicals can reduce Fe(III) to Fe(II), propagating the chain reaction. The chain reaction is terminated by radical dimerization, as in reaction 6, or by reaction of the organic radical with Fe(II). The same radical terminating reactions have been used to explain various inhibition effects (Walling and Kato, 1971).

In homogeneous systems, contaminant reaction kinetics follow the second-order rate equation,

$$\frac{d[R]}{dt} = -k_{\bullet OH,R}[R][\bullet OH] \quad (8)$$

where $k_{\bullet OH,R}$ is the compound-specific reaction rate constant for reaction of the target compound with •OH. It is assumed that upon initiation of the Fenton's reaction, the concentration of •OH rises quickly and stabilizes at a near-steady concentration within a very short period of time (seconds or less). A steady-state approximation for •OH concentration is frequently assumed for kinetic analysis so that pseudo-first-order decay kinetics are often the basis of kinetic analyses of contaminant destruction:

$$\frac{d[R]}{dt} = -k'[R] \quad (9)$$

where *k'* is defined as

$$k' = k_{\bullet OH,R}[\bullet OH]_{ss} \quad (10)$$

Pseudo-first-order kinetics are only expected, however, if the hydroxyl radical concentration is essentially constant. Furthermore, it is expected that $[\bullet OH]_{ss}$ will depend on total iron, H_2O_2 concentration, pH, and temperature. At a constant total iron concentration, the near-steady •OH concentration may be fairly insensitive to H_2O_2 concentration (Huling et al., 2000a). If H_2O_2 concentration is low, for example, the Fenton's mechanism slowed, which limits the rate of production of radicals. However, the overall rate of •OH scavenging may also be relatively low. If, on the other hand, excess H_2O_2 is present, it acts as both a source of radicals and a scavenger for •OH.

$$\bullet OH + H_2O_2 \rightarrow HO_2\bullet + H_2O \quad (11)$$

However, it has been shown that because H_2O_2 both generates and consumes •OH, the steady concentration of •OH, and thus the pseudo-first-order rate constant for target destruction, are not strongly influenced by H_2O_2 concentration over a broad range of conditions. Therefore, small fluctuations in H_2O_2 have little effect on the observed pseudo-first-order rate constant for contaminant destruction via oxidation with •OH in homogeneous Fenton systems. Although not explicitly studied in this or previously published work, the near-steady superoxide radical concentration is expected to be insensitive to small fluctuations in H_2O_2 concentration (analogous to •OH radical as discussed previously).

Copper as a Fenton Metal

There is considerable debate regarding the status of copper as a Fenton metal. Although copper cycles between the Cu(I) and Cu(II) oxidation states via reaction with H_2O_2, hydroxyl radicals are not generally produced (Masarwa et al., 1988). Nevertheless, the reaction of the cuprous ion and hydrogen peroxide (reaction 12) results in the formation of a copper complex, $(H_2O)_m\, Cu^+\bullet O_2H^-$, that may react with organics present in solution. In acidic solution and in the absence of organics, the copper complex decomposes into free cupric ion and hydroxyl radicals (reaction 13) (Masarwa et al., 1988).

$$Cu^+ + H_2O_2 \rightarrow Cu^+\bullet O_2H^- + H^+ \quad (12)$$

$$(H_2O)Cu^+\bullet O_2H^- \rightarrow Cu^{2+} + \bullet OH + 2OH^- \quad (13)$$

Cupric copper can also react with organic radicals (reaction 14). The Cu(I) product of reaction 14 can either react with Fe(III) to regenerate Fe(II) or with H_2O_2 to produce cuprous ions (Walling and Kato, 1971). Since an array of unidentified organic radicals may be produced during Fenton-driven decomposition of target contaminants, particularly in the presence of non-target organics, this pathway may be of practical importance in environmental applications. The reaction of Cu(II) with R• is comparable to Fe(III) reduction (reaction 4). The reduction of Fe(III) by Cu(I) (reaction 15) and subsequent reaction of Fe(II) with H_2O_2 would increase the overall rate of •OH generation (Walling and Kato, 1971).

$$R\bullet + Cu(II) \rightarrow Cu\ (I) + \text{products} \quad (14)$$

$$Cu(I) + Fe(III) \leftrightarrow Fe(II) + Cu(II) \quad (15)$$

Walling and Kato (1971) indicated that iron undergoes electron-transfer during reaction with R•, whereas the copper reaction can involve either complexation (reaction 16) or reduction via formation of an organo-copper intermediate (reactions 16 and 17).

$$R\bullet + Cu^{2+}(H_2O)_n \rightarrow RCu^{2+}(H_2O)_n \quad (16)$$

$$RCu^{2+}(H_2O)_n \rightarrow ROH + Cu^+(H_2O)_{n-1} + H^+ \quad (17)$$

Furthermore, they found evidence that organic radicals with strong electron withdrawing groups (e.g. Cl^-) are preferentially reduced by ferrous iron. Trichloroethene radical, for example, would satisfy requirements for such a reaction.

Cu(II) is a weaker oxidizing agent than Fe(III), and therefore less capable of oxidizing R• (as in reaction 4) by outer-sphere electron transfer. Instead, the reaction involves formation of an organo-copper intermediate (Walling, 1975). Comparison of oxidation rates attributable to Cu(II) and Fe(III) indicated that Cu(II) oxidations were slower, but that ligand-Cu(II) exchanges were fast (Walling, 1975).

Cu(II) and Cu(s) are thermodynamically favored over Cu(I) as shown by the following reactions (Holleman and Wiberg, 2001; Cotton et al., 1999):

$$Cu^+ + e^- = Cu\ (s) \qquad E^o = 0.52\ V \qquad (18)$$

$$Cu^+ = Cu^{2+} + e^- \qquad E_H{}^o = -0.16\ V \qquad (19)$$

$$2Cu^+ = Cu\ (s) + Cu^{2+} \qquad \Delta E^o = 0.36\ V \qquad (20)$$

At equilibrium, only low concentrations of Cu(I) ($<10^{-2}$ M) can exist in aqueous solutions (Cotton et al., 1999). Stability differences arise in part because the energy of hydration of Cu^{2+} is much higher than that of Cu^+ (2100 vs. 582 KJ/mol), all of which helps to explain why Cu(I) does not normally exist in aqueous solution, but rather disproportionates to Cu and Cu(II) (Heslop and Robinson, 1967):

$$K = \frac{\left[Cu^{2+}\right]}{\left[Cu^{+}\right]^2} \approx 10^6 \qquad (21)$$

However, Cu^{2+} is favored with anions unable to make covalent bonds or bridging groups (e.g. SO_4^{2-}) (Cotton et al., 1999). Copper participates in outer sphere electron transfers as opposed to inner sphere electron transfers in which the transfer of electrons occurs through a chemical bridge. The ligand covalently links the two metal redox centers and typically has more than one lone electron pair, serving as an electron donor to both the reductant and the oxidant (www.wikipedia.com). The coordination chemistry of the Cu^{2+} ion is dominated by nitrogen- and oxygen-donating ligands followed by chloride and sulfur-containing groups (King, RB. 2006).

Fenton-Driven GAC Regeneration

Contaminant Removal and Destruction Mechanisms

Removal of adsorbates from GAC may be kinetically limited by any of four distinct steps: desorption from the GAC surface, “1”; pore and surface diffusion, “2”; film transport, “3”, in which the film thickness (δ) is inversely related to the local bulk velocity; and removal of reactant from bulk aqueous phase, “4”, due to reaction and advective transport. In most cases, intraparticle effects (pore diffusion-“2” and/or desorption-“1”) control the observed rate of transfer from the particle to the bulk aqueous phase (Crittenden et al., 1987).

Figure 2 illustrates the possible sources of rate limitation experienced by a desorbing species. Partitioning between the solid and liquid within a pore is governed by the surface desorption rate or equilibrium condition “1”. Once the contaminant is in the liquid within a pore, intraparticle transport “2” is largely governed by molecular diffusion. At the surface of the particle, transport into the bulk aqueous phase can be limited by molecular diffusion across a mass transfer boundary layer. Removal from the bulk aqueous phase relies on a mixture of convection and (in the presence of Fenton’s reagents) reaction.

Because hydroxyl radicals are extremely reactive and short-lived, they do not persist any significant distance beyond the point where they are generated. Thus, if the Fenton’s reagents are primarily present in the bulk phase (as opposed to in the pore volume of the GAC), it is reasonable to hypothesize that the reaction of the target compound with hydroxyl radicals will occur mainly in the bulk aqueous phase. This physical model represents a hypothesis to be tested using experimental carbon recovery data.

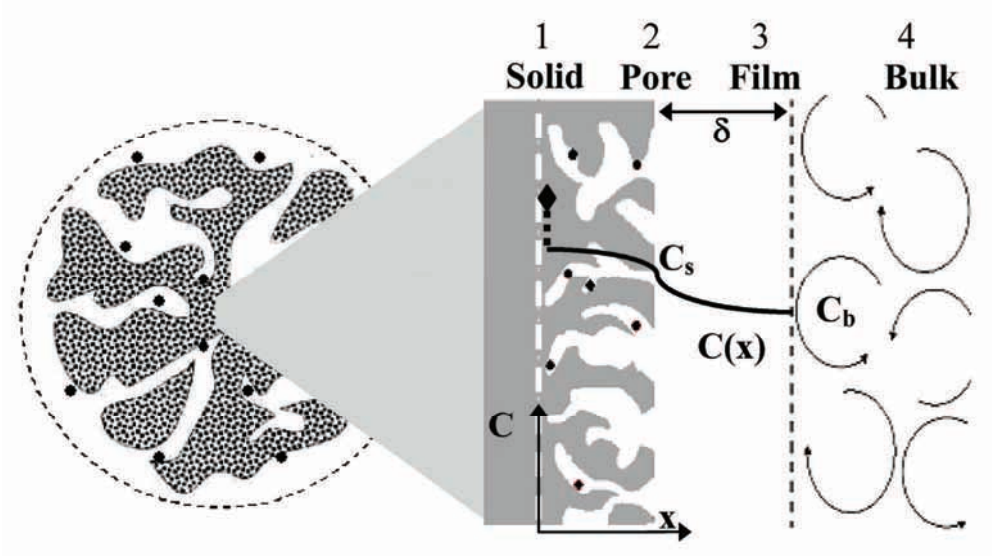

Figure 2. Potential sources of rate limitation for desorption of adsorbate from the GAC (solid) to the bulk fluid. 1.Desorption from solid to liquid phase. 2.Diffusive transport within the pores (pore or surface diffusion). 3.Diffusive transport through a quiescent film surrounding the particle. 4.Convective transport or reaction in bulk fluid.

In the general case, it is possible that carbon recovery kinetics are limited by either the rate of reaction of target contaminants with Fenton-dependent radicals, by the rate of desorption of contaminants from the particle surface or by a combination of pore and surface diffusion. This physical description provides a starting point for model development and data analysis.

To provide a foundation for transport characterization, the physical processes of chemical adsorption will be briefly covered. Convection along the column’s axial direction and axial dispersion are the mass transport mechanisms in the bulk aqueous phase (Ma et al., 1996). If these processes are rapid compared to other transport steps, the bulk aqueous phase can be modeled as well mixed. Molecules from the bulk are transported across a boundary layer. The thickness of this hydrodynamic boundary layer is reduced when fast convective mixing occurs in

the bulk phase; the resistance to overall diffusive transport is often neglected in fast flowing, expanded bed columns (Noll et al., 1992). Upon reaching the adsorbent surface, molecules diffuse into or out of the interior of the particle through an intricate porous network (Figure 3).

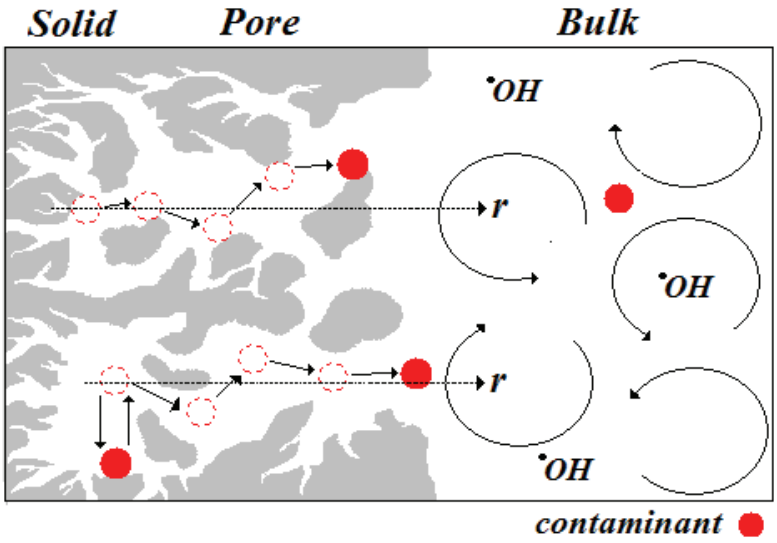

Figure 3. GAC particle cross-section. A tortuous path is experienced by desorbing particles on the particle surface and in the intra-particle aqueous phase.

Intraparticle diffusion describes the mass transport of adsorbate molecules within GAC, and consists of pore-volume and surface diffusion. Pore-volume diffusion, which characterizes contaminant transport through the porous, fluid-filled void, is normally expressed in terms of an effective diffusion coefficient ($D_{ef,p}$) that is lower than the molecular diffusivity (D_{mol}). This arises because the diffusive path experienced by the adsorbate during radial transport can be exceptionally tortuous (Figure 3). In the absence of other diffusive mechanisms, an inverse relationship exists between $D_{ef,p}$ and pore space tortuosity, τ,

$$\tau = \frac{D_{mol}}{D_{ef,p}} \tag{22}$$

where D_{mol} is the contaminant molecular diffusivity (cm^2/s), and $D_{ef,p}$ is the effective pore-volume diffusivity (cm^2/s). Conversely, a direct relationship exists between particle porosity and the $D_{ef,p}$. The effective pore-volume diffusion coefficient approaches the liquid-phase molecular diffusion coefficient as porosity approaches 1.0 (Furuya et al., 1996).

Surface diffusion describes concentration-driven contaminant transport on the particle surface. The mechanism is analogous to pore-volume diffusion but occurs on the internal surface of the particle. Due to an aqueous concentration gradient within the pores, a surface gradient will also exist on the pore surface in the same direction as the aqueous-phase gradient (Yang, 1987). Such a (surface) gradient is assured if adsorption/desorption reactions on the

particle/pore wall are relatively fast. Surface diffusion occurs by molecular hopping between adsorption sites. Thus, surface diffusion depends on the ability of molecules to overcome an energy barrier. Molecules can also desorb to the intra-particle fluid by overcoming a similar desorptive energy barrier. A simplifying assumption that is often made for modeling purposes is that adsorption and desorption processes are much faster than diffusive transport (Crittenden et al., 1986). Under these circumstances, local equilibrium is assumed to exist between the local sorbed and intraparticle aqueous contaminant concentrations, and the interfacial flux can be characterized by an adsorption isotherm.

As for pore-volume diffusion, calculating surface diffusion flux in GAC requires estimation of a tortuosity factor. Although the tortuosity factor for surface diffusion is not necessarily equal to that of porous contaminant transport within the same structure, the same τ is usually assumed for both diffusion modes (Yang, 1987). The relative contributions of surface and pore diffusion to the overall rate of intraparticle transport are a function of adsorbate affinity for the surface as well as other factors, making empirical determination of an overall diffusion constant a necessity. Several researchers have established that surface diffusion is also related to the solid phase (adsorbed) concentration and temperature (Furuya et al., 1987; Sudo et al., 1978; Suzuki and Fujii, 1982). Consequently, determination of accurate kinetic and equilibrium data across the gamut of experimental conditions is generally required for adequate surface diffusion characterization.

For design, surface and pore diffusion are often combined into a single term, the apparent diffusivity (D), and an overall mass transfer rate is established from recovery data. General conclusions can be deduced from such an analysis - mainly the relative importance of individual transport mechanisms. However, mechanism-specific transport rates cannot be established. To verify the importance of diffusive transport to overall recovery kinetics in the Fenton-based treatment scheme considered here, the effect of particle size on recovery rate can be examined in fixed-bed columns. That is, a specific pore-diffusion-limited process would yield faster particle recovery kinetics (transport to the bulk liquid phase) as the size of the particles decreases. The importance of this transport mechanism can be determined by measuring the rate of carbon recovery from several GAC populations that differ in size.

A Fenton-dependent GAC recovery (kinetic) model was developed based on assumptions that (i) particle surface and proximate pore water concentrations of the contaminant are at equilibrium and (ii) overall recovery kinetics are limited by pore diffusion or a combination of surface and pore diffusion. An analytical solution governing contaminant removal kinetics from carbon was developed and compared to experimental recovery profiles. Calibration was based on a single fitting parameter, τ. To validate the pore diffusion approximation, a single τ must fit the desorption profiles of compounds with differing sorption characteristics. Similarly, a single, unique τ must fit these same desorption profiles for a surface and pore diffusion approximation to be validated.

Theoretical Considerations – Fenton's Treatment for GAC Regeneration

This section discusses possible scenarios and theoretical considerations that may take place in heterogeneous systems. It should be clear to the reader that the discussion encompasses theoretical speculations as opposed to a supportable set of hypotheses related to the physical-chemical events in these experiments.

In heterogeneous systems, there exist a variety of scenarios in which pseudo-first-order recovery kinetics could be expected. Similar to homogeneous reaction kinetics, Fenton-dependent recovery rates in expanded-bed heterogeneous trials may be limited by the bulk-phase reaction of the target with the •OH. Since the overall rate of contaminant loss is related to the •OH concentration present in the bulk, a steady state approximation for •OH would lead to pseudo-first-order kinetics. Under these circumstances, the bulk liquid-phase concentration of contaminant must be in approximate equilibrium with its adsorbed concentration throughout the recovery period. Therefore, an approximately linear adsorption isotherm would be an additional, necessary condition for first-order kinetics. In such a case, the observed recovery rate would be directly related to the second-order rate constant for the aqueous-phase reaction.

Alternatively, it is possible that the reaction rate of the •OH with the adsorbed contaminant limits overall recovery kinetics. In these circumstances, the bulk aqueous-phase concentrations of H_2O_2, total iron and (therefore) •OH would seemingly extend to the carbon surface, where the reaction rate would depend on the abundance of adsorbed contaminant (Figure 4). The bulk aqueous-phase contaminant concentration would be essentially zero, or at least much less than the equilibrium aqueous-phase concentration. If the concentration of the aqueous-phase radical is steady, the rate of target destruction will be proportional to the adsorbed concentration under surface-reaction limited conditions.

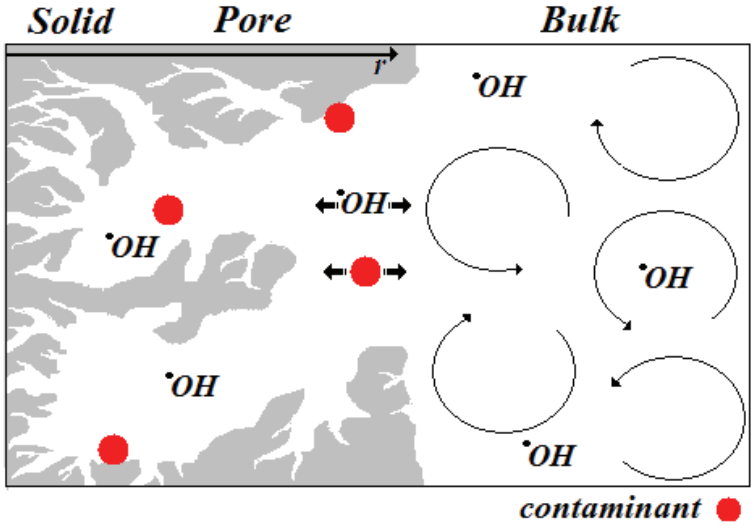

Figure 4. Intraparticle porous transport of hydroxyl radical to GAC particle surface.

Intraparticle transport mechanisms, such as pore and surface diffusion and surface desorption may also limit carbon recovery in heterogeneous systems (Figure 5). If the overall rate of contaminant destruction were limited by the rate of chemical desorption from the carbon surface, first-order kinetics would be expected. That is, the overall

desorption rate of compound disappearance would be proportional to the adsorbed concentration. There are, however, some underlying assumptions here, such as the equivalence of adsorption sites on the carbon surface. Thermodynamic equivalence must exist among the carbon adsorption sites, so that rapid desorption from less energetically favorable sites does not result in recovery rates that are initially faster, and subsequently slower, than predicted from a single first-order kinetic relationship.

Finally, first-order recovery kinetics might be expected if the overall rate of compound disappearance were controlled by intraparticle diffusive transport to the bulk solution (Figure 5). No fraction of the carbon surface, however, could be kinetically inaccessible relative to the remainder of the surface. This restriction seems unlikely considering that relatively small pores within the particle interior typically dominate carbon surface area. Therefore, kinetic equivalence of adsorption sites in the particle interior and those at the surface, in terms of accessibility to the bulk solution, seems improbable (Knudsen effects). The loss of contaminant from the carbon surface would, under those circumstances, be proportional to the aqueous-phase concentration in equilibrium with the sorbed concentration of contaminant. The diffusion coefficient for intraparticle transport is related to a geometric tortuosity factor, τ, and reflects, at least to a degree, the physical characteristics of the adsorbent (22).

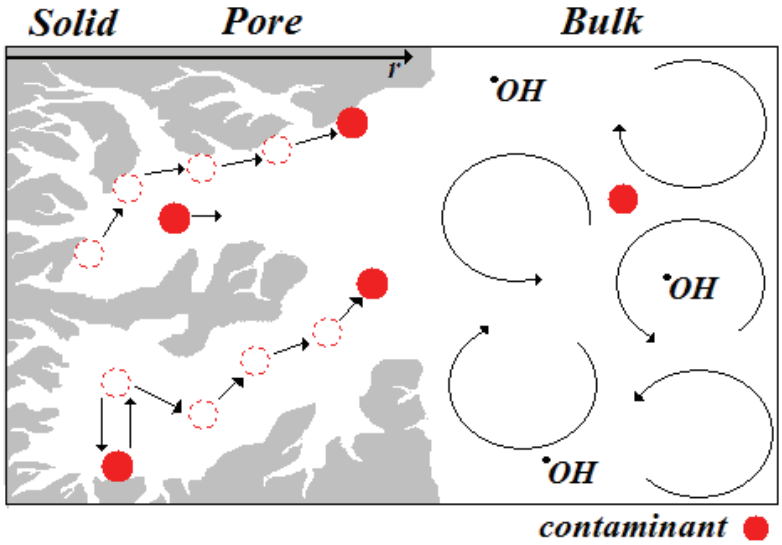

Figure 5. Pore and surface diffusion, and surface desorption of contaminant within a GAC particle pore.

In summary, the rate of disappearance of initially adsorbed contaminants can be proportional to the mass of target in the heterogeneous system under a variety of circumstances. Chemical contaminants that react slowly with •OH may accumulate in the bulk liquid-phase reflecting a reaction-limited rate of chemical destruction. Chemicals that are insoluble or show a very high affinity for solid surfaces (e.g. carbon) may experience overall rates of Fenton-driven transformation that are limited by pore and surface diffusion or by the rate of desorption from the surface. Each situation could yield pseudo-first-order recovery kinetics.

Project Objectives

The project seeks to increase the knowledge and applicability of an innovative means of destroying GAC-sorbed VOCs without the need to remove the sorbent from the adsorption reactor. The project focuses on laboratory bench-scale experimentation, evaluation and modeling combined with limited pilot-scale field testing.

The specific laboratory objectives were:

- Investigate the use of reductants and electron shuttles, other than hydrogen peroxide to accelerate the Fenton-driven process for organics degradation.
- Evaluate the effect of chloride build-up in the Fenton reagent regenerant solution during chlorinated organic degradation.
- Establish the relative merits of regenerant liquid amended versus surface precipitated iron for catalyzing Fenton's reaction.
- Identify the mechanism and rate limiting step(s) for Fenton reagent destruction for a range of chlorinated organics.
- Evaluate the dependence of reaction kinetics and efficiency on solution pH.
- Provide a scoping level evaluation of the relative economics of Fenton reagent regeneration of VOC-bearing GAC versus conventional off-site thermal regeneration or hazardous waste disposal.

The specific field testing objectives were:

- Provide proof of concept of Fenton's reagent, in-place regeneration of VOC-laden GAC.
- Establish basic performance characteristics and challenges for field use of Fenton's reagents for GAC regeneration.
- Establish the effect on GAC adsorption capacity of multiple regenerations by Fenton's reagents.
- Establish a scoping level estimate of field scale economics of the process.

Materials and Methods

Chemicals

Purified water (Milli-Q™ Water System by Millipore) was used in all experiments. The following chemicals were obtained from Sigma-Aldrich: carbon tetrachloride, CT (99.9% HPLC grade), 1,1,1-trichloroethane, TCA (>99%), hexachloroethane, HCA, ferric sulfate [$Fe_2(SO_4)_3$•$5.6H_2O$], cupric sulfate pentahydrate ($CuSO_4$•$5H_2O$), hydroxylamine hydrochloride (H_3NO•HCl; minimum 99%), copper (I) chloride (CuCl; 97%), 1,4-benzoquinone (1,4-BQ; 98%), hydroquinone (HQ; 99%), 9,10-anthraquinone 2,6-disulfonic acid disodium salt (>98%). Hydrogen peroxide (30%, reagent grade) and methanol (HPLC grade) were from Fischer Scientific. Ultra resi-analyzed tetrachloroethylene (PCE), methylene chloride (CH_2Cl_2), trichloroethylene (TCE), chloroform (CF), *n*-heptane, 1,10-phenanthroline monohydrate, ferrous sulfate hepta hydrate ($FeSO_4$•$7H_2O$), and hydrochloric acid were from J.T. Baker. Titanium sulfate solution was obtained from Pfaltz and Bauer, and sulfuric acid, ethyl acetate, ammonium acetate, and 1,2-dichloroethane (DCA) were from EM Science. Potassium permanganate and isopropyl alcohol were obtained from EMD Pharmaceuticals, and ferrous ammonium sulfate [$FeSO_4(NH_4)_2SO_4$•$6H_2O$] from Spectrum Chemical Mfg. Corporation. All chemicals were reagent grade or better and were used as obtained.

Analytical

Target Organic Compounds

The target VOCs (methylene chloride, chloroform, carbon tetrachloride, 1,2-dichloroethane, 1,1,1-trichloroethane, trichloroethylene, tetrachloroethylene) were analyzed using a modified version of the EPA method 551.1, "Determination of Chlorinated Solvents by Liquid-Liquid Extraction and Gas Chromatography with Electron-Capture Detection." Samples were prepared for analysis by placing 20-µL (15-µL in some experiments) in a 2-mL glass crimp-top vial containing 1 mL of heptane. Using an auto sampler 1 µL of the extract was injected into a Hewlett Packard 5890 Gas Chromatograph (GC, Palo Alto, CA) equipped with a DB-624 fused silica capillary column (J & W Scientific, Fulsom, CA; 0.53 mm ID, 30 m in length). The GC used an electron-capture detector (ECD) for quantification of chlorinated compounds. Nitrogen and helium were used as the make-up and carrier gases. The gas flow rate was 26 mL/min. The temperatures of the detector and inlet were 275°C, and 150°C, respectively. The oven temperatures ranged from 35°C to 100°C and the sample run times were 5-20 minutes, depending on the

compound analyzed. A chlorinated compound (e.g. carbon tetrachloride) was added to each sample as an internal standard to adjust for instrument error and sample size inaccuracy. A response factor was obtained from the calibration curve relating the response of the analyte to that of the internal standard. This factor was then used to determine the analyte concentrations. A calibration curve was run prior to all analysis; samples were diluted as needed. To ensure proper results and monitor instrument performance, a check standard was run every tenth sample. The percent deviation between check standards was no larger than 5%, indicating proper operation of the GC. A more complete description of procedures for adjustment of analyte concentrations using the internal standard is in the Quality Assurance Project Plan (QAPP) submitted to EPA project officers prior to beginning project trials (November, 2003).

Hydrogen Peroxide

Hydrogen peroxide was analyzed using a peroxytitanic acid colorimetric method (Boltz and Holwell, 1978), as modified by Teruya (2000). The procedure was as follows. The sample (50 μL) and 50 μL of titanium sulfate (Pfaltz and Bauer, Inc., Waterbury, CT) solution were added to 4.9 mL of deionized water. Titanium sulfate was provided in stoichiometric excess to react with H_2O_2 leading to color development and quenching the Fenton reaction. After 1 hour, color development was measured at a wavelength of 407 nm using a Hitachi U-2000 doubled-beamed spectrophotometer (Hitachi Corporation, Schaumburg, IL). Samples were diluted with deionized water as necessary to fall within the range of the standards.

pH

A Hach One pH/ISE meter (Hach Company, Loveland, CO) was used to monitor the pH of the solution containing Fenton's reagents. The meter was calibrated using standard pH calibrating buffers (pH 2 and 4) from VWR (Aurora, CO).

Iron

Total iron content of all the samples was analyzed using the phenanthroline method (Standard Methods for the Examination of Water and Wastewater, 1995).

Quality Assurance

The utmost care was taken to assure the quality of laboratory work. In accordance with the Quality Assurance Project Plan (QAPP), the lab maintained logbooks, internal standards, proper storage of samples, and check standards. The Quality Assurance Officer specified all analytical methods, evaluated analysts for competency to perform the analyses, and monitored all phases from sample collection to disposal. The project was subject to audit by EPA and

quarterly audits by the Quality Assurance Officer. These audits consisted of reviews of analytical methods, analyst familiarity with methods, reviews of standard solution quality, reviews of calculations, and instrument performance.

Experimental

General

Experiments were conducted in either batch or column reactors. In general, batch reactors were used to investigate homogeneous Fenton reaction kinetics. Experiments in bench-scale column reactors were designed to examine the role of mass transfer limitations to Fenton-driven carbon recovery rates and to expose key operational characteristics of the Fenton-dependent carbon regeneration mechanism. It is not known with certainty, for example, whether compound desorption must precede reaction with Fenton-derived free radicals and (consequently) whether desorption rates control overall process kinetics. Column reactors were also designed and tested at the field-scale. Isotherms for target compounds were developed by varying the mass of carbon in a series of batch reactors that contained identical masses of the target contaminant. Masses of carbon and contaminant were estimated in advance to provide a broad range of aqueous-phase concentrations following attainment of equilibrium.

Batch Kinetic Experiments

Reaction vessels consisted of 65-mL glass vials, capped with mini-inert valves. Chemicals in the reaction mixtures always included PCE or CT (the target compounds in these experiments), ferric iron (added from a pH-adjusted solution of ferric sulfate), and H_2O_2 (added to achieve target initial concentrations from a 30% stock solution). Depending on experimental objectives, one of several quinones, copper, hydroxylamine or radical ($\bullet OH/O_2\bullet^-$) scavengers were at times part of the reacting mixture. Reactors were filled to near capacity and placed in an Orbit Shaker Bath for temperature control. In a subset of the experiments, H_2O_2 and/or PCE were periodically replenished. Both PCE and CT degradation was studied in the presence of radical scavengers in Fenton's reaction. In these experiments, the same 65-mL vials were utilized but with 5 mL headspace.

Experiments with 0.5 mM total iron were run at room temperature (22-24°C). When total iron was 0.1 mM, the temperature was maintained at 30-31°C. Experiments involving quinones were conducted at room temperature (22-24°C). Experiments studying the effect of pH, Cl^- accumulation and radical scavengers in Fenton's reaction were at 32°C. Temperatures in the range 8.8-54.4°C were also explored in the experiments designed to establish the effect of copper addition on Fenton's (iron based) reaction for PCE decomposition.

Adsorption Isotherms

Isotherms were obtained for each of seven chlorinated target compounds (Table II). For each compound, five 160-mL glass serum bottles containing varying masses of carbon (1-6 grams) were filled with water containing the

respective target chemical and crimp sealed. A blank (compound solution with no carbon) was utilized when running all isotherms. The measurement of this blank was used as the C_o (initial concentration).

Water at near-saturation levels with contaminant was used to initially load the target VOC into the serum bottle to avoid co-solvent effects and/or adsorption of neat-phase contaminant directly onto the carbon. The serum bottles were placed in a temperature-controlled water bath (32°C) equipped with a shaker element. The bottles were allowed to equilibrate for at least 36 hours. The liquid phase was then sampled and analyzed for the contaminant by GC-ECD. The mass adsorbed on the carbon was determined from the difference between the initial (saturated water) concentration and the liquid concentration following adsorption. Isotherm data were fitted using a Freundlich model. Model parameters were determined via simple linear regression analysis of the log-transformed data.

Column Experiments

GAC Selection and Preparation

Granular activated carbon (URV-MOD 1, Calgon Corporation, Pittsburgh, PA) was used in all trials. This experimental-type carbon was selected because of its relatively high iron and low manganese contents. The GAC was steam-activated to minimize reactivity with H_2O_2 (Huling et al., 2005a). It is a bituminous coal, 8 x 30 mesh (effective size 0.6-2.4 mm), with a specific surface area of 1290 m^2/g and pore volume of 0.64 mL/g (Huling et al., 2005a). Physical properties of this experimental carbon provided by the Calgon Corporation are summarized in Table III. The 8×30 mesh size fraction was used in expanded-bed column and isotherm adsorption experiments. In fixed-bed studies, sieve-sorted particle distributions of 1.0-1.18 mm, 1.4-1.7 mm, and 2.0-2.38 mm were used. Calgon URV-MOD 1 carbon was sieve sorted using USA Standard test sieves with ASTM-11 specification.

Table II. Chemical Properties of the Organic Compounds Studied

Name	Formula	Log K_{ow} [a]	$k_{M,OH}$ $(M^{-1} s^{-1})$ [b]	Diffusivity (cm^2/s) [c]	Adsorbed concentration (mg/g) [d]	Freundlich Parameters [e]	
						K (mg/g) $(L/mg)^{1/n}$	1/n
Methylene Chloride (MC)	CH_2Cl_2	1.15	9.00E+07	1.21E-05	275	0.07	1.06
1,2-DCA	$C_2H_4Cl_2$	1.47	7.90E+08	1.01E-05	146	0.04	1.33
1,1,1-TCA	$C_2H_3Cl_3$	2.48	1.00E+08	9.24E-06	20	0.65	0.87
Chloroform (CF)	$CHCl_3$	1.93	5.00E+07	1.04E-05	188	1.48	0.77
Carbon Tetrachloride (CT)	CCl_4	2.73	2.00E+06	9.27E-06	N/A	12.30	0.59
TCE	C_2HCl_3	2.42	2.90E+09	9.45E-06	103	5.82	0.70
PCE	C_2Cl_4	2.88	2.00E+09	8.54E-06	11	45.66	0.56

Note: $k_{M,OH}$ is the second-order rate constant for the reaction of hydroxyl radical with the target organic compound.

Source: [a]Swarzenbach et al., 1993; [b]www.rcdc.nd.edu, except carbon tetrachloride (Haag and Yao, 1992); [c]calculated from Wilke-Chang equation (Logan, 1999); [d]From analysis of initial carbon concentration for carbon recovery experiments (data at 32ºC); [e]From isotherm data obtained in this lab at 32ºC.

Table III. Physical Properties of Calgon URV-MOD 1

Property	Value
BET Surface Area (95% CI)	1290 m^2/g ± (1260-1330 m^2/g)
Total Pore Volume (95% CI)	0.643 mL/g ± (.613-.673 mL/g)
Micropore	0.386 mL/g
Meso & Macropore	0.257 mL/g
Porosity	0.592

Source: Huling et al., 2005a.

Prior to use in experiments, GAC was dried overnight at 103°C to obtain the dry weight. Dried carbon was cooled in a vacuum dessicator, and then wetted with de-ionized water from a Milli-Q-water system. To guarantee a fully hydrated surface, the suspended carbon was shaken at room temperature for 24 hours prior to contaminant loading. Loading of a target contaminant onto the carbon was done in an aqueous-phase suspension to avoid co-solvent effects, and the adsorbed mass was determined by GC-ECD analysis, and verified by determining the difference between pre- and post-adsorption liquid-phase concentrations. Pre-loading of carbon for bench-scale experiments was accomplished by placing 10-16 g of GAC into 1.00 L of water containing the experiment-specific target contaminant. Normally, the water was nearly saturated with the target at room temperature prior to the introduction of carbon. The 1-L batch reactors with negligible headspace were then sealed and tumbled for approximately 60 hours (room temperature) for attainment of equilibrium between the dissolved and adsorbed chemical. Final (measured) adsorbed concentrations are provided in Table II.

Iron-Amended GAC Preparation

In one set of trials, iron was precipitated on the GAC surface to evaluate the effectiveness of using iron-amended GAC versus providing iron in the bulk solution. These trials were conducted in bench-scale column reactors using GAC loaded with either TCE or PCE as the target VOCs.

To precipitate iron on the surface of the carbon, an iron solution was equilibrated with the carbon for approximately 4 days. The iron loading was based on a critical iron loading on GAC particles that was established by Huling et al., (2007). The critical loading was established as the GAC-bound level that maximized the rate of H_2O_2 consumption for the iron-amended GAC in water plus H_2O_2. To prepare the iron solution, $FeSO_4 \cdot 7H_2O$ was dissolved in water to obtain 2.2 g/L Fe (0.039 M Fe). Ten grams of dry GAC were placed in each vial with 30 mL of the iron solution. Sulfuric acid was added as necessary to maintain the pH of the iron-GAC solution near 2.5 during the equilibrium process (~4 days). After 4 days, the pH was increased to 3.0 using a solution of NaOH. The liquid was analyzed for total iron using the phenanthroline method. Subsequently, the iron-amended GAC from each vial was combined in a beaker, dried, weighed and utilized in the column experiments. For analysis of the iron content on the carbon, 5 g of iron-amended and background (clean) GAC were crushed to homogenize the samples. Replicates of the

crushed GAC samples were analyzed by Shaw Environmental, Inc., under EPA direction. Samples were prepared by microwave extraction and filtration and analyzed by ICP-OES (Perkin Elmer Optima 3300DV ICP). A standard operating procedure for determination of total nitric acid extractable metals from solids and sludges was used.

Extraction of VOCs from GAC

Four organic solvents were evaluated in terms of their ability to extract PCE from activated carbon. The extracting solvents analyzed were heptane, pentane, ethanol, and ethyl acetate, and the target organic compound was tetrachloroethylene (PCE). Results are summarized in Figure 6. Five identical samples of carbon were loaded with equal masses of PCE and subsequently extracted with one of the four solvents. Extraction mixtures were sampled at 6, 12, and 24 hours and analyzed by GC-ECD.

Of the four solvents, ethyl acetate provided the highest extraction efficiency (≥93%) after 12 hours. All other solvents took considerably longer. Table IV contains the percent recovery of PCE in the same experiment.

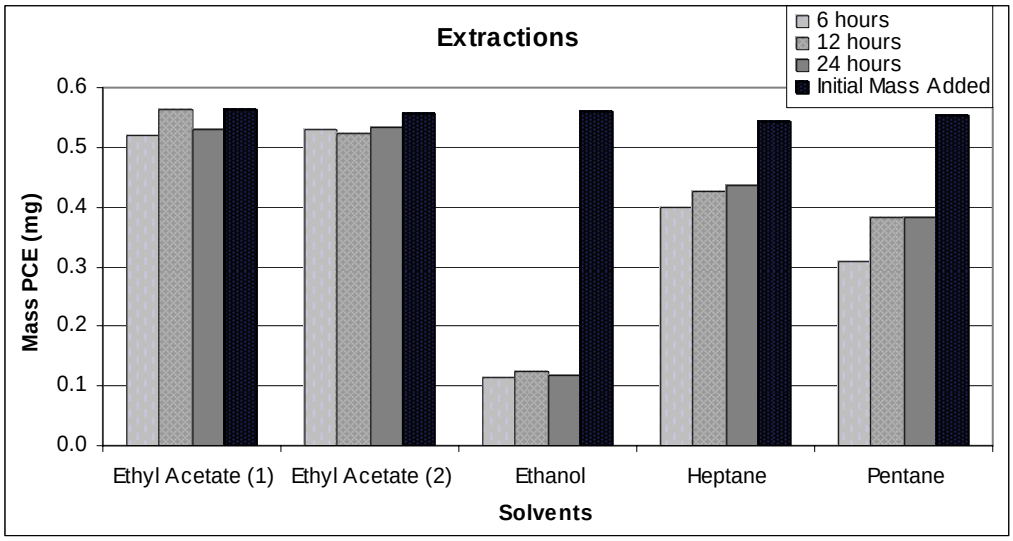

Figure 6. PCE extraction efficiencies in four different solvents.

Table IV. Extraction Efficiencies

Solvent	6 hours	12 hours	24 hours
Ethyl Acetate (1)	92 %	100 %	94 %
Ethyl Acetate (2)†	95 %	93 %	95 %
Ethanol	20 %	22 %	21 %
Heptane	71 %	76 %	77 %
Pentane	55 %	68 %	68 %

Note: † A second trial using ethyl acetate was conducted and verified performance.

A period of 12 hours was considered adequate for extraction of PCE from the activated carbon using ethyl acetate. Based on these results, all subsequent extractions of chlorinated solvents from GAC used ethyl acetate solvent and a 12-hour extraction period.

Sample Analysis

In all column experiments, representative volumes of carbon (0.5-0.7 grams) were withdrawn from the reactor, weighed, and extracted in ethyl acetate in crimp sealed vials. After the 12-hour extraction period, samples were prepared for analysis by withdrawing a 20-µL sample of ethyl acetate from the crimped carbon vials, and injecting it into a 2-mL glass crimp top vial containing 1 mL of heptane. The mass of VOC in the heptane was subsequently quantified by GC-ECD (see earlier description). Liquid samples from the reactor bulk fluid were collected at the same time as the GAC samples to measure contaminant desorption rates and to complete a mass balance. Liquid-phase contaminant levels were monitored in the bulk aqueous-phase by placing samples from the reservoir (Figure 7) in 1-mL crimp sealed vials. Dilutions were performed in heptane as needed, and 1.00 µL was then injected in the GC-ECD. An internal standard, appropriate for each compound, was added to each sample to analyze and adjust for instrumentation inconsistencies. Analyte-specific internal standards were selected based on GC peak retention times, to produce sufficient separation between the target and the internal standard. The oven temperature and run time were also selected based on chromatographic peak analysis. Oven temperatures ranged from 60°C-100°C (inlet temperature: 200°C, detector temperature: 275°C) with run times of 4-9 minutes, depending on the compound being analyzed. A calibration curve was established prior to all analyses.

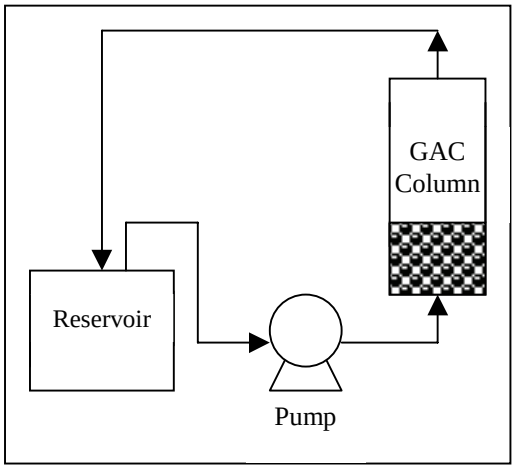

Figure 7. Expanded bed desorber setup.

Desorption Rate Experiments

Expanded-bed column experiments were performed at a temperature of 32°C (± 2°C) using a Chromaflex® borosilicate glass chromatography column with a 2.5-cm inner diameter and 15-cm length (obtained from VWR). In these experiments, the temperature was controlled by means of a water bath.

The column was fitted with 2.5-cm inner diameter PTFE frits tapped with 5/8-inch Swagelok stainless steel fittings that fed to 5/8-inch Teflon tubing. A 6-600 rpm Masterflex® peristaltic pump transported the bulk liquid in an up-flow mode through the column at a flow rate of 950 mL per minute, a volume flow-rate sufficient to expand the carbon bed and ensure proper mixing. To improve hydrodynamic mixing, a 5-cm Chromaflex® extension packed with 3-mm glass beads was added to the column influent (Figure 7).

Desorption rates were measured by circulating clean (contaminant free) water through the column. That is, elution water did not contain Fenton's reagents. Two methods were used in this type of experiment. In the first, the water was recirculated through the reservoir (T = 32ºC) and the contaminant was stripped from the reservoir using a bubbler. MC, CF and TCE were used in these trials. Later, similar experiments were run by wasting the column effluent rather than stripping and recirculating it. In this case, tap water was employed (T = 29ºC). It should be noted that even thought no efforts were made to analyze the tap water in these experiments, the typical ion concentrations in Tucson groundwater are all below the levels that are known to have an effect on reaction rates for Fenton's reaction (see section entitled, Effect of Cl^- on PCE Degradation by Fenton's Reaction).

In both trials, water was passed through the pre-loaded columns at rates designed to minimize aqueous-phase contaminant concentrations at the column exit, so that rates of mass transport from the carbon surface to bulk solution were not affected by the bulk liquid-phase concentration. In this manner, contaminant transport kinetics from surface to bulk could be established directly. Desorption kinetics were established by periodically measuring both residual contaminants on carbon samples and the contaminant concentration in the liquid exiting the column. In these trials MC, TCA and TCE were used as the VOC targets, and the results were used in the modeling efforts described later.

Regeneration Rate Experiments

Regeneration kinetics were first studied by circulating Fenton's reagents through a fluidized bed of pre-loaded GAC as described for the desorption rate experiments above. Column recovery was monitored by periodically withdrawing carbon samples and extracting residual contaminants for analysis (see earlier descriptions). Preliminary experiments of this type were conducted at room temperature. When it became apparent that room temperature was subject to significant uncontrolled changes, temperature was controlled at 32ºC in subsequent experiments. In the initial bench-scale column experiments, VOC-loaded carbon was packed into a Chromaflex® borosilicate glass chromatography column, I.D.=2.5 cm, L=15 cm, V=85 mL (Ace Glass, Inc., Louisville, KY). Fenton's reagents were prepared on the day of use. During regeneration, a 10 mM Fe (ferric sulfate) solution was recirculated in up-flow mode through the column at a rate sufficient to expand the carbon bed by approximately 50%. To initiate recovery,

0.2 M H_2O_2 was added to the recirculating fluid. At 10-60 minute intervals, sufficient H_2O_2 was added to restore the original concentration. This generally produced an H_2O_2 concentration that differed from the original concentration by less than 50% (data not shown). Periodically the reagent circulation was stopped, while carbon samples were withdrawn from the top and bottom of the column for extraction and analysis of the target compound. Extraction periods were 12 hours in ethyl acetate on a shaker table. Extracts were analyzed using GC-ECD with the methods described below. Carbon samples were then dried at 103°C and weighed. Data are reported as the mean results of the values for samples from the top and bottom (one each) of the fluidized bed. Aqueous-phase samples were taken from the recirculation reservoir for analysis of the target compound, reaction by-products and residual hydrogen peroxide.

In iron-amended GAC trials, the reservoir contained water (no iron solution). A smaller reservoir size was utilized in these experiments (approx. 400 mL). Hydrogen peroxide was added using a peristaltic pump (as described previously), but the rate of addition necessary to maintain a constant H_2O_2 concentration was relatively low (see discussion). In these experiments, the pH was uncontrolled, but monitored.

Fixed-Bed Desorption Experiments

Fixed bed (as opposed to the previously described fluidized bed) experiments were conducted using an Emerson mechanical vacuum pump rated at 1725 rpm to draw water through a contaminant-loaded carbon bed in a down-flow direction. The pump was connected to an enclosed reservoir by 1/4-inch Teflon tubing, which fed a 1 L Pyrex® filter flask that acted as a support base for the reactor assembly. The reactor consisted of a 350-mL borosilicate graduated funnel with removable support screen (Chemglass®). Prior to experiments, carbon was sieve-sorted and 8-9 grams of each sample fraction (1.0-1.18 mm, 1.4-1.7 mm, and 2.0-2.38 mm) were equilibrated for 24 hours with an initially saturated water solution. The aqueous-phase was then decanted off, and the loaded GAC was transferred to the funnel assembly. Deionized water was drawn through the carbon bed at a rate of 200 mL per hour. A constant volume of 250 mL of deionized water was maintained above the carbon bed using a 1-100 rpm Masterflex® peristaltic pump, which pumped deionized water from a reservoir at room temperature (32°C ± 2°C). The fixed-bed adsorber design is presented in Figure 8.

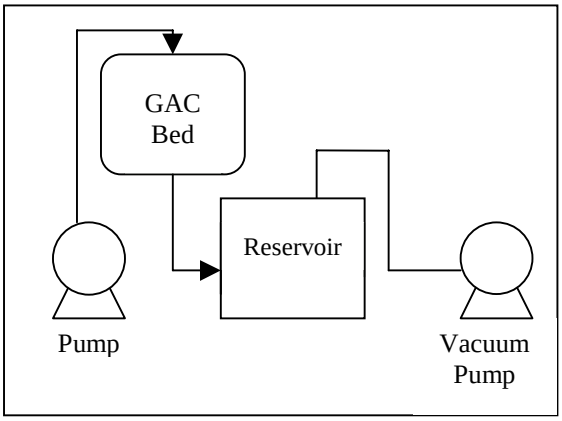

Figure 8. Fixed bed desorber setup with mechanical vacuum pump.

Representative samples of carbon were removed from the funnel over the course of each 250-minute experiment, extracted with ethyl acetate on a shaker table for 24 hours, and analyzed for residual contaminant, per above.

Field-Scale Column Experiments

Fenton-driven carbon regeneration was applied to soil vapor extraction (SVE) gas at the Park-Euclid (Arizona) State Superfund site, in which the primary contaminants are perchloroethene, trichloroethene, dichloroethene isomers, and the volatile hydrocarbon components of diesel fuel. Local groundwater and soil gases have been studied intensively so that the extent and severity of pollution are well characterized. A side stream was taken off the full-scale SVE system at the field site to provide a source of SVE gases (containing mainly TCE and PCE) to the project's GAC column. The carbon was packed into a borosilicate glass chromatography column, I.D.=5.00 cm, L=30.0 cm, V=600.0 mL. The gas flow rate passing through the column was 4.0 cfm. Column effluent was returned to the SVE system. The carbon was typically loaded for approximately 72 hours. After loading, the carbon was regenerated in place via Fenton's reaction, reloaded with contaminant, and re-regenerated to study process feasibility (see Figure 9). During regeneration, solid and aqueous-phase samples were withdrawn and extracted as in the bench-scale experiments (see Figure 10). Initially, hydrogen peroxide was added to the 7-liter reservoir to maintain a near-constant concentration (0.2 M) throughout the regeneration period. Less frequent pulse additions of H_2O_2 were later used as a strategy to reduce H_2O_2 utilization during carbon recovery.

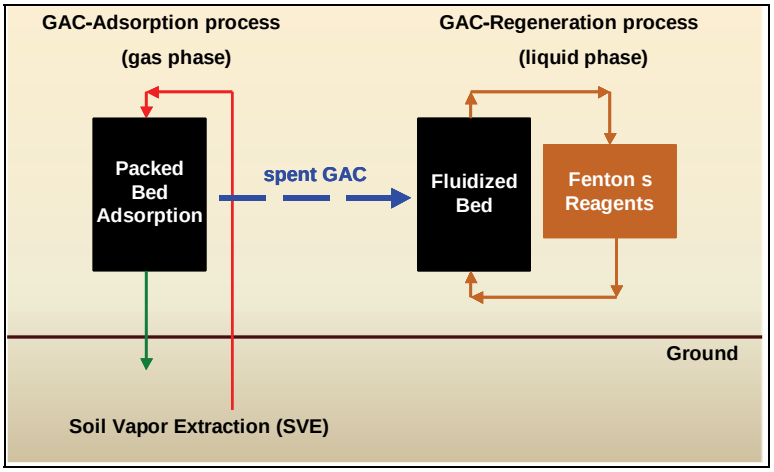

Figure 9. SVE-GAC system at field site.

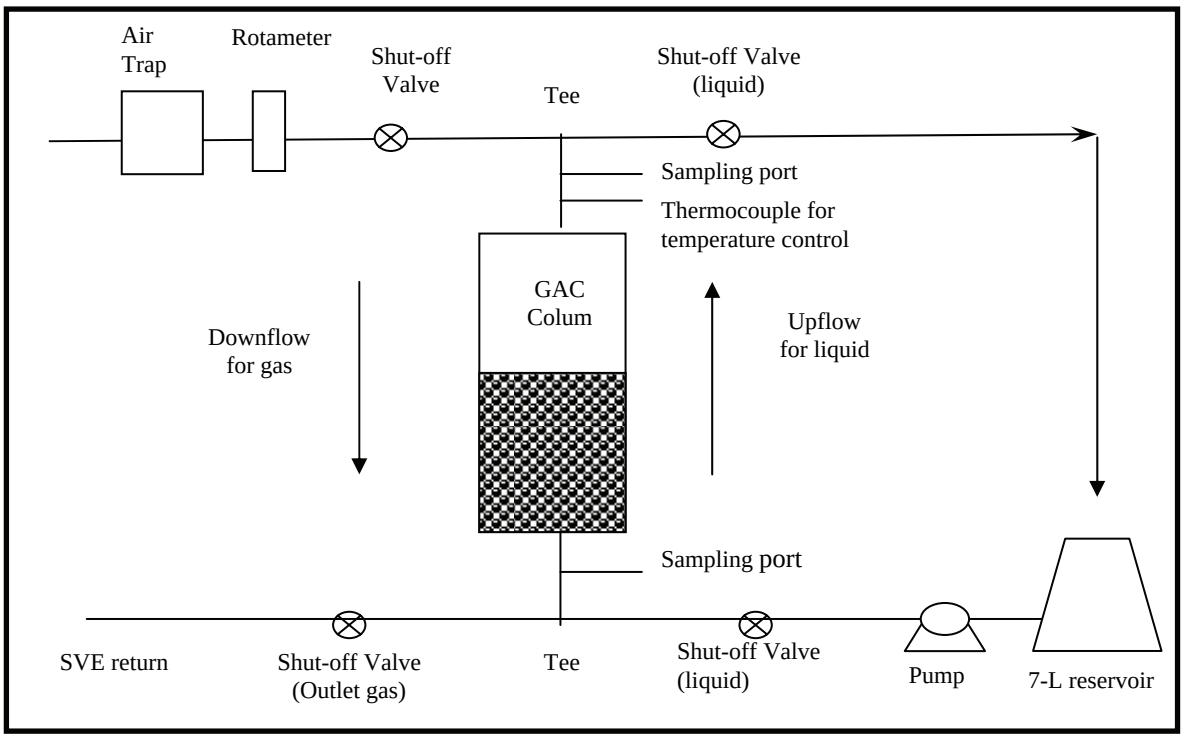

Figure 10. Diagram of the field experimental set-up for GAC-regeneration experiments. The carbon was loaded in a down flow mode and regenerated in an up flow mode. Column ID = 50 mm, L = 300 mm, 0.60 L, HRT (column) = 2 sec., HRT (reservoir) = 0.9 min, pH = 2.0, $[Fe(III)]_T$ = 10 mM, and $[H_2O_2]_o$ =0.38M.

Results and Discussion

Homogeneous Experiments

Dependence of PCE Reduction Kinetics on Total Iron

Preliminary experiments were carried out at initial concentrations of 0.10 M H_2O_2, pH 2.0, and either 0.1, 0.5 or 2.0mM Fe_T (added as Fe(III)). Starting PCE concentrations were 50 μM. PCE disappearance obeyed first order kinetics (Figure 11) even though there was no attempt to maintain H_2O_2 at a constant level over the 2-hour experiments. The magnitude of the first order rate constant varied directly with total iron concentration. At the highest total iron concentration (2.0 mM), the half time for PCE disappearance was 19 minutes. The reaction proceeded with essentially no lag following the addition of H_2O_2, indicating that near steady concentrations of iron species and hydroxyl radical were established quickly.

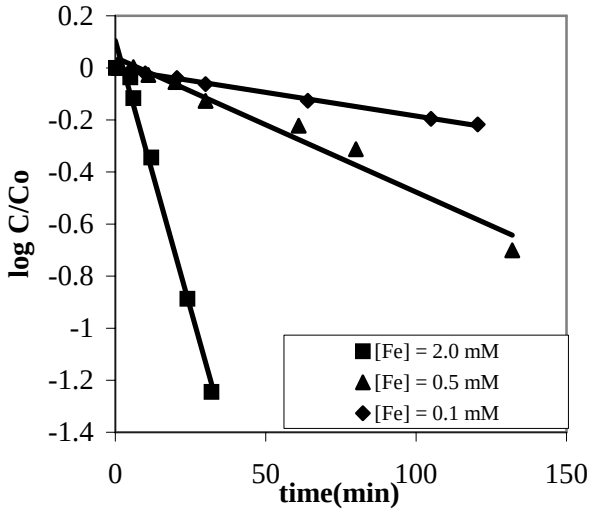

Figure 11. Effect of iron concentration on PCE disappearance at a fixed initial hydrogen peroxide concentration of 0.10 M. Total iron concentrations were 0.1 mM(♦), 0.5 mM (▲), and 2.0 mM (■). The data yield pseudo-first-order rate constants k_1 of 0.0018 min^{-1} (♦), 0.0047 min^{-1} (▲), and 0.0366 min^{-1} (■), respectively.

The pseudo-first-order rate constant for PCE disappearance in the experiment with a total iron concentration of 2.0 mM was about 20 times that of the experiment with $[Fe]_T = 10^{-4}$ M. However, the rate constant for PCE destruction at $[Fe]_T = 5 \times 10^{-4}$ M was unexpectedly low. There is no convincing explanation for the seeming inconsistency.

Rate Enhancement via Hydroxylamine (NH_2OH) Addition

Many investigators have shown that Fenton-driven reaction rates are initially very fast but subsequently decelerate rapidly when iron is provided as Fe(II) (Chen and Pignatello, 1997; Gallard and De Laat, 2000; Poppe, 2001). The observation directly supports assertions that Fe(III) reduction limits the overall rate of radical generation and, in these cases, contaminant destruction. On this basis, it was hypothesized that chemical reductants that convert Fe(III) to Fe(II) faster than the reaction of Fe(III) with H_2O_2 would increase the overall rate of hydroxyl radical formation and the rate of PCE disappearance. Several chemical additives were tested as potential means to circumvent or accelerate this rate limiting step in the simple Fenton's reagent system.

In the first experiments, identical reaction mixtures were established in two parallel reactors with $[Fe(III)]_T$ = 0.5 mM, $[H_2O_2]_o$ = 0.1 M, pH = 2.0, and $[PCE]_o$ = 70 μM. Eighteen minutes after the start of the experiment, 0.1 M NH_2OH (a common reductant used to convert Fe(III) to Fe(II)) was added to one of the two reactors. After an additional 21 minutes, a second, identical dose of hydroxylamine was provided to the same reactor. The aqueous-phase PCE concentration was measured as a function of time.

NH_2OH addition dramatically increased the specific rate of PCE disappearance, decreasing the half time for PCE disappearance from 148 minutes to, at least initially, less than five minutes (Figure 12). It is also apparent that the hydroxylamine-dependent (specific) rate of PCE conversion was not sustained over the course of the experiment, probably due to hydroxylamine consumption. Because hydroxylamine concentration was not monitored, this explanation cannot be established directly. The second hydroxylamine addition at 39 minutes also increased the specific rate of PCE disappearance, although more modestly. It is hypothesized that reaction products from the first stages of the experiment consumed a significant fraction of the radicals generated at that point. Accumulation of reaction intermediates could also account for the observed decrease in the specific rate of PCE disappearance during minutes 20-39 of the experiment. It seems likely, then, that although NH_2OH addition initially greatly enhanced Fenton-dependent contaminant transformations, consumption of NH_2OH and the consequent need for semi-continuous chemical addition limits the utility of such strategies for enhancing PCE degradation rates.

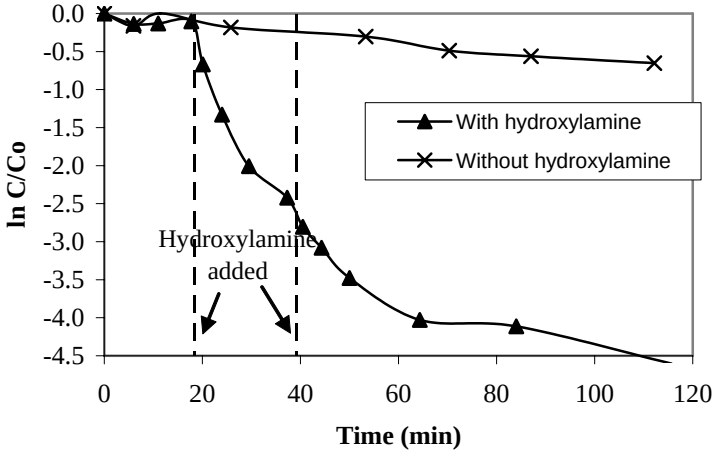

Figure 12. PCE degradation with hydroxylamine as a reducing agent. T=22-24°C. Initial concentrations: $[Fe(III)]_T$ = 0.50 mM, $[H_2O_2]$ = 0.10 M, pH= 2.0, and [PCE]= 70E-4 M. Hydroxylamine doses (0.01 M) were added to the system at 18 and 39 min.

Quinone Addition

Quinone addition was investigated as a means for accelerating the rate limiting step, Fe(III) reduction, in the Fenton's mechanism. Quinones are effective agents for facilitating electron transfer to Fe(III) (Fredrickson et al., 2000). The mechanism involves a series of 1-electron transfers that yield a semiquinone radical intermediate (Chen and Pignatello, 1997). The initial reductant in this reaction series is thought to be the superoxide radical produced via Fenton's mechanism (Figure 13). These experiments do not distinguish between superoxide or hydroxyl radicals as participants in PCE transformation. Later experiments using IP as an •OH radical scavenger, however, suggest that •OH is the primary reactant with PCE (see later section on superoxide radical effects). Three different quinones were tested in these experiments (Figure 14). It was hypothesized that the more complex structure of 9,10-anthraquinone-2,6-disulfonic acid (AQDS) might protect the molecule against radical attack, preserving or extending its ability to shuttle electrons to the Fe(III) target.

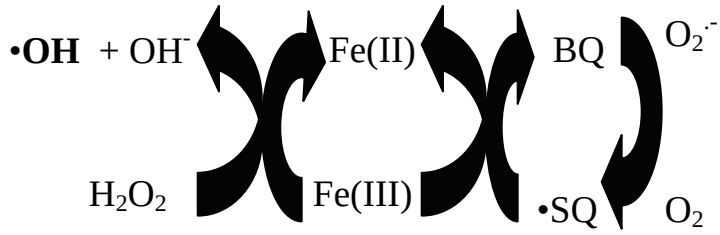

Figure 13. Simplified quinone mechanism (adapted from Chen and Pignatello, 1997). •SQ stands for semiquinone radical, and O_2•$^-$ for superoxide radical.

Quinones were tested by adding them at concentrations up to 5×10^{-4} M to Fenton reagents consisting initially of 5×10^{-4} M Fe_T (initially as Fe(III)), 0.10 M H_2O_2, pH 2.0 and 70 μM PCE. All experiments were at room temperature (22-24ºC). Initial PCE conversion rates increased monotonically with increasing initial quinone concentration (Figure 15). Addition of 5×10^{-5} M hydroquinone, for example, doubled the initial rate of PCE disappearance. An additional 10-fold increase in the hydroquinone concentration, to 5×10^{-4} M, increased the initial rate constant of PCE disappearance by another factor of two. It is apparent that for periods approaching an hour hydroquinone addition increased the overall rate of Fe(III) reduction and, consequently, the concentration of hydroxyl radicals in these experiments.

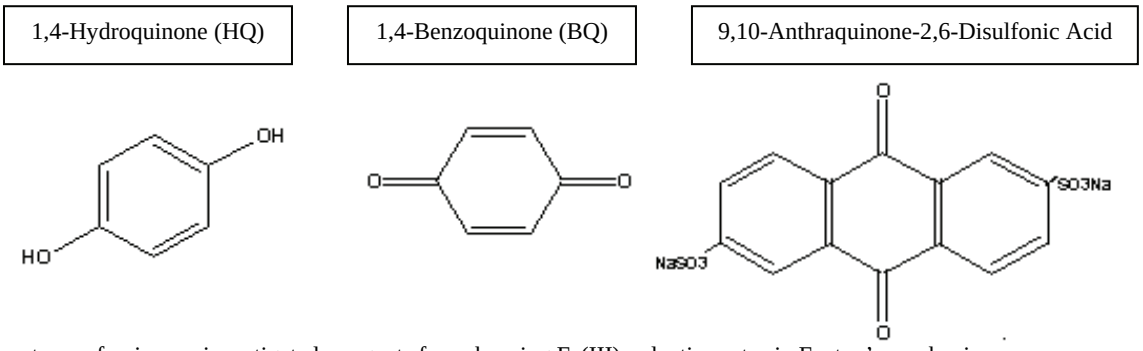

Figure 14. Structures of quinones investigated as agents for enhancing Fe(III) reduction rates in Fenton's mechanism.

A summary of quinone-dependent first-order rate constants is provided as Table V. First-order rate constants represent reaction kinetics at the outset of the experiment, before the specific rates of PCE disappearance decreased as a consequence of quinone destruction or accumulation of reaction intermediates. Initial rates of PCE disappearance are plotted as a function of the hydroquinone addition in Figure 16. A linear relationship between the specific rate of PCE loss and the initial hydroquinone concentration is evident.

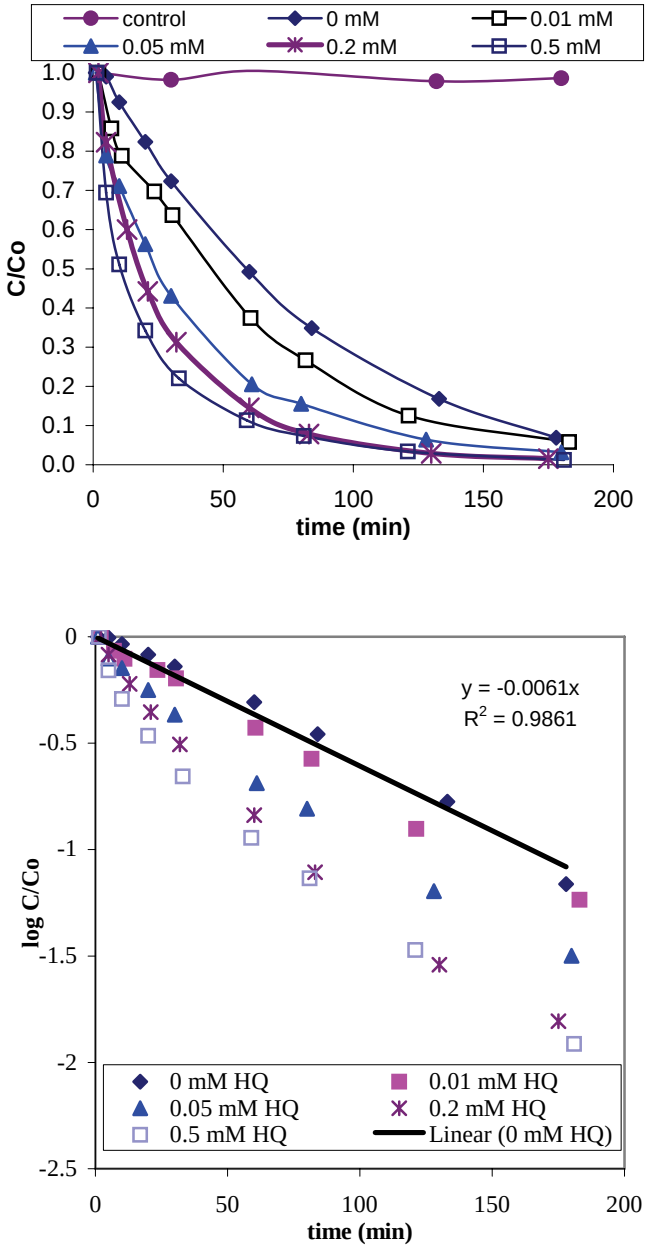

Figure 15. PCE degradation as a function of 1,4-hydroquinone added.
Initial conditions: $[Fe(III)]_T$ = 0.5 mM @ pH = 2.06, $[H_2O_2]_o$ = 0.10 M (0.25%), $[PCE]_o$ = 4E-5M.

Table V. First-Order Rate Constants for PCE Disappearance as a Function of the Initial Hydroquinone Concentration

HQ (mM)	$k_1(min^{-1})$	R^2
0.5	1.89E-02	0.946
0.4	1.59E-02	0.947
0.3	1.41E-02	0.972
0.2	1.28E-02	0.979
0.05	8.30E-03	0.996
0.01	6.90E-03	0.998
0.005	6.60E-03	0.989
0	4.45E-03	0.990

Note: Values were derived via linear regression using the (semi-log) transformed data from Figure 15. In general, only the first 4-5 data points (first 30-min) from each experiment were used. R^2 values are included to illustrate goodness of fit.

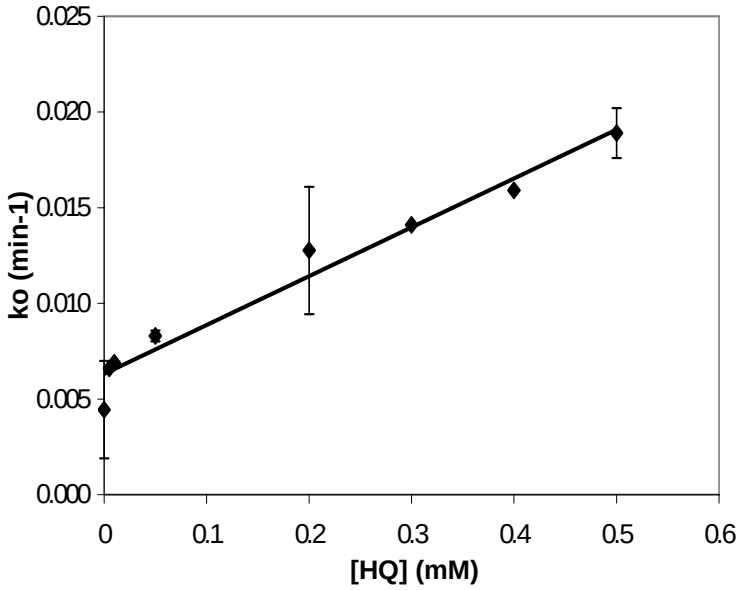

Figure 16. Initial first order rate constants for different hydroquinones concentrations. When two or more experiments were run at a single HQ concentration, symbols indicate average values. Error bars represent ± 1 standard deviation (n=3).

Inspection of the Figure 15 data indicates that, in the presence of hydroquinone, the specific rate of PCE conversion decreased continuously during the course of each three-hour experiment. It was therefore posited that Fenton-derived radicals gradually destroy HQ. To test this hypothesis, the reaction time for PCE destruction was extended by renewing the PCE and H_2O_2 concentrations in both the HQ-free control and the reactor initially amended with 0.5 mM HQ (Figure 17). The kinetic advantage initially afforded by HQ addition was completely absent in the second half of the experiment. Results strongly suggest that HQ no longer served as an electron shuttle after the first three-hour period of the experiment. Others have noted that quinone function is rapidly lost in the presence of reactions that yield hydroxyl radicals (Chen and Pignatello, 1997). The practical implication of these results is that

hydroquinone addition can accelerate Fenton-driven conversions only briefly unless the quinone concentration is periodically renewed. Practical and economic considerations probably dictate against this.

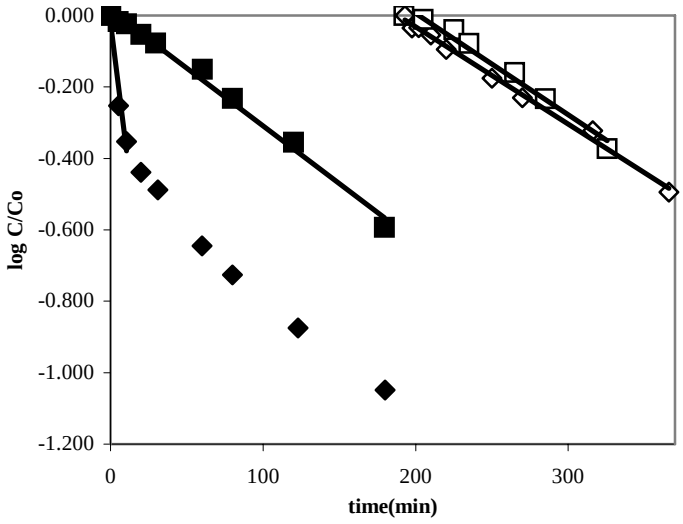

Figure 17. Two-period hydroquinone addition experiment comparing the performances of Fenton's mechanism for PCE destruction, with (♦/◊) and without (■/□) 5×10^{-4} M hydroquinone addition. The second period of the experiment involved reestablishment of initial conditions via PCE and H_2O_2 addition after the first three hours of the experiment. Initial conditions: $[Fe(III)]_T$ = 0.5 mM, $[H_2O_2]$ = 0.10 M, [PCE] = 7.26×10^{-5} M, pH=2.0, room temperature.

Experiments with 1,4-benzoquinone (BQ) were parallel in design and similar in result to those involving HQ. Reactors, reaction mixtures and physical conditions of the experiments were identical to those described for HQ. The initial BQ concentration was varied from 0.0 to 0.5 mM. Initially, the specific rates of PCE disappearance were significantly enhanced by addition of BQ (Figure 18), although a saturation effect was apparent: BQ concentrations ≥ 0.3 mM all produced approximately the same effect on reaction kinetics (Figures 18 and 19). PCE disappearance was initially 7 times faster in the reactor amended with 0.3 mM BQ than in the BQ-free reactor. However, prior to the end of the first 5-hour phase of the experiment, the kinetic advantage offered by BQ addition was entirely lost and likely reversed. After 5 hours, H_2O_2 and PCE concentrations were restored to their original levels in the reactors that initially contained 0.0 or 0.3 mM BQ. The BQ-free control clearly outperformed the BQ-amended reactor at that point (Figure 20). It is hypothesized, but not verified, that organic residuals derived from the destruction of quinones served as radical scavengers, thus depleting the •OH radical pool available for PCE depletion.

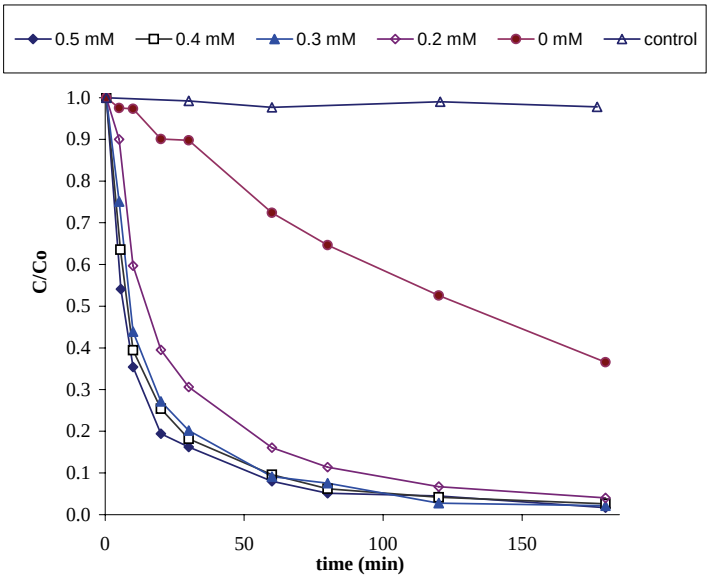

Figure 18. Effect of initial benzoquinone concentration on the Fenton-dependent rate of degradation of PCE. Initial conditions: $[Fe(III)]_T$ = 0.5 mM, pH = 2.0, $[H_2O_2]$ = 0.10 M, [PCE] = 8E-5 M. The control had no H_2O_2.

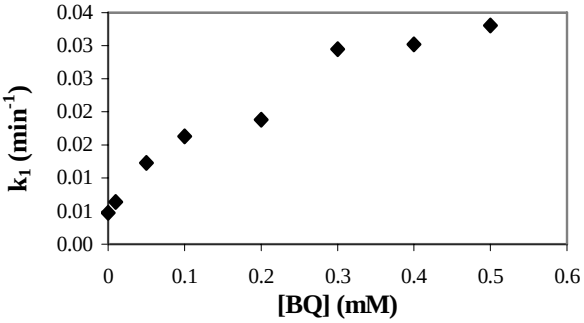

Figure 19. Effect of initial benzoquinone concentration on the observed first-order rate constant for Fenton-dependent PCE disappearance. Initial conditions are given in Figure 18.

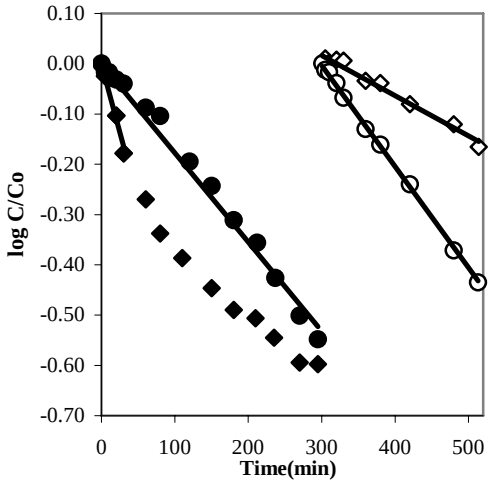

Figure 20. Effect of 0.3 mM BQ addition on the (log transformed) PCE concentration. Initial conditions: $[Fe(III)]_T$= 0.5 mM, $[PCE]_o$ = 1E-4 M, $[H_2O_2]_o$ = 0.10 M, pH = 2.0. PCE and H_2O_2 concentrations were restored to original levels after 300 minutes. The slopes for the segments of straight lines are 0.0018 min^{-1}(●) and 0.0020 min^{-1}(○) for the BQ-free reactors and 0.0055 min^{-1}(♦) and 0.0008 min^{-1}(◊) for BQ-amended reactors. Closed symbols indicate the original reactors.

Experiments with 9,10-anthraquinone-2,6-disulfonic acid (AQDS) produced similar results to the BQ and HQ trials. That is, the initial catalytic effect was quickly lost, and the AQDS-free control outperformed the amended reactor in the second phase of the experiment (Figure 21). It is apparent that addition of functional groups to the quinone did not enhance quinone longevity. Neither did the added functional groups make organic by-products from quinone destruction less effective radical scavengers. Again, the experiment highlights the practical limitations of quinone addition for enhancement of Fenton-driven destruction of hazardous organic compounds.

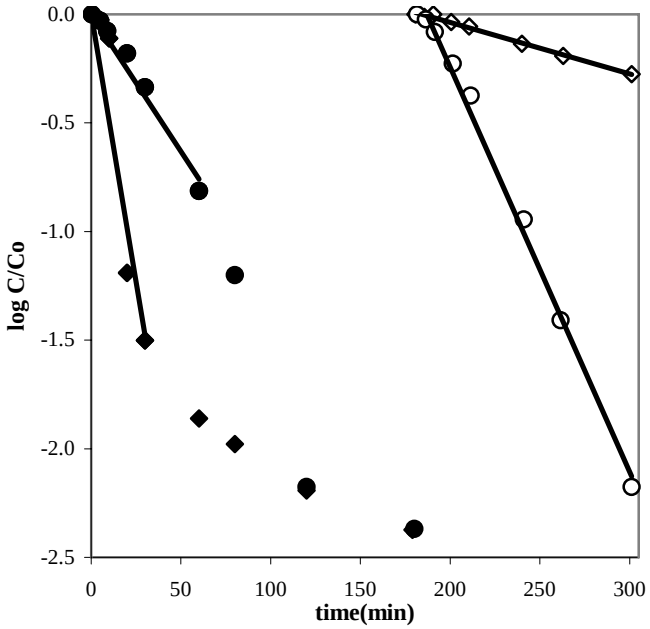

Figure 21. Effect of 0.5 mM AQDS addition to Fenton's reagents for PCE transformation. Log-transformed PCE data are on the ordinate. Initial conditions: $[Fe(III)]_T$=0.05 mM, $[H_2O_2]$=0.10 M, [PCE]=9.9×10^{-5} M, pH= 2.1. Initial PCE and H_2O_2 levels were restored after 180 minutes. The slopes for the segments of straight lines are 0.0126 min^{-1}(●) and 0.0186 min^{-1}(○) for the AQDS-free reactors and 0.0492 min^{-1}(♦) and 0.0024 min^{-1}(◊) for AQDS-amended reactors. Closed symbols indicate the original reactors.

Copper Effects

Based on the findings of Walling and Kato (1971), it was hypothesized that the presence of copper in solution can propagate hydroxyl radical chain reactions, possibly enhancing the rate of PCE destruction in homogeneous experiments. To test this hypothesis, initial experiments were conducted in which 0.0, 5×10^{-4} M (Figure 22), 2.0×10^{-3} M, 4.0×10^{-3} M and 2.0×10^{-2} M Cu(II) were added to the aqueous-phase system that consisted of 5×10^{-4} M Fe(III), 0.10 M H_2O_2 and 10^{-4} M PCE. The initial pH was 2.1, and the experiment was conducted at room temperature. Negative controls contained 5×10^{-4} M Cu(II), but lacked either iron or H_2O_2. In both controls, the loss of PCE was negligible over the 5-hour experiments. Rate dependence on copper concentration proved to be complex.

At Cu/Fe molar ratios from 4-80, however, rates of PCE degradation were enhanced by copper addition. Process kinetics remained first-order in PCE, but the apparent first-order rate constant was increased more than two-fold at [Cu(II)] = $4x10^{-3}$ M (Figure 23). Unlike the quinone and hydroxylamine trials, PCE conversion kinetics remained first

order throughout each experiment since copper was conserved during the radical generation and reaction process. Presumably the concentrations of copper species changed little over the course of the experiment, following establishment of near-steady conditions in the first minutes of each experiment.

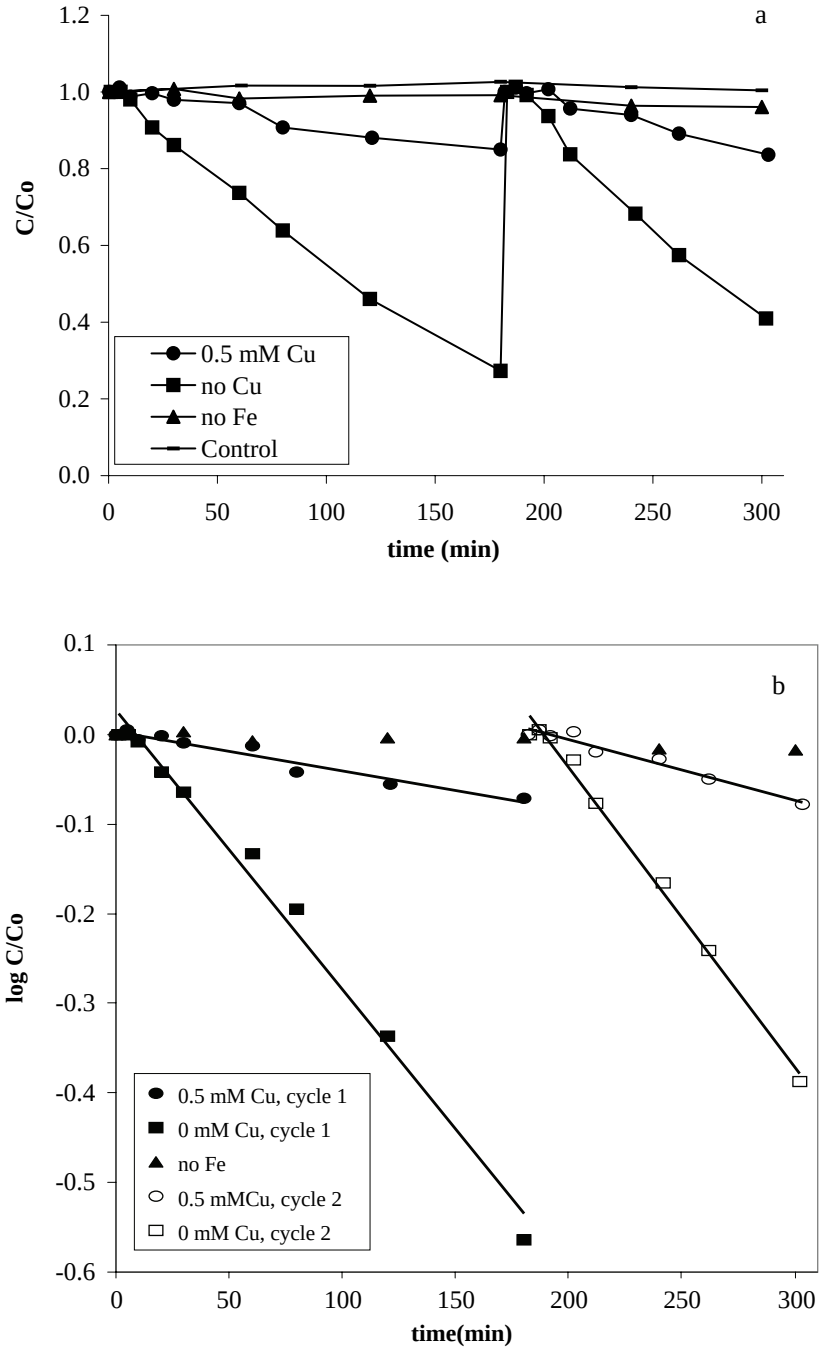

Figure 22(a)(b). Effect of 5×10^{-4} M Cu(II) addition on the Fenton-driven rate of PCE destruction. Initial conditions: $[Fe(III)]_T$ = 0.5 mM, $[H_2O_2]_o$ = 0.10 M, [PCE] = 10^{-4} M, pH = 2.1, room temperature. At 180 minutes, PCE and H_2O_2 were added to the system to reestablish their initial conditions.

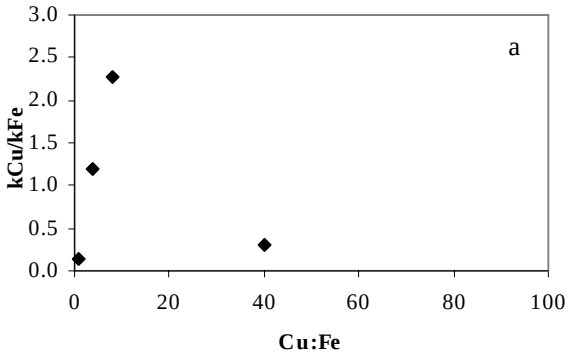

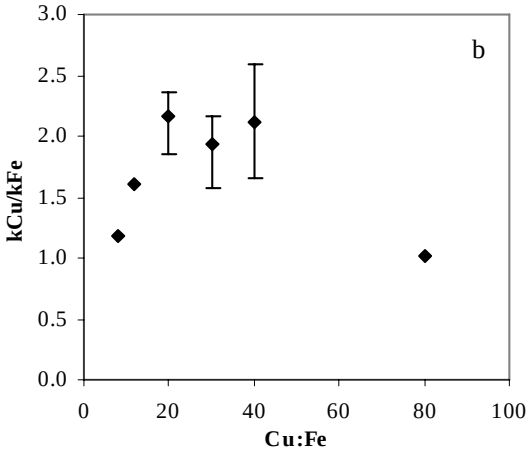

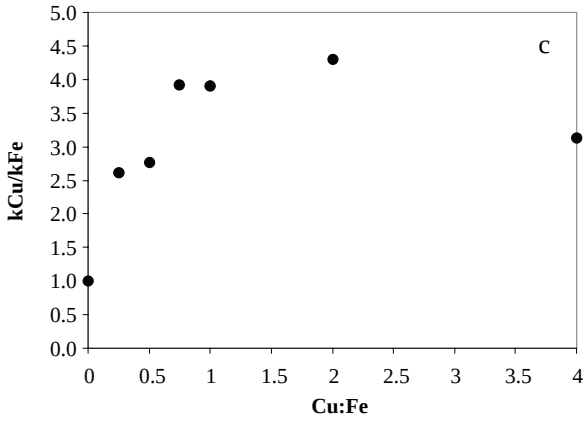

Figure 23. Effect of Cu(II) addition on the pseudo-first-order rate constant for Fenton-driven PCE transformation. Initial conditions: (a)$[Fe(III)]_T$ = 0.5 mM, $[H_2O_2]_o$ = 0.10 M, $[PCE]_o = 5\times10^{-5}$, [Cu(II)] from 0 to 20 mM, pH = 2.1, room temperature; (b) $[Fe(III)]_T$ = 0.1 mM, $[H_2O_2]_o$=0.10 M, $[PCE]_o=10^{-4}$ M, [Cu(II)] from 0 to 8 mM, pH = 2.1, T = 30ºC. (c) $[Fe(III)]_T$ = 0.1 mM, $[H_2O_2]_o$=0.10 M,$[PCE]_o=6x10^{-5}$ M, [Cu(II)] from 0 to 0.4 mM, pH = 2.0, T = 30ºC. Rate constants obtained at other temperatures were corrected to 30ºC using the Arrehenius plot (see Figure 24). Ordinate values are the ratio of rate constants measured in the presence and absence of copper at the molar Cu:Fe ratio indicated. Symbol indicates the average value. Error bars were calculated for some data points (n≥3) using the standard deviations.

The same series of copper-addition experiments were repeated using a total ferric iron concentration of $1.0x10^{-4}$ M, with Cu/Fe (molar ratios) from zero to 80 (T = 30ºC). Results (Figure 23b) were similar to those obtained with 0.5 mM total iron. Cu:Fe ratios from 20-40 increased the pseudo-first-order rate constant for PCE disappearance by a factor ≥ 2.0.

Mechanism of Rate Enhancement by Copper

The acceleration of PCE degradation by copper addition at Cu/Fe ratios near 10:1 can be explained in the following way. The reaction of Cu(I) with H_2O_2 may be slow or proceed without the production of hydroxyl radicals. This is supported by the lack of PCE degradation in mixtures that initially contained Cu(II), H_2O_2, and PCE but with no iron present. For the case with both Cu and Fe present, if the reaction of Cu(II) with H_2O_2 is fast, the Cu(I) formed may reduce Fe(III) to yield Fe(II) and regenerate Cu(II). In the Fenton's system without copper amendment, iron reduction limits the rate of hydroxyl radical generation, thus, acceleration of ferrous iron production by copper addition would increase the overall rate of hydroxyl radical generation, and thus the pseudo-first-order rate constant for PCE disappearance. That is, the following sequence of reactions would yield additional free radicals and accelerate PCE oxidation:

$$Cu(II) + H_2O_2 \leftrightarrow Cu(I) + O_2\bullet^- + 2H^+ \quad (23)$$

$$Cu(I) + Fe(III) \leftrightarrow Fe(II) + Cu(II) \quad (15)$$

$$Fe(II) + H_2O_2 \rightarrow Fe(III) + \bullet OH + OH^- \text{ (as above)} \quad (2)$$

Superoxide radicals produced in reaction 23, may reduce another metal ion yielding molecular oxygen. The cuprous ion may also terminate the chain reaction that propagates the PCE conversion reaction. That is,

$$Cu(I) + R\bullet \rightarrow Cu\ (II) + R^- \quad (24)$$

The ability of copper addition to accelerate PCE degradation is fairly modest, at least at room temperature. Nevertheless, Cu(II) solubility is greater than that of iron so that copper addition may provide attractive benefits in the pH range where the rate is limited by iron solubility. Furthermore, copper-dependent effects on contaminant treatment kinetics may be greater at higher temperatures.

Temperature Effects

Dependence of the first-order rate constant for PCE disappearance on temperature was established for both copper-free and copper-amended reaction mixtures. It is apparent that the copper-dependent mechanism of PCE destruction is more sensitive to temperature than is the conventional (Cu-free) Fenton-driven mechanism. Arrhenius plots corresponding to the Cu-free and Cu/Fe = 8:1 cases (Figure 24) provided different activation energies and pre-exponential factors, indicating that the addition of copper to the Fenton's reactants alters the mechanism of destruction, including the rate-limiting step. In the copper-free solution, at least, rate limitation is thought to arise

from reduction of Fe(III)-peroxo complexes by H_2O_2. The greatest benefit of copper addition, in terms of accelerated PCE destruction was achieved in the highest temperature range investigated (40 – 54°C). At 54°C, the expected rate constant for PCE transformation was increased almost four-fold by copper addition at an 8:1 molar (Cu/Fe) ratio. At 30°C, rates with and without copper addition were essentially indistinguishable. Because Fenton's reaction is exothermic, reaction heat could enhance the benefits of copper addition to hydroxyl radical generation and PCE degradation rates. Iron was provided at nearly its solubility limit in these experiments (at pH 2.0 Fe(III) solubility is about $2x10^{-3}$ M). Therefore, acceleration of Fenton's reaction via further iron addition is infeasible. Thus, copper addition offers an attractive method for further enhancing reaction rates, particularly at higher temperatures.

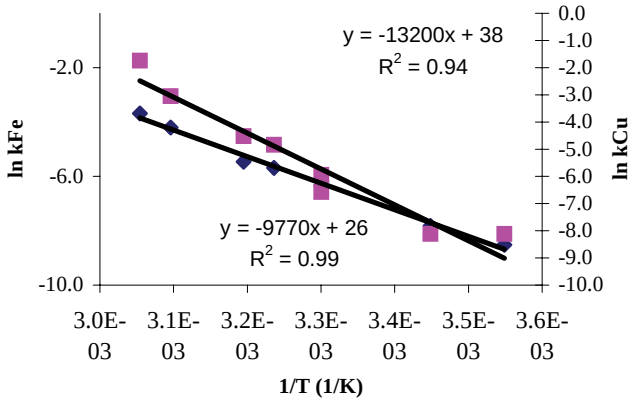

Figure 24. Arrhenius plots for copper-free and fixed Cu:Fe ratio (8:1) cases. Initial concentrations: $[Fe(III)]_T$ = 0.1 mM, $[H_2O_2]_o$ = 0.10 M, $[PCE]_o = 9.0\times10^{-5}$ M. Temperature range: 8.8-54.4°C. Symbols used: ♦ Fenton's system without copper and ■ Fenton's system with copper.

Homogeneous Model Formulation

A. Simplified Fenton Mechanism

In Fenton's mechanism, successive reactions of hydrogen peroxide cycle iron between the plus two and plus three oxidation states, generating two radical species (•OH, and HO_2•/O_2•$^-$) in each cycle. The radicals produced are capable of oxidizing/reducing many organic targets per the following simplified mechanism:

$$Fe(III) + H_2O_2 \rightarrow Fe(II) + HO_2\bullet + H^+ \quad (1)$$

$$Fe(II) + H_2O_2 \rightarrow Fe(III) + \bullet OH + OH^- \quad (2)$$

$$\bullet OH + R \rightarrow OH^- + \bullet R \quad (3)$$

B. Complications in the Actual Fenton Reactions

A mathematical model based on the kinetic model of De Laat and Gallard (1999) is presented in this section. The model describes the decomposition of hydrogen peroxide by iron in a homogeneous aqueous solution, taking into account the rapid formation and the slower decomposition of Fe(III)-hydroperoxo complexes ($Fe^{III}(HO_2)^{2+}$ and $Fe^{III}(OH)(HO_2)^+$). The objective of this modeling effort is to achieve a better understanding of the effect that the

operational parameters in Fenton's reaction, such as pH and initial concentrations of H_2O_2 and iron, have on the utility of the system for degradation of organic toxins.

i. Complexation with H_2O_2 and Complex Disproportionation – Implication for pH Effects on Rate of Reaction

Gallard *et al*. (1999) identified two ferric hydroperoxo complexes by spectrophotometric analysis. These two complexes are formed rapidly after mixing Fe(III) and H_2O_2 in solution. The species are formulated as $[Fe^{III}]^{3+}$, (HO_2^-) (or $Fe^{III}(HO_2)]^{2+}$; I_1) and $[Fe^{III}](OH)]^{2+}$, (HO_2^-) (or $[Fe^{III}](OH)(HO_2)]^+$; I_2), which are in acid base equilibrium ($K_{I1/I2}$ = 1.8 x10^{-4} M) (Table VI). Once generated, these species are assumed to decompose to Fe^{2+} and HO_2• (Table VI).

The reaction rate constants and the equilibrium constants for the species involved in the Fenton's reaction and included in the model are listed in Table VI. Reactions (1) to (5) are sufficiently fast to be at equilibrium in this application.

Table VI. Reaction Mechanism for Fe(III)-Catalyzed Decomposition of H_2O_2 (25 °C; I = 0.1 M)

No	Reaction	Constants
(1)	$Fe^{3+} + H_2O \leftrightarrow FeOH^{2+} + H^+$	K_1= 2.9 x 10^{-3} M
(2)	$Fe^{3+} + 2H_2O \leftrightarrow Fe(OH)_2^+ + 2H^+$	K_2= 7.62 x 10^{-7} M^2
(3)	$2Fe^{3+} + 2H_2O \leftrightarrow Fe_2(OH)_2^{4+} + 2H^+$	$K_{2,2}$ = 0.8 x 10^{-3}M
(4)	$Fe^{3+} + H_2O_2 \leftrightarrow Fe^{III}(HO_2)^{2+} + H^+$	KI_1 = 3.1 x 10^{-3}
(5)	$FeOH^{2+} + H_2O_2 \leftrightarrow Fe^{III}(OH)(HO_2)^+ + H^+$	KI_2 = 2.0 x 10^{-4}
(6a)	$Fe^{III}(HO_2)^{2+} \rightarrow Fe^{2+} + HO_2$•	$k_{6,I1}$ = 2.7 x 10^{-3} s^{-1}
(6b)	$Fe^{III}(OH)(HO_2)^+ \rightarrow Fe^{2+} + HO_2$• + OH^-	$k_{6.I2}$ = 2.7 x 10^{-3} s^{-1}
(7)	$Fe^{2+} + H_2O_2 \rightarrow Fe^{3+} + $•$OH + OH^-$	k_7 = 63.0[a] M^{-1} s^{-1}
(8)	$Fe^{2+} + $•$OH \rightarrow Fe^{3+} + OH^-$	k_8 = 3.2 x 10^8 M^{-1} s^{-1}
(9)	•$OH + H_2O_2 \rightarrow HO_2$• + H_2O	k_9 = 3.3 x 10^7 M^{-1} s^{-1}
(10a)	$Fe^{2+} + HO_2$• $\rightarrow Fe^{III}(HO_2)^{2+}$	k_{10a} = 1.2 x 10^6 $M^{-1}s^{-1}$
(10b)	$Fe^{2+} + O_2$•$^- + H^+ \rightarrow Fe^{III}(HO_2)^{2+}$	k_{10b} = 1.0 x 10^7 M^{-1} s^{-1}
(11a)	$Fe(III) + HO_2$• $\rightarrow Fe^{2+} + O_2 + H^+$	k_{11a} < 2 x 10^3 M^{-1} s^{-1}
(11b)	$Fe(III) + O_2$•$^- \rightarrow Fe^{2+} + O_2$	k_{11b} = 5 x 10^7 M^{-1} s^{-1}
(12a)	HO_2• $\rightarrow O_2$•$^- + H^+$	k_{12a} = 1.58 x 10^5 s^{-1}
(12b)	O_2•$^- + H^+ \rightarrow HO_2$•	k_{12b} = 1 x 10^{10} M^{-1} s^{-1}
(13a)	HO_2•+ HO_2• $\rightarrow H_2O_2 + O_2$	k_{13a} = 8.3 x 10^5 M^{-1} s^{-1}
(13b)	HO_2• + O_2•$^-$ + $H_2O \rightarrow H_2O_2 + O_2 + OH^-$	k_{13b} = 9.7 x 10^7 M^{-1} s^{-1}
(14a)	•$OH + HO_2$• $\rightarrow H_2O + O_2$	k_{14a} = 0.71 x 10^{10} M^{-1} s^{-1}
(14b)	•$OH + O_2$•$^- \rightarrow OH^-$+ O_2	k_{14b} = 1.01 x 10^{10} M^{-1} s^{-1}
(15)	•$OH + $•$OH \rightarrow H_2O_2$	k_{15} = 5.2 x 10^9 M^{-1} s^{-1}

Note: [a] Apparent second-order rate constant for the reaction of H_2O_2 with Fe(II) at pH < 3.5.
Source: De Laat and Gallard, 1999. De Laat and Gallard (1999) fit k_6 to the experimental data (pH <3.5), where I_1 is the predominant Fe(III)-hydroperoxy complex.

In a constant volume batch system, the reactions listed in Table VI lead to the following mass balances:

$$d[Fe^{2+}]/dt = k_6([I_1]+ [I_2]) - k_7[Fe^{2+}][H_2O_2] - k_8[Fe^{2+}][\bullet OH] - k_{10a}[Fe^{2+}][HO_2\bullet] - k_{10b}[Fe^{2+}][O_2\bullet^-] + k_{11a}[Fe(III)][HO_2\bullet] + k_{11b}[Fe(III)][O_2\bullet^-] \quad (25)$$

$$d[Fe(III)]_T/dt = -d[Fe^{2+}]/dt \quad (26)$$

$$d[H_2O_2]/dt = - k_7[Fe^{2+}][H_2O_2] - k_9[H_2O_2][\bullet OH] + k_{13a}[HO_2\bullet][HO_2\bullet] + k_{13b}[O_2\bullet\text{-}][HO_2\bullet] + k_{15}[\bullet OH]^2 \quad (27)$$

$$d[\bullet OH]/dt = k_7[Fe^{2+}][H_2O_2] - k_8[Fe^{2+}][\bullet OH] - k_9[H_2O_2][\bullet OH] - k_{14a}[\bullet OH][HO_2\bullet] - k_{14b}[\bullet OH][O_2\bullet^-] - 2k_{15}[\bullet OH]^2 \quad (28)$$

$$d[HO_2\bullet]/dt = k_6([I_1]+[I_2]) + k_9[H_2O_2][\bullet OH] - k_{10a}[Fe^{2+}][HO_2\bullet] - k_{11a}[Fe(III)][HO_2\bullet] - k_{12a}[HO_2\bullet] + k_{12b}[O_2\bullet^-][H^+] - 2k_{13a}[HO_2\bullet]^2 - k_{13b}[O_2\bullet^-][HO_2\bullet] - k_{14a}[\bullet OH][HO_2\bullet] \quad (29)$$

$$d[O_2\bullet^-]/dt = -k_{10b}[Fe^{2+}][O_2\bullet^-] - k_{11b}[Fe(III)][O_2\bullet^-] + k_{12a}[HO_2\bullet] - k_{12b}[O_2\bullet^-][H^+] - k_{13b}[O_2\bullet^-][HO_2\bullet] - k_{14b}[\bullet OH][O_2\bullet^-] \quad (30)$$

The total concentration of Fe(III) and the concentration of non-hydroxy Fe(III) species are given by:

$$[Fe(III)]_T = [Fe(III)] + [I_1] + [I_2] \quad (31)$$

$$[Fe(III)] = [Fe^{3+}] + [FeOH^{2+}] + [Fe(OH)_2^+] + 2[Fe_2(OH)_2^{4+}] \quad (32)$$

The system of nonlinear ordinary differential equations was solved numerically using the fourth-order Runge-Kutta method. Quasi-steady-state conditions were assumed for radical species ($d[\bullet OH]/dt = d[HO2\bullet]/dt = d[O_2\bullet^-]/dt = 0$) and their concentrations were obtained using Newton's method. The reaction parameters (pH, $[H_2O_2]_o$, $[Fe(III)]_o$), rate constants and equilibrium constants were specified as inputs to the program (for nomenclature of variables - see Appendix A.1). Model details are provided in Appendix A. The concentration - time profiles for H_2O_2, and Fe^{2+} were calculated by the program, and the concentration of H_2O_2 predicted by the model was compared to experimental measurements and/or published data when available.

ii. Model Limitations

Precipitation reactions of Fe(III) have not been incorporated in the model, hence the model should not be applied in situations where Fe(III) precipitation is expected or observed (typically pH> 3.0).

Differences between the experimental conditions in our study and those employed in the investigation by De Laat and Gallard (1999) are worth mentioning. De Laat and Gallard conducted their kinetic study at 25.0 °C and I = 0.1 M ($HClO_4/NaClO_4$), while our experiments were performed at 31±1°C (water bath), and the ionic strength varied from trial to trial but was typically about 0.02 M. In contrast to De Laat and Gallard's use of ferric perchlorate salt, ferric sulfate salt was used in all experiments and the pH was adjusted using sulfuric acid (H_2SO_4), to avoid adding background chloride in the system. In Fenton's reaction, destruction of chlorinated compounds results in

accumulation of chloride ions in solution. Therefore, ferric sulfate was chosen over ferric chloride for iron addition, to avoid the complication of a high initial chloride ion concentration when attempting to sort out chloride effects. Ferric sulfate was preferable to ferric perchlorate since a rate constant for the reaction of the hydroxyl radical and sulfate was found in the literature (3.5×10^5 $Lmol^{-1}s^{-1}$, Radiation Chemistry Data Center, 2003). No value was found for the hydroxyl radical and perchlorate reactions.

iii. Inorganic Radical Formation

a. Chloride, Perchlorate, Sulfate and Nitrate

De Laat *et al*., (2004) studied the effect of chloride, perchlorate, sulfate and nitrate ions on the rate of decomposition of H_2O_2 and transformations of organic compounds (atrazine, 4-nitrophenol, and acetic acid) by Fenton's reaction. They observed that the rates of reaction between iron (added as Fe(II)) and H_2O_2 were increased by specific anions. Relative effects were in the order of $SO_4^{2-}>ClO_4^-=NO_3^-=Cl^-$. When iron was provided as Fe(III), sulfate and chloride decreased both the decomposition rate of H_2O_2 and the rate of disappearance of specific organic targets. It was suggested that the latter observation was due to decreased formation of Fe(III) - hydroperoxy complexes, and that H_2O_2 does not complex with Fe(III)-sulfato complexes (De Laat and Giang Le, 2005). The pseudo-first-order kinetic constant (k_{obs}) for the initial rate of decomposition of H_2O_2 by Fe(III) decreased by 30%, and almost 20% of the iron was complexed as sulfato-Fe(III) at pH 2.0, I = 0.2 M, $[SO_4^{2-}]$ = 2 mM (lowest concentration studied in the range 0-200 mM). Almost complete inhibition of the rate was observed at $[SO_4^{2-}]$ = 67 mM, where 93% of iron was complexed with sulfate (De Laat and Giang Le, 2005). Nevertheless, under our experimental conditions, sulfate ($[SO_4^{2-}]$ = 1.5 mM) effects on H_2O_2 decomposition were not evident.

In the study by De Laat et al., (2004), inhibitory effects observed in the presence of chloride (100 mM) or sulfate (33.33 mM) were explained by a decrease in the hydroxyl radical production rate due to the formation of non-reactive (with H_2O_2) Fe(III) complexes and the formation of inorganic radicals from •OH ($SO_4^{\bullet -}$ and $Cl_2^{\bullet -}$) that are less reactive than •OH. The same study suggested that kinetic models validated in $NaClO_4/HClO_4$ solutions should not be used to predict Fenton reaction rates in the presence of chloride and sulfate. Moreover, De Laat and Giang Le (2006) recently showed that in the presence of 50 mM chloride, 20% of the Fe(III) was complexed by the Cl^-, decreasing the H_2O_2 degradation rate by 23%.

Tables VII - IX provide reaction rates for the decomposition of hydrogen peroxide and the fraction of Fe(III) that is complexed with the different anions at the concentrations given.

Table VII. Apparent First-Order Rate Constant for the Decomposition of H_2O_2 (k_{obs})

Anion	[Fe(III)] (μM)	$[H_2O_2]$ (mM)	[Anion] (mM)	Complexes Fe(III) (%)	k_{obs} (min^{-1})
Perchlorate	200	10	100	0	$4.67x10^{-3}$
Nitrate	200	10	100	0	$4.66x10^{-3}$
Chloride	200	10	100	21.0	$3.95x10^{-3}$
Sulfate	200	10	33.33	83.7	$7.37x10^{-4}$

Source: De Laat et al., (2004)

Table VIII. Measured Pseudo-First-Order Kinetic Constants (k_{obs}) for the Initial Rate of Decomposition of H_2O_2 –Sulfate Effect

I(M)	$[SO_4^{2-}]_o$ mM	$[H^+]_o$ (mM)	$[Fe(III)]_o$ mM	$[H_2O_2]_o$ (mM)	pH	Complexes Fe(III) (%)	k_{obs} (10^{-5} s^{-1})	($[•OH]/[SO_4•^-]$)
0.2	0	10	1.0	49.9	2.00	0	10.46	
0.2	2	10	1.0	50.0	2.01	19.6	8.04	4418
0.2	5	11	1.0	50.1	2.00	38.8	5.78	1688
0.2	10	11.5	1.0	49.7	2.01	57.3	4.02	855
0.2	20	13.5	1.0	49.4	2.01	74.6	2.41	419
0.2	40	19	1.0	49.3	2.00	87.0	1.25	193
0.2	66.67	25	1.0	48.9	2.01	92.8	0.79	114
0.6	200	40	1.0	48.5	2.02	97.7	0.53	51

Note: T = 25.0±0.5°C; ionic strength adjusted with $NaClO_4$.
Source: De Laat and Giang Le (2005).

Table IX. Measured Pseudo-First-Order Kinetic Constants (k_{obs}) for the Initial Rate of Decomposition of H_2O_2 –Chloride Effect

I(M)	$[Cl^-]_T$ mM	$[Fe(III)]_o$ mM	$[ClO_4^-]_o$ (mM)	$[H_2O_2]_o$ (mM)	pH	Complexes Fe(III) (%)	k_{obs} (10^{-5} s^{-1})	($[Cl_2•^-]/[•OH]$)
0.2	0	1.0	200	49.9	2.00	0	10.46	0
0.2	50	1.0	150	49.5	2.00	17.2	8.07	$6x10^2$
0.2	100	1.0	100	49.7	2.00	30.6	6.80	$1.6x10^2$
0.2	200	1.0	0	50.2	2.02	49.6	5.12	$3.8x10^3$
0.2	400	1.0	0	50.5	2.02	49.6	5.16	$3.8x10^3$
0.4	500	1.0	0	48.2	2.00	65.5	3.81	$8.4x10^3$
0.5	800	1.0	0	47.5	2.00	71.2	3.56	$1.1x10^4$
0.8	1000	1.0	0	48.6	1.92	84.5	2.67	$1.8x10^4$

Note: $[[HClO_4]_o$ = 10 mM in all experiments.
Source: De Laat and Giang Le (2006).

b. Carbonate ($CO_3^{\cdot -}$) and Carboxyl ($CO_2^{\cdot -}$) Radicals

Carbonate system effects may be important in reactions involving oxygen containing free radicals. Michelson and Maral (1983) reported an increase in the oxidation of luminal by hydrogen peroxide in the presence of bicarbonate and carbonate anions. The following mechanism was proposed:

$$H^+ + O_2^{\cdot -} + HCO_3^- \rightarrow CO_3^{\cdot -} + H_2O_2 \quad (33)$$

$$2H^+ + 2O_2^{\cdot -} \rightarrow H_2O_2 + O_2 \quad (34)$$

$$H_2O_2 + CO_3^{2-} \rightarrow HO^{\cdot} + HO^- + CO_3^{\cdot -} \quad (35)$$

The increase in luminal destruction was attributed to reaction with the carbonate radical. The carbonate radical is much less reactive than the hydroxyl radical, but enjoys a relatively long lifetime (Michelson and Maral, 1983).

Both the superoxide and hydroxyl radicals (produced in the Fenton's reaction) are able to react with carbonate ions (CO_3^{2-}) to produce carbonate radicals ($CO_3^{\cdot -}$). In addition, reduction of carbonate by superoxide radical can produce formate radicals:

$$H^+ + CO_3^{2-} + O_2^{\cdot -} \rightarrow CO_2^{\cdot -} + O_2 + HO^- \quad (36)$$

However, the formate radical so formed further reacts to reform carbonate radical via:

$$H^+ + CO_3^{2-} + CO_2^{\cdot -} \rightarrow CO_3^{\cdot -} + HCOO^- \quad (37)$$

Thus, each pathway yields carbonate radicals from superoxide radicals.

The carboxyl radical anion ($CO_2^{\cdot -}$) is widely used in free-radical studies due to its ease of formation in aqueous solutions by ionizing radiation, and its excellent reductive properties [$E(CO_2/CO_2^{\cdot -})$=-1.9V] (Flyunt et al., 2001) (Table X). The product of the bimolecular decay of $CO_2^{\cdot -}$ depends strongly on the pH of the solution with an inflection point at pH 3.8. In acidic solution, CO_2 is the main product, while in neutral to basic solution oxalate is dominant. To explain the dependence of product formation on pH, Flyunt et al., (2001) proposed that $CO_2^{\cdot -}$ radicals react mainly (>90%) by head-to-tail recombination to form an intermediate. In this mechanism, rearrangement of the intermediate competes with the proton-assisted disproportionation reactions.

Table X. Carboxyl Radical Anion, $CO_2^{\cdot -}$, Properties

$E(CO_2/CO_2^{\cdot -})$	-1.9V
$pKa(\cdot CO_2H)$[1]	2.3
Bimolecular decay rate constant[2]	$2k \approx 1.4 \times 10^9$ $dm^3 mol^{-1} s^{-1}$
Products[3]	CO_2 and oxalate anion

Note: [1]determined by pulse radiolysis with conductometric detection,
[2]independent of pH in the range 3-8 at constant ionic strength, [3]depend on pH.
Source: Flyunt et al., 2001.

The carboxyl radical has also been reported to enhance HCOOH oxidation kinetics by assisting in the redox cycling of iron (Duesterberg et al., 2005).

$$CO_2^{\cdot -} + Fe(III) \rightarrow CO_2 + Fe(II) \quad (38)$$

In the absence of oxygen, Fe(II) concentrations are higher due to the absence of autoxidation, which leads to higher steady-state hydroxyl radical concentrations in Fenton-driven systems. However, in the presence of oxygen (air-saturated solutions) rate enhancement is diminished by competition for the organic intermediates. With O_2 present, the carboxyl radical reacts at diffusion-limited rates to yield CO_2 and superoxide radicals

$$CO_2^{\cdot -} + O_2 + H^+ \rightarrow CO_2 + HO_2\cdot/O_2^{\cdot -} \quad (39)$$

Oxygen is the primary carboxyl radical scavenger. The superoxide radicals produced can then reduce Fe(III) or oxidize Fe(II) in the Fenton system. In the presence of oxygen, organic radicals are converted into species that can both oxidize and reduce Fe. Under anoxic conditions, only reducing species are available.

The large difference in species profiles between air-saturated and deaerated experiments demonstrates that oxygen reactions should be included in the kinetic models to accurately simulate system behavior. However, under this project's experimental conditions, oxygen is always present in the aqueous solutions (see oxygen generation section). Thus, the effect of the carboxyl radical is not likely to be significant in our system.

c. Radical Formation Kinetics and Reactivity

Hydroxyl radical scavenging by bicarbonate (HCO_3^-) or carbonate (CO_3^{2-}) should not have been an issue in project's trials due to the low pH. At a pH <3, both ions are present at low concentrations.

Hydroxyl radical reaction rates with perchlorate are not available in the literature. If a perchlorate radical is formed by reaction, it does not affect the rate of hydrogen peroxide decomposition by either Fe(II) or Fe(III), as discussed above. Even though nitrate radicals can be formed by reaction of hydroxyl radicals with nitric acid ($k_{OH,HNO3} = 5.3x10^7\ M^{-1}\ s^{-1}$, www.rcdc.nd.edu), their formation does not affect the rate of reaction in the Fenton's system.

Hydroxyl radical reaction rates with sulfate, hydrogen peroxide, chloride and PCE under conditions expected here are compared in Table XI. The data indicate that hydroxyl radicals are consumed mainly by reacting with hydrogen peroxide, PCE, and chloride (produced from PCE dechlorination) and to a much lesser extent, sulfate. Hence, the computer modeling efforts neglected sulfate effects on •OH.

Table XI. Rate Constants for Potential Hydroxyl Radical Sinks

	$^{*}k_{OH}$, M^{-1} s^{-1}	Concentration, M	Rate, s^{-1}
SO_4^{2-}	$3.5x10^5$	$15x10^{-5}$	52.5
H_2O_2	$3.3x10^7$	0.1	$3.3 x10^6$
Cl^-	$3.0x10^9$	$200x10^{-6}$	$6.0x10^5$
PCE	$2.0x10^9$	$50x10^{-6}$	$1.0 x10^5$

Note: $[Fe(III)]_T$ = 0.1mM, $[SO_4^{2-}]=(3/2)[Fe(III)]_T$ since the source of sulfate in our experiments is the $Fe_2(SO_4)_3$, $[PCE]_o$ = 50μM, $[Cl^-]_o$=0 but $[Cl^-]_f = 4x[PCE]_o$ when mineralization is complete.
Source: *www.rcdc.nd.edu.

Moreover, typical groundwater concentrations of chloride and sulfate in Tucson, AZ where the field studies were conducted are 0.45 mM and 0.50 mM, respectively. At these concentrations, the effect of the anions on H_2O_2 consumption is insignificant, but buildup of chloride from the dechlorination of compounds like PCE/TCE may eventually interfere with •OH generation and degradation kinetics. Nitrate and perchlorate do not seem to affect the rate of H_2O_2 reactions in Fenton systems (De Laat et al., 2004). Typical groundwater concentrations of nitrate and perchlorate in Tucson, AZ are low - less than 1 mg/L and < 0.01 mg/L, respectively.

C. Model Applications

i. Simulation of H_2O_2 Decomposition.

The rate limiting step in Fenton-dependent destruction of organic compounds is typically the disproportionation of the ferric hydroperoxy species ($k_{6,I1}$ and $k_{6,I2}$ of Table VI). In the De Laat and Gallard (1999) formulation, these rate constants were assumed to be equal, and their value was obtained by fitting experimental data. However, experimental trials in that study were conducted at much higher ionic strengths and lower hydrogen peroxide concentrations than those used in the present work. Efforts to validate use of the De Laat/Gallard constant for simulations relevant to our chemical conditions are recommended as follow-on research.

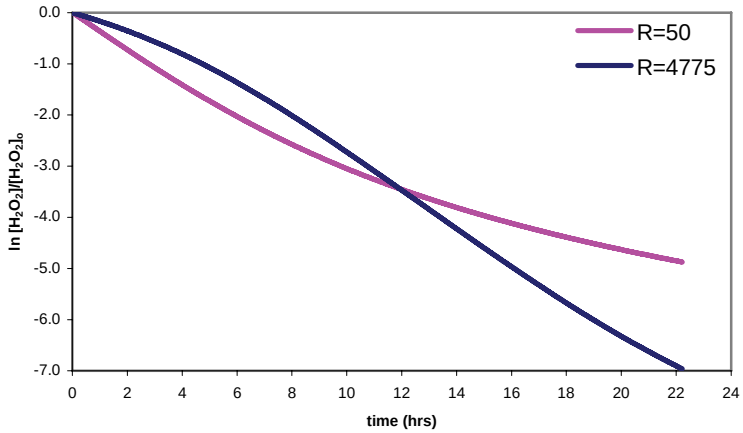

Figure 25. Simulation of H_2O_2 decomposition at initial concentrations of 0.01 and 0.955M at a constant Fe(III) concentration. Initial conditions: pH = 3.0 (25°C, I=0.1M; $R=[H_2O_2]_o/[Fe(III)]_o$, $[Fe(III)]_o=2x10^{-4}$ M. Data from De Laat and Gallard, 1999.

ii. Effect of pH on the Observed Rate Constant for Decomposition of H_2O_2 by Fe(III)

The effect of pH on Fenton kinetics has been studied extensively (Burbano et al., 2005; Kremer, 2003; De Laat and Gallard, 1999). The k_{obs} for the decomposition of H_2O_2 by catalytic iron increases with pH in the range 1-3.2, but decreases above pH 3.2. This decrease can be attributed to the precipitation of Fe(III), as confirmed by measurements of dissolved Fe(III) concentrations (De Laat and Gallard, 1999).

In an effort to validate our mathematical model, the effect of pH on the observed first-order rate constant (k_{obs}) for the decomposition of H_2O_2 in Fenton's mixtures was simulated (Figure 26) and compared to data from De Laat and Gallard (1999). This study's model produced similar results prior to pH 3, after which Fe(III) precipitation began. However, constant initial rates were not obtained at each pH indicating that the simulation efforts are not satisfactory. Future research is recommended to resolve these discrepancies.

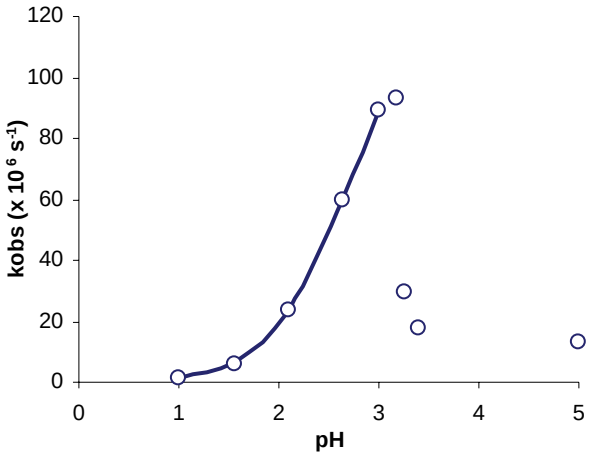

Figure 26. Computer simulation showing the effect of pH on the simulated first order rate constant for the decomposition of H_2O_2 by Fe(III) (solid line). Initial conditions: $[Fe(III)]_o$=200μM, $[H_2O_2]_o$=10mM. Data points (observations) were obtained from De Laat and Gallard, 1999 and the continuous line indicates the computer generated simulation.

iii. Non-Halogenated Organics Degradation in Homogeneous Systems

Table XII shows hydroxyl radical reaction rate constants for non-halogenated organics (i.e. formic acid) that were studied previously. These constants were incorporated into the mathematical model in order to analyze the transformation rates of the target compounds. Duesterberg *et al.* (2005) studied the effect of oxygen and by-product formation on the oxidation rate of HCOOH in a Fenton's system with initial Fe(II) concentrations of 100-200 μM and H_2O_2 concentrations from 0.2 - 2.2 mM. It was reported that the intermediate, carboxyl radical, enhances oxidation efficiency by assisting in the redox cycling of iron. However, in the presence of molecular oxygen the improvement was attenuated.

In our experiments, we made no effort to remove oxygen as it was generated. The effect of the carboxyl radical was neglected at initial formic acid concentrations that were low relative to the dissolved oxygen concentration (DO_{sat} = 2.7x10^{-4} M at 25°C) (Duesterberg, et al. 2005). That is, under the experimental conditions

employed in the simulation, the intermediate generated by reaction 1 (Table XII) is assumed to be oxidized immediately to CO_2. Therefore, a simplified version of the oxidation pathway of formic acid (Table XII) was included in our mathematical model to simulate formic acid degradation in Fenton's reaction (Figure 27). The mathematical model (see Appendix A.2 for coding) simulates satisfactorily the oxidation of HCOOH (Figure 27) as reported by Duesterberg et al (2005) in an Fe(II)/H_2O_2 system.

Table XII. Additional Second Order Reaction Rate Constants for Organic Targets with •OH

No.	Reactions	constants
(1)	$\bullet OH + HCOOH \rightarrow CO_2 + HO_2\bullet/O_2\bullet^-$	$k_{17} = 6.5 \times 10^8\ M^{-1}s^{-1}$ [a]
(2)	$PCE + \bullet OH \rightarrow \bullet CCl_2CCl_2OH \rightarrow (CO_2 + HCl)$	$k_{21} = 2.0 \times 10^9\ M^{-1}s^{-1}$ [b]
(3)	$Cl^- + \bullet OH \rightarrow ClOH^-$	$k_{22} = 3.0 \times 10^9\ M^{-1}s^{-1}$ [b]
		$k_{22} = 4.3 \times 10^9\ M^{-1}s^{-1}$ [c]

Source: [a]Duesterberg et al., 2005; [b]www.rcdc.nd.edu; [c] Buxton et al., 1988.

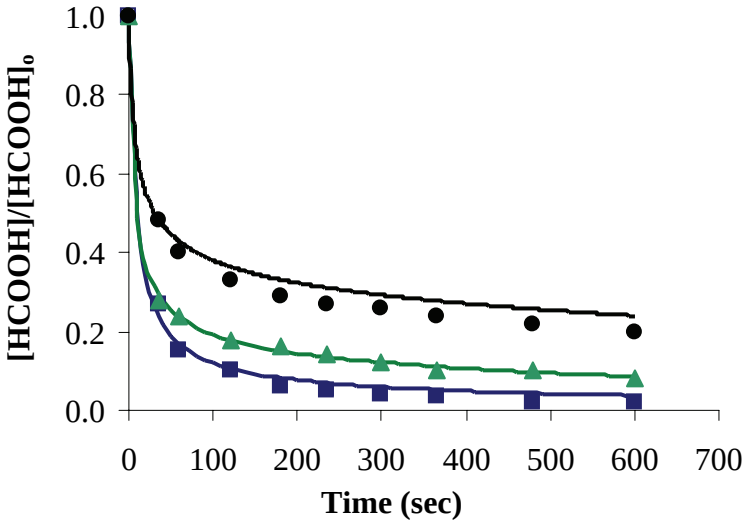

Figure 27. Computer simulation (solid lines) for the simplified oxidation of formic acid (HCOOH) in a H_2O_2/Fe(II) system (pH = 3). Experimental data (symbols) were obtained from Duesterberg et al., 2005. $[HCOOH]_o$=200 nM, $[H_2O_2]_o$=1.1 mM (■) or 2.2 mM (▲,●),$[Fe(II)]_o$=200μM (■,▲) or 100μM (●).

iv. PCE Destruction Kinetics Considering Cl^- Effects

Published second-order rate constants for the chloride ion reaction with the hydroxyl radical (reaction 3, Table XII) indicate chloride should be a significant, unavoidable radical scavenger in Fenton's destruction of chlorinated organics. In our model, the chloride ion is considered a conservative species. It reacts with the hydroxyl radical and generates a radical that does not participate in the organic degradation pathway, and then is regenerated by radical-radical reaction, resulting in reestablishment of the chloride ion.

Figure 28 shows the effect of different second-order reaction rate constants for the reaction of hydroxyl radical with the chloride ion. The literature value ($k = 3.0 \times 10^9$ $M^{-1}s^{-1}$) employed in this simulation was obtained in a system with $[Cl^-] = 1.2$ M (Grigor'ev *et al.*, 1987), which exceeds the range of concentrations studied here. The chloride rate constant was reported to decrease as $[Cl^-]$ increased in the range 3.5-12.2 M (Grigor'ev *et al.*, 1987). The lack of a reasonable model fit suggests that the literature value for the reaction constant may not be accurate at the much lower chloride concentrations of our experiments. Using k_{22} (rate constant for reaction of •OH and Cl^-, Table XII) as a fitting parameter, the model (see Appendix A.3) was applied to our experimental data to find reasonable empirical values for k_{22}. The data fall in between the simulation trials with k_{fit} of 0 – 3×10^9 $M^{-1}s^{-1}$. A k_{fit} value of 1.0×10^9 $M^{-1}s^{-1}$ is near optimal.

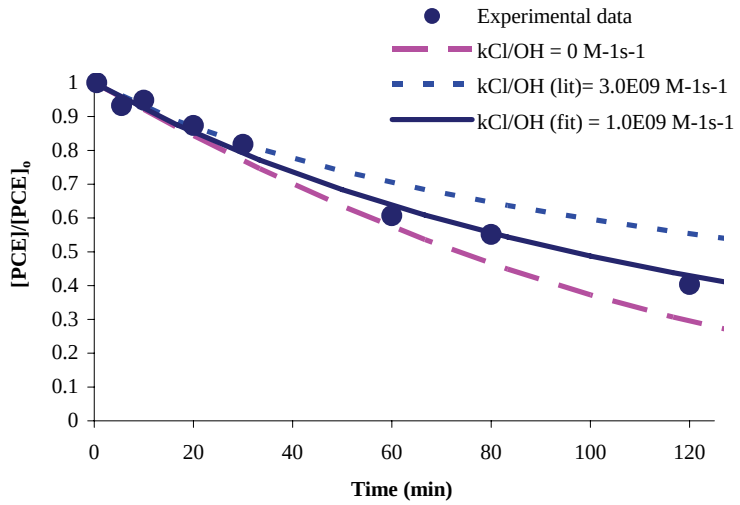

Figure 28. PCE degradation and model fits using various second-order •OH reaction rate constants ($k_{Cl,OH}$) for the reaction with Cl^- ion. The Cl^- is produced from PCE dechlorination and no Cl^- was added initially to the solution. Initial conditions: $[Fe(III)]_o$=0.1 mM, $[H_2O_2]_o$= 0.11 M, $[PCE]_o$=6.52E-5 M , pH = 2.0, T= 31±1°C. A literature value ($k_{Cl,OH} = 3.0 \times 10^9$ $M^{-1}s^{-1}$), one k_{fit} and one neglecting the reaction of •OH with Cl^- were used for the simulation trials.

D. Simulation of Fenton's Reaction for PCE Degradation

i. pH Effect

Numerous studies have shown that the Fenton-dependent rates of degradation of H_2O_2 and organic compounds are optimum near pH 3 (Gallard and DeLaat, 2000; Arnold *et al.*, 1995; Sedlak and Andren, 1991). In this section, experimental data for the degradation of PCE in the pH range 0.9-3.0 are reported and compared to simulations using the mathematical model (see Appendix A.3) described previously.

The PCE transformation rate increases with increasing pH (0.9-3.0), with a maximum near pH 3 (Figure 29). Most of the rate acceleration was evident in the pH range 2.1-3.0. PCE degradation experiments at pH>3.0 are not presented because precipitation (as indicated by solution turbidity) was observed. The effect of the precipitated

Fe(III)-species on the PCE degradation rate is not completely understood. Precipitated Fe(III)-species are not likely to form complexes with hydrogen peroxide, which changes the rate of decomposition of H_2O_2 and that of any organic target in solution. The concentration of the Fe(III)-hydroperoxy species is greater at pH 3 than 2, which explains why Fenton's reaction is faster at pH 3.

Time dependent PCE concentrations are compared to model predictions in Figure 29. The simulations are not in good agreement with the experimental data, but model and experiment agree on the general effect of increasing pH. That is, increasing pH is expected to accelerate PCE degradation. At every pH except pH = 0.9, however, the model over-predicts the PCE transformation rate. Furthermore, the model predicts greater sensitivity to pH values from 0.9 to 2.1 than was observed.

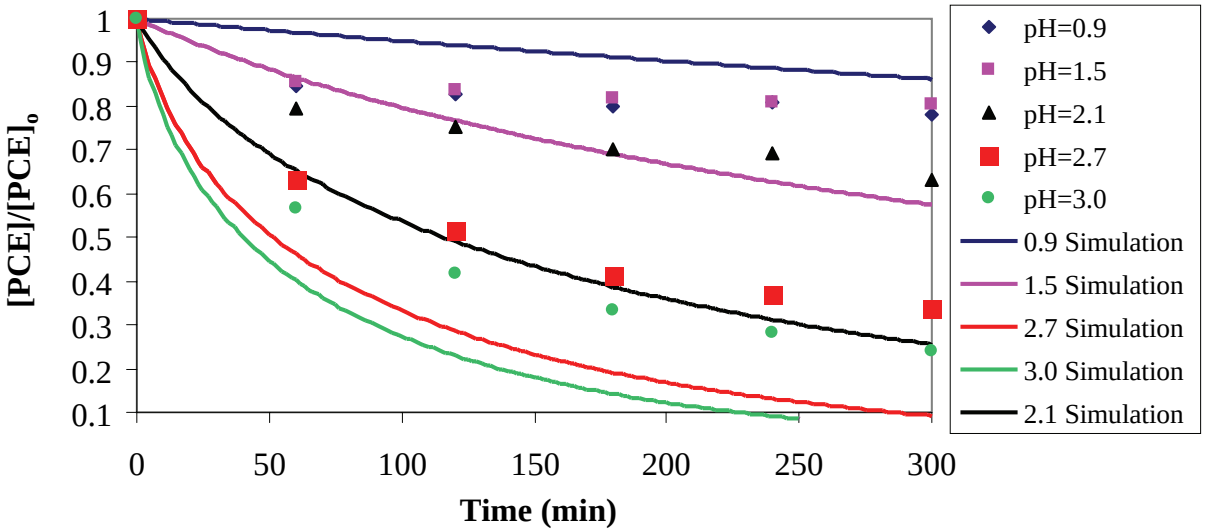

Figure 29. Effect of pH on the PCE degradation rate in Fenton's reaction. Initial conditions: $[Fe(III)]_o$ =0.103 mM, $[H_2O_2]_o$=0.11 M, $[PCE]_o$= 62 μM, T = 31±1°C. A literature value ($k_{Cl,OH}$ = 3.0 x 10^9 $M^{-1}s^{-1}$) was utilized in all simulations trials.

Degradation of PCE and other chlorinated solvents yields chloride ions that can accumulate in solution. Chloride ion is a hydroxyl radical scavenger. Reported values for the rate constant for reaction of Cl^- with •OH are near that of PCE (Table II and XII). If mineralization is complete and the rate of production of chloride ion is four times the rate of PCE destruction, then the accumulation of chloride in the regenerant solution should be considered in terms of its effect on Fenton-dependent reactions.

To further investigate chloride ion effects, PCE degradation experiments were conducted in which the initial chloride ion concentrations were varied from 0 – 0.058 M. Figure 30 shows the effect of chloride on the decomposition rate of PCE in Fenton's reaction. PCE loss decreases with increasing Cl^- concentration in the range 0 – 0.058 M Cl^-. At $[Cl^-]$=0.058 M, the observed first-order rate constant for PCE transformation was about one-fourth that of the chloride-free solution. The results show that the accumulation of chloride ion in the Fenton's

solution can markedly decrease the rate of organic degradation. The accumulation of chloride in the regenerant due to the destruction of the target is a key aspect of the application of this process for the regeneration of chlorinated solvents adsorbed to the GAC. It is important to evaluate how much chloride would be added to a regenerating solution during one carbon recovery event and at what stage chloride accumulation will matter. A simplistic, yet illustrative, approach is taken below to quantify the chloride accumulation from PCE destruction at the field-scale.

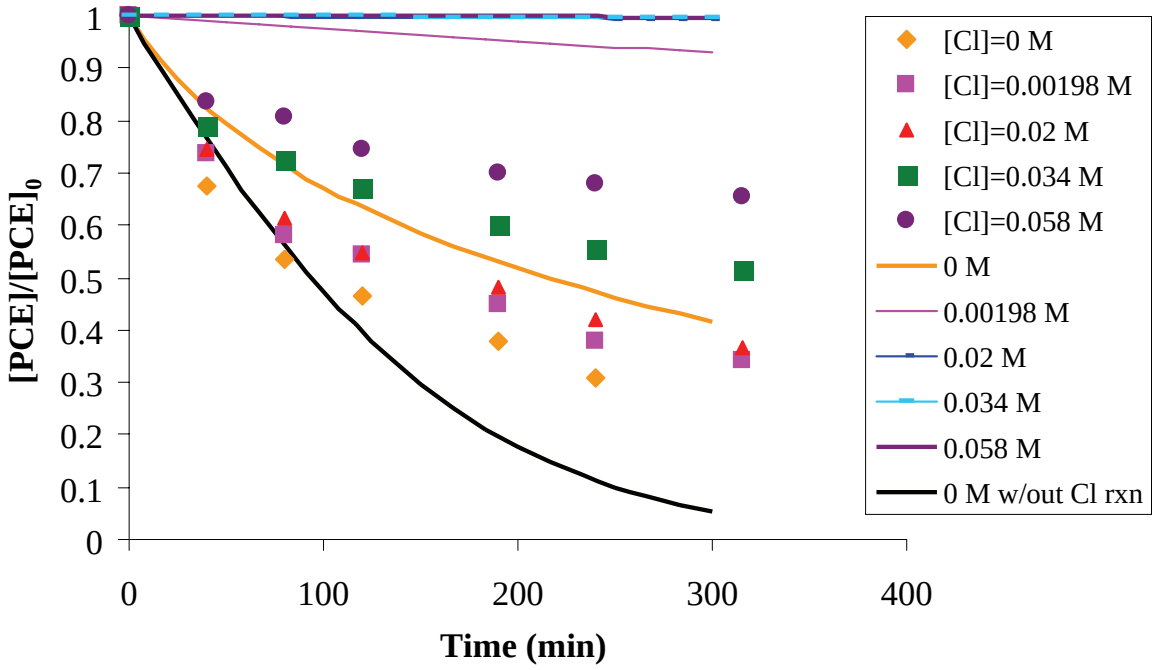

Figure 30. Effect of chloride ion concentration on the PCE degradation rate in Fenton's reaction. Initial conditions: $[Fe(III)]_o$ =0.09 mM, $[H_2O_2]_o$=0.11 M, $[PCE]_o$= 87 μM, pH = 2.0, T = 31±1°C. Chloride concentrations: 0 M - 0.058 M. Model simulations are shown by lines without data points.

ii. Cl^- Effect

The reaction rate of chloride with the hydroxyl radical alone cannot fully explain the Cl^- effect observed (Figure 30). The rate constant ($k_{Cl,OH}$ = 3.0 x 10^9 $M^{-1}s^{-1}$) used in the mathematical model may not be appropriate for our experimental conditions, as discussed in the earlier section. Data and fit of the mathematical model for PCE degradation (accounting for reaction of Cl^- with •OH) were presented previously (Figure 28). The data fall between the simulation trials using k_{fit} of 0 – 3x 10^9 $M^{-1}s^{-1}$. A value to 1 x 10^9 $M^{-1}s^{-1}$ provided the best fit.

The problem is to determine the $[Cl^-]$ in the regeneration water produced from PCE dechlorination during Fenton's reaction and then predict its impact. The solution strategy was to calculate the ΔCl^- concentration attributable to one regeneration of the spent carbon and compare that concentration to Cl^- levels shown to impair Fenton-dependent process performance. Conditions were selected to mimic observations in field-scale

experiments. Those conditions included mass of PCE on the carbon at breakthrough, regenerant volume and fractional recovery during the regeneration event.

Assumptions:

(i) PCE concentration in the solid, C_s = 250 mg/g

(ii) 50% PCE degradation/regeneration

(iii) 4 moles of Cl^- produced/mole PCE degraded

(iv) Bulk density of GAC = 0.5 kg/L

(v) 8 L of regenerant for recovery of 1 L of (unexpanded) carbon

The mass of PCE on the carbon at saturation is

$$\frac{0.5 kgGAC}{Lbed} \times \frac{0.250 kgPCE}{kgGAC} \times \frac{1 Lbed}{8 Lwater} \times 0.5(recovery\_efficiency) = \frac{7.8 gPCE}{Lwater}$$

and the resultant fractional Cl^- mass is

$$\frac{142 gCl^- / mol}{165.83 gPCE / mol} \times \frac{7.8 gPCE}{Lwater} = \frac{6.68 gCl^-}{L} \times \frac{molCl^-}{35.5 gCl^-} = 0.19 MCl^-$$

a. Complexation of Cl^- with Fe(III)

Iron(III)-chlorocomplexes ($FeCl_2^+$ and $FeCl_2^+$) are the predominant Fe(III) species at [Cl^-] above 200 mM. The rate of decomposition of hydrogen peroxide decreases 49% at 200 mM Cl^-, and almost 84% at 1 M Cl^- (De Laat and Giang Le, 2006). In our analysis, 190 mM Cl^- is produced per regeneration, which could have a significant impact on the rate of decomposition of H_2O_2 (Table XIII).

Based on this analysis, use of regenerant solution for multiple regeneration events would not be recommended due to the rate-suppressing effects of chloride ion accumulations.

Table XIII. Calculated Effect of Chloride and Perchlorate Ion Concentrations on Rate of Hydrogen Peroxide Degradation in Fenton's Reaction

I, M	[Cl^-], mM	$[ClO_4]_o$, mM	pH_o	$[H_2O_2]_o$, mM	α (%)	α (I_a + I_b) (%)	k_{obs} (10^{-5})
0.2	0	200	2.00	49.9	0	1.29	10.46
0.2	200	0	2.02	50.2	49.6	0.65	5.12
0.4	400	0	2.00	48.2	65.5	0.43	3.81
1	1000	0	1.76	46.1	90.7	0.09	1.64

Note: $[HClO_4]_o$=10mM except 15mM for 1000mM Cl^-, $[Fe(III)]_o$=1mM. α represents the molar fraction of Fe(III) present as iron(III)-chlorocomplexes, α (I_a + I_b) represents the fraction of Fe(III)-hydroperoxy species, and k_{obs} the rate of H_2O_2 decomposition.
Source: De Laat, J. and Giang Le, T. (2006)

b. Ionic Strength Effects

Although not incorporated into the model formulation, Table XIV illustrates the expected dependence of the Fe(III) equilibrium constants on the ionic strength of the solution. Because the equilibrium constants for the Fe(III) species dominating in the sub-neutral pH range where the project trials were conducted are affected by factors of up to five, it is recommended that ionic strength corrections be incorporated in future modeling work.

Table XIV. Equilibrium Constants as a Function of Ionic Strength

		Ionic Strength (M)					
Reaction		0	0.1	0.2	0.5	0.6	1
$Fe^{3+} + H_2O \leftrightarrow FeOH^{2+} + H^+$	$\log K_1$	-2.19	-2.63	-2.72	-2.79	-2.79	-2.72
$Fe^{3+} + 2H_2O \leftrightarrow [Fe(OH)_2]^+ + 2H^+$	$\log K_2$	-5.67	-6.33	-6.47	-6.57	-6.57	-6.47
$2Fe^{3+} + 2H_2O \leftrightarrow [Fe_2(OH)_2]^{4+}$	$\log K_{2,2}$	-2.95	-2.95	-2.95	-2.95	-2.95	-2.95

Source: De Laat and Giang Le, 2005.

c. Temperature Effects

The effect of temperature on reaction rate constants is analogous to its effect on equilibrium constants (Morel and Hering, 1993). In general, rate constants increase with increasing temperature. As a rule of thumb, rate constants double for every 10°C increase in temperature. The exponential effect of temperature arises from the exponential temperature dependence of viscosity (η). Since the rate constant is inversely proportional to viscosity, then

$$k \propto \exp(-E_a/RT)$$

This dependence corresponds to the empirically derived Arrhenius equation:

$$k = A\exp(-E_a / RT)$$

where E_a is the activation energy of the reaction and A is the preexponential factor.

From the Arrhenius plot (Figure 24),

$$\ln k = -9770(1/T) + 26$$

we can adjust the rate constants from De Laat and Gallard's model rate constant for a temperature of 25°C (Table VI) to our experimental conditions (T = 30°C). Table XV shows the temperature corrections for some of the reactions in the model.

Table XV. Equilibrium Constants as a Function of Temperature

Reaction	Constants	Temperature (°C) 25	30
$Fe^{3+} + H_2O \leftrightarrow FeOH^{2+} + H^+$	K_1	$2.9x10^{-3}$ M	$5.0x10^{-3}$ M
$Fe^{3+} + 2H_2O \leftrightarrow [Fe(OH)_2]^+ + 2H^+$	K_2	7.62×10^{-7} M^2	$1.31x10^{-6}$ M^2
$2Fe^{3+} + 2H_2O \leftrightarrow [Fe_2(OH)_2]^{4+} + 2H^+$	$K_{2,2}$	0.8×10^{-3}M	1.4×10^{-3}M

Source: De Laat and Gallard, 1999.

d. Role of Superoxide Radical ($O_2\bullet^-$) in Fenton's Reaction

i. Background and Reactions Involving $O_2\bullet^-$

A number of studies suggest that a subset of the environmental contaminants of interest, including carbon tetrachloride (CT) and N-nitrosodimethylamine (NDMA), are transformed by a non-hydroxyl radical mechanism that probably involves direct attack by the superoxide radical anion (Roberts and Sawyer, 1981; Stark and Rabani, 1999; Watts et al., 1999; Teel and Watts, 2002; Smith *et al*., 2004; Kommineni *et al*., 2003).

Although the superoxide radical is a relatively weak reductant (Table XVI), $O_2\bullet^-$ is an effective nucleophile in aprotic solvents (Roberts and Sawyer, 1981). As such, it may react readily with heavily halogenated targets such as PCE and carbon tetrachloride. The reductive transformation of CT in dimethyl sulfoxide by $O_2\bullet^-$ follows second order kinetics with a rate constant, k = 3800 M^{-1} s^{-1} (Teel and Watts, 2002). However, the role of perhydroxyl radical, $HO_2\bullet$, in CT reduction was held to be negligible. Since the pKa for $HO_2\bullet$ in water is 4.8, the utility of superoxide radical as a reductant in the destruction of CT and similar (heavily halogenated) targets may be largely confined to waters with pH > 4.

Table XVI. Standard Redox Potentials

Equilibrium	E^o (V)
$Li^+_{(aq)}/Li_{(s)}$	-3.03
$K^+_{(aq)}/K_{(s)}$	-2.92
$Ca^{2+}_{(aq)}/Ca_{(s)}$	-2.87
$Na^+_{(aq)}/Na_{(s)}$	-2.71
$Mg^{2+}_{(aq)}/Mg_{(s)}$	-2.37
$Al^{3+}_{(aq)}/Al_{(s)}$	-1.66
$Zn^{2+}_{(aq)}/Zn_{(s)}$	-0.76
$Fe^{2+}_{(aq)}/Fe_{(s)}$	-0.44
$Pb^{2+}_{(aq)}/Pb_{(s)}$	-0.13

Equilibrium	E^o (V)
$H^+_{(aq)}/½H_{2(g)}$	0
$O_{2(aq)}/O_2\bullet^-_{(g)}$	**0.137[a]**
-pulse radiolysis (duroquinone-superoxide)	**0.13[a]**
- irradiated solutions	**0.33[b]**
-DMF	**0.86[b]**
-DMSO	**0.78[b]**
$Cu^{2+}_{(aq)}/Cu_{(s)}$	0.34
$Ag^+_{(aq)}/Ag_{(s)}$	0.8
$Au^{3+}_{(aq)}/Au_{(s)}$	1.5

Note: The standard reduction potential is that of the hydrogen electrode under standard conditions (1 M or 1 atm and pH 0.0). At pH 7.0, the potential of the hydrogen electrode is -. 42 V. Solvents: dimethyl sulfoxide (DMSO), dimethylformamide (DMF).
[a]The standard reduction potential for the couple $O_{2(aq)}/O_2\bullet^-_{(g)}$ = 0.137 V was calculated from reversible electrochemical cell measurements without a liquid junction.
Source: URL http://www.chemguide.co.uk/physical/redoxeqia/ecs.html#top (Dec 2005), except $O_2\bullet^-$ ([a]Petlicki and van de Ven, 1998; [b]Smith et al., 2004).

ii. Solvent Effects on O_2•$^-$ Reactivity in Aqueous Solutions

CT degradation in solutions containing KO_2 was reported to be insignificant compared to the loss in control reactors (deionized water). Only 25% of CT was lost over 2 hrs under the experimental conditions (1 mM CT, 2 M KO_2, 33 mM purified NaOH, 1 mM DTPA, pH = 14, T= 4±1°C) (Smith *et al.*, 2004). The kinetics of this reaction, however, are substantially improved via the addition of specific organic co-solvents (Smith *et al.*, 2004). In alkaline solutions (pH = 14) with H_2O_2 (as HO_2^-), cosolvent enhancement of CT transformation by O_2•$^-$ was reported in the following order: acetone > 2-propanol > ethanol > H_2O_2 (as HO_2^-) > methanol> ethylene glycol. In Fenton's reaction, the kinetics of CT degradation increased as a function of acetone concentration in the range 0.01 M < [Acetone] < 1 M (Smith *et al.*, 2004). At sufficiently high concentrations (> 0.1 M), HO_2^- increased the observed rate of CT transformation. It was concluded that the superoxide radical, and not HO_2^-, initiated CT transformation in this reaction mixture, and that HO_2^- increased the reactivity of O_2•$^-$ with CT through a co-solvent effect (Smith *et al.*, 2004). Others (Peyton *et al.*, 1995) have noted enhancement of degradation kinetics due to ethanol addition during H_2O_2/UV treatment of water containing CT.

The products of CT reaction with O_2•$^-$ included primarily carbon dioxide and phosgene (Smith *et al.*, 2004). Both products are consistent with a reductive mechanism initiated via nucleophilic attack by O_2•$^-$ on CT.

A number of independent investigators have noted that the reaction of CT with •OH is slow (< $2x10^6$ M^{-1} s^{-1} Haag and Yao, 1992; <$6x10^5$ M^{-1} s^{-1} Buxton *et al.*, 1988). These observations support the existence of a reductive pathway involving superoxide radicals in Fenton-based systems. Moreover, inverse relationships between rates of hydrogenolysis of chlorinated targets and carbon-chlorine bond energies and/or the energy of formation of chloromethyl radicals from their chlorinated parents have been repeatedly shown for a number of relevant reductive systems (Liu *et al.*, 2000). Carbon tetrachloride and other heavily halogenated targets are particularly well suited to transformation via hydrogenolysis due to their low carbon-chlorine bond energies (Table XVII).

Table XVII. Carbon-Chlorine Bond Dissociation Energies for Chlorinated Compounds

Species	Abbreviation	Experimental enthalpies (C-Cl) (kcal/mol)	Theoretically calculated D(C-Cl) (kcal/mol)
CCl_4	CT	72.0 ± 2.1	72.65
$CHCl_3$	CF	77.8 ± 1.4	77.54
CH_2Cl_2	DCM	82.1 ± 1.3	81.85
CH_3Cl	CM	83.5 ± 0.9	NA
CCl_2=CCl_2	PCE	91.0	94.52
CCl_2=CHCl	TCE	93.3	93.56
CCl_2=CH_2	1,1-DCE	93.8	93.67
trans-CHCl=CHCl	trans-DCE	88.7	97.33
cis-CHCl=CHCl	cis-DCE	88.2	98.98

Table XVII (continued). Carbon-Chlorine Bond Dissociation Energies for Chlorinated Compounds

Species	Abbreviation	Experimental enthalpies (C-Cl) (kcal/mol)	Theoretically calculated D(C-Cl) (kcal/mol)
$CHCl=CH_2$	VC	107.6 ± 2.3	NA
C_2Cl_6	HCA	71.2 ± 3.3	68.83
C_2HCl_5	PCA	68.4 ± 3.6	68.95
$CHCl_2CHCl_2$	1,1,2,2-TeCA	NA	74.65
CCl_3CH_2Cl	1,1,1,2-TeCA	NA	70.19
$CH_2ClCHCl_2$	1,1,2-TCA	NA	76.04
CH_3CCl_3	1,1,1-TCA	NA	73.6
CH_2ClCH_2Cl	1,2-DCA	82.8 ± 2.8	82.23
CH_3CHCl_2	1,1-DCA	79.2 ± 2.7	79.12
C_2H_5Cl	CA	84.4 ± 0.8	84.13

Note: Experimental enthalpies for C-Cl bond dissociation were derived from enthalpies of formation. Theoretical calculations of D(C-Cl) values were performed at G2MP2 level using Gaussian 94.
Source: Liu et al., 2000.

The existence of a reductive transformation pathway for CT in Fenton's solutions was supported by observation of CT reactivity in the presence of •OH-scavenging reactants at concentrations that should have quenched •OH reaction with CT (Smith *et al.*, 2004). A reductive mechanism for CT degradation was also suggested by the results of experiments in which excess $CHCl_3$ was added to react with superoxide radicals (Teel and Watts, 2002). Reduction pathways have been proposed for other advanced oxidation processes (Stark and Rabani, 1999; Glaze *et al.*, 1993).

iii. Fenton-Driven Transformation of PCE

Advanced oxidation processes are known to promote both oxidative and reductive contaminant transformations. In TiO_2-mediated photocatalysis, for example, PCE degradation occurs via both oxidative and reductive pathways (Glaze *et al.*, 1993). It was suggested that the reductive pathway involved electrons that were elevated to the conduction band by photons and produced di-chlorinated byproducts. The oxidative pathway involved semiconductor holes and produced both mineralized products and tri-chlorinated intermediates. Peyton *et al.* (1995) observed products from reductive transformations of chlorinated target compounds in UV/ozone reactors, and Watts *et al.* (1999) indicated that in Fenton systems, PCE is degraded exclusively by hydroxyl radicals only when reducing species are consumed by a suitable radical scavenger. In soil systems, PCE desorption was enhanced via co-solvent addition (Watts *et al.*, 1999), suggesting that similar methods could be used to circumvent transport/desorption limitations to PCE recovery in heterogeneous systems such as the GAC adsorption/destruction system described elsewhere in this report.

Our own (previous) investigation and work by others showed that PCE destruction by Fenton's reagents in homogeneous, aqueous solutions is fast (Figure 31). Here PCE reached the method detection limit after about 100 minutes. Again, halogenated intermediates derived from PCE conversion were not detected via GC/ECD analysis of reactor contents at any time during the experiments. The published second-order rate constant for PCE reaction with hydroxyl radical is 2.0×10^9 M^{-1} s^{-1} (www.rcdc.nd.edu). This is near the diffusion limitation. Addition of 1.0 M IP stabilized the PCE concentration in the same two-hour experiments. Results suggest that under the conditions used here (low pH), reaction with hydroxyl radical accounts for observable PCE degradation. In this system, under these conditions, it seems that a reductive pathway for initiation of PCE destruction can be neglected. Reduction reactions may still play a role, however, in subsequent transformations involving reaction intermediates.

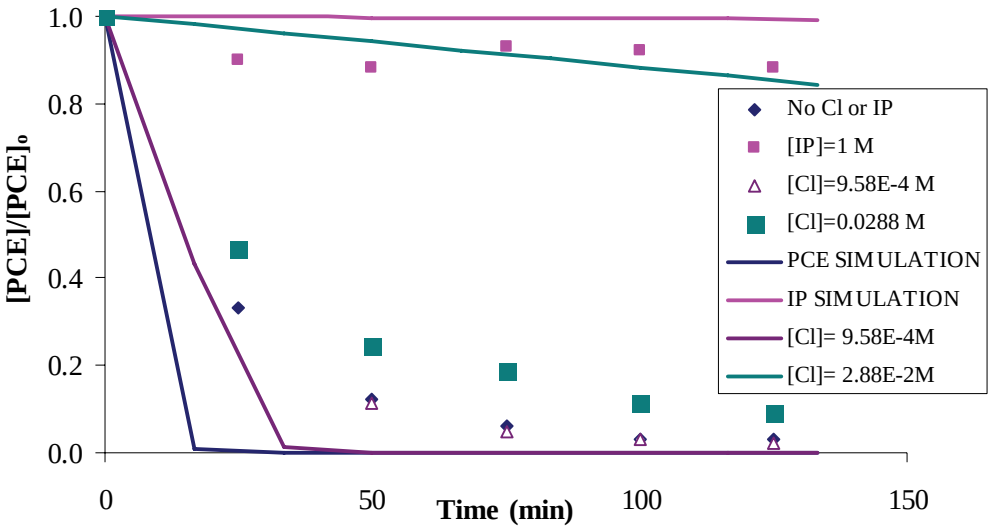

Figure 31. Effect of Cl^- and IP as •OH radical scavengers on PCE transformation rate in Fenton's system. Initial conditions: $[Fe(III)]_T$ = 0.389 mM, $[H_2O_2]_o$ =0.3 M, pH = 2.8, $[PCE]_o$ = 61 μM, $[IP]_o$= 1 M, T = 31± 1 °C. Data points represent the experimental data and the continuous lines the simulation using the mathematical model described previously in this report.

Consistent inhibition of PCE transformation was observed in a series of experiments with Fenton's reagents at various concentrations of chloride ion. The experiments were originally designed to investigate the inhibitory effect of Cl^- on reactions involving •OH. The second-order rate constant for the reaction between Cl^- and •OH is 3.0×10^9 M^{-1} s^{-1} (http://www.rcdc.nd.edu/) making the chloride ion a strong candidate for inhibition of Fenton-driven oxidations. Here it seems, however, that PCE oxidation by •OH was essentially eliminated by IP addition, leaving chloride ion no role to play. Figure 32 is included only to show the consistency of experiments illustrating the reaction antagonism produced through IP addition.

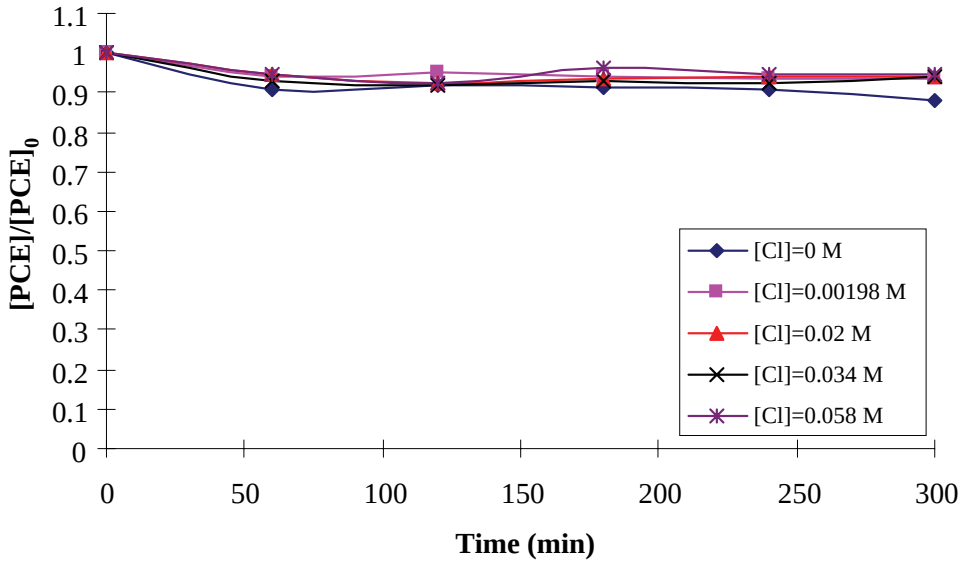

Figure 32. Effect of Cl^- concentration on PCE transformation in Fenton's reaction with IP as•OH radical scavenger. Initial conditions: $[Fe(III)]_T$ = 0.238 mM, $[H_2O_2]_o$ =0.3 M, pH = 2.2, $[PCE]_o$ = 53μM, $[IP]_o$ = 1 M, $[Cl^-]_o$ = 0 M - 0.058 M,, T= 31±1°C.

Elimination of hydroxyl radical-dependent reaction pathways by IP addition and competition for Fenton-derived hydroxyl radicals might have been expected. The initial concentration of IP (1 M) was more than 16,000 times that of PCE (61 μM) (Figure 31). Since reported second-order rate constants for reaction of IP and PCE are similar (Table VII), the very high concentration of IP employed should have virtually eliminated the direct reaction of •OH with PCE (or Cl^-) in these experiments. A comparison of reaction rates for PCE, H_2O_2 and IP with hydroxyl radical follows:

$$\frac{d[PCE]}{dt} = k_{PCE,\cdot OH}[PCE][\cdot OH] \qquad k_{PCE,\cdot OH} = 2.0x10^9 M^{-1}s^{-1} \tag{39}$$

$$\frac{d[H_2O_2]}{dt} = k_{H_2O_2,\cdot OH}[H_2O_2][\cdot OH] \qquad k_{H_2O_2,\cdot OH} = 3.3x10^7 M^{-1}s^{-1} \tag{40}$$

$$\frac{d[IP]}{dt} = k_{IP,\cdot OH}[IP][\cdot OH] \qquad k_{IP,\cdot OH} = 1.9x10^9 M^{-1}s^{-1} \tag{41}$$

If $[\cdot OH]_{ss}$=1.0x10^{-12} M and $[PCE]_o$ = 61μM, $[H_2O_2]_o$ =0.3 M, $[IP]_o$ = 1 M, then it is clear that the IP rate exceeds by nearly four orders of magnitude that of PCE.

$$\frac{d[PCE]}{dt} = 2.0x10^9[61x10^{-6}][1.0x10^{-12}] = 1.22x10^{-7} Ms^{-1} \tag{42}$$

$$\frac{d[H_2O_2]}{dt} = 3.3x10^7[0.3][1.0x10^{-12}] = 9.9x10^{-6} Ms^{-1} \tag{43}$$

$$\frac{d[IP]}{dt} = 1.9x10^9[1][1.0x10^{-12}] = 1.9x10^{-3} Ms^{-1} \tag{44}$$

Since IP, PCE and H_2O_2 all compete for the same hydroxyl radical pool and the IP is in excess, it is expected that the direct PCE reaction with OH will be essentially eliminated through the addition of IP.

a. Inhibition of PCE Oxidation by Cl^-

The oxidation of chloroalkenes such as PCE by •OH is expected to yield primarily mineralized products (CO_2 and HCl). No chlorinated intermediates were detectable via GC/ECD during the course of these experiments. There was no attempt to measure CO_2 evolution, however. Under these conditions, the accumulation of Cl^- due to target compound mineralization may eventually inhibit •OH-dependent pathways, as radical consumption by Cl^- begins to rival H_2O_2 as a sink for hydroxyl radicals.

Here PCE degradation was modestly impeded at the highest concentration of chloride addition (0.0288 M). However, at a concentration near 1 mM, Cl^- had essentially no effect on PCE transformation kinetics (Figure 31).

iv. CT Transformation in the Presence of 2-propanol

Here we measured Fenton-dependent CT degradation kinetics in the presence and absence of 2-propanol (IP), hydroxyl radical scavenger (Smith et al., 2004; Watts et al., 1999). Data were compared to previously published results and to predictions obtained using a mathematical model (described subsequently). The importance of light to observed transformations was investigated by comparing CT reaction rates in the presence and absence of room light. Carbonyl-photosensitized destruction of CT in the simultaneous presence of acetone and isopropanol was reported previously (Betterton et al., 2000).

All experiments were run at 31±1°C in 65-mL (batch) threaded Pyrex tubes that were sealed with mini-inert caps to permit sampling for residual CT without opening the reactors. Reactors were sampled 5-8 times over the course of each experiment. The 15-µL samples were transferred to 1 mL of heptane in GC vials for analysis via gas chromatography using an electron-capture detector. Duplicates of each reaction mixture/treatment were provided. When duplicate reactors provided conflicting results, experimental results were discarded and the trial was repeated. Initial reactor conditions are provided in figure captions.

Room lighting had no effect on observed reaction kinetics (Figure 33). That is, CT transformation kinetics were essentially independent of light/dark conditions for paired reactors in room lighting and minimal light. Thirty percent of the CT originally present was lost over 2.5 hours in reactors containing Fenton's reagents plus IP in both the presence and absence of room light. The disappearance of CT was clearly dependent on Fenton's reaction, as indicated by control reactors that lacked either hydrogen peroxide or iron. In no case did light induce CT transformation in the absence of Fenton's reagents.

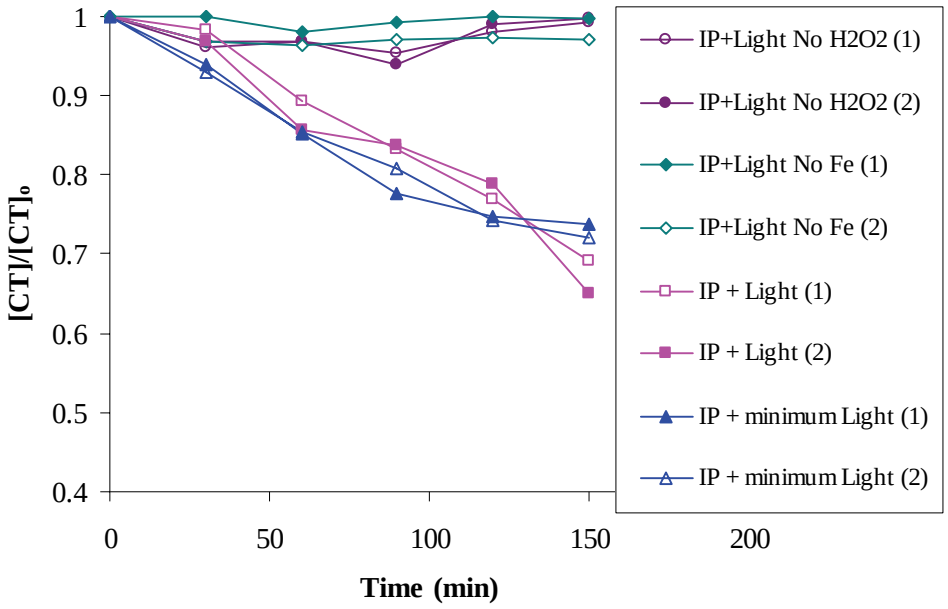

Figure 33. Effect of light on transformation rates of carbon tetrachloride (CT) in the presence of isopropanol (IP) as an OH radical scavenger. Initial conditions: $[Fe(III)]_T$ = 0.26 mM , $[H_2O_2]_o$=0.21 M, $[CT]_o$ = 0.81 mM, pH =2.1, T=31±1°C

Acceleration of CT transformation kinetics in the presence of 1.0 M IP was clearly evident (Figure 34). Again, room light had no effect on reaction kinetics. In the presence of IP, CT was completely consumed in 10-15 hours. In the absence of IP, Fenton's reaction produced ~50% reduction in CT concentration during the 28-hour experiment. With IP present, reaction kinetics were zero-order in CT for the first 10 hours of the experiment, during which time CT removals approached 90%. No chlorinated intermediates were observed in the GC/ECD analysis.

The role of IP in Fenton-driven CT transformations remains obscure despite the careful work of Smith *et al.* (2004), in which co-solvent effects were firmly established. That work was conducted at the opposite end of the pH spectrum (pH = 14) and lacked a detailed mechanistic explanation for co-solvent effects. It is possible, for example, that IP serves primarily as a hydroxyl radical scavenger ($k = 1.9 \times 10^9$ M^{-1} s^{-1}, Buxton, 1988; $k = 1.6 \times 10^9$ M^{-1} s^{-1}, www.rcdc.nd.edu), eliminating heterogeneous radical-radical extinctions involving hydroxyl and superoxide radicals per

$$\bullet OH + HO_2\bullet/O_2\bullet^- \rightarrow H_2O/OH^- + O_2 \qquad k = (0.71\text{-}1.01) \times 10^{10}\ M^{-1}\ s^{-1} \qquad (33)$$

This explanation seems unlikely, however, in light of the low, steady concentrations of radicals in these reactors and the presence of other effective radical scavengers, including H_2O_2 itself.

That is, reaction (33) would tend to lower quasi-steady levels of superoxide radicals in IP-free reactors. In this way, IP addition might increase the observed rates of superoxide radical-dependent pathways, including CT transformation. However, this mechanism is thought to play a minimal role in IP-dependent kinetic effects. At the concentration provided, H_2O_2 is already a capable scavenger for hydroxyl radicals. The rate constant for •OH

reactions with H_2O_2 is $3.3x10^7$ M^{-1} s^{-1} (De Laat and Giang Le, 2005). Calculations show the overwhelming majority of hydroxyl radicals produced in these experiments were consumed by that reaction. The importance of •OH scavenging by H_2O_2 on Fenton-dependent contaminant transformations was the subject of extensive previous commentary (Huling *et al.*, 1998). Thus, the contribution of the hypothesized radical-radical extinction pathway to regulation of •OH levels in Fenton reactions is probably small compared to those of alternative scavenging reactions.

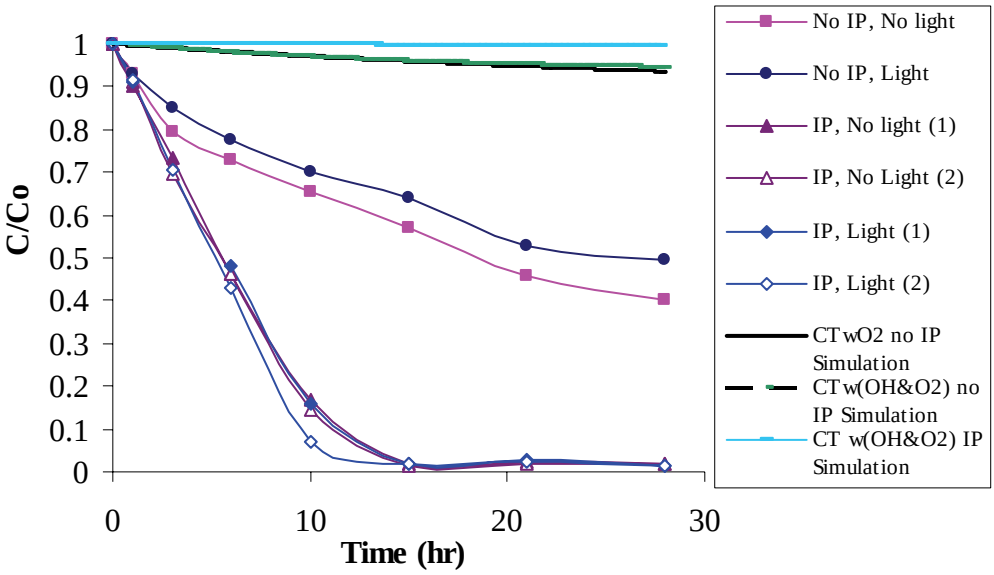

Figure 34. Effect of isopropanol (an •OH radical scavenger) on the degradation of CT. Initial conditions: $[Fe(III)]_T$ = 0.11 mM , $[H_2O_2]_o$=0.23 M ,$[CT]_o$ = 0.35 mM, pH =2.1, T=31±1°C.

It is also possible that hydroxyl radicals participate in hydrogen abstraction reactions with isopropanol of the form

$$\bullet OH + IP + H^+ \rightarrow IP\bullet + H_2O \quad (45)$$

The isopropanol radicals so formed may participate in reactions of the form

$$CT + IP\bullet \rightarrow Acetone + CT\bullet + HCl \quad (46)$$

where CT• is the trichloromethyl radical. Betterton *et al.* (2000) proposed a chain reaction for CT destruction in which reaction (46) was among the initiation steps. A reaction of this form and antecedent chain reaction could account for the observed IP-dependent acceleration of the low-pH, Fenton-dependent destruction of CT.

Nevertheless, a series of additional experiments was performed to clarify the role of IP in promoting Fenton-dependent CT transformations. Because superoxide radical rapidly reduced quinones (Watts *et al.*, 1999), benzoquinone (*p*-isomer k = ~10^9 $M^{-1}s^{-1}$, Chen and Pignatello, 1997) was added to a series of reaction mixtures (with and without IP) in an effort to scavenge $O_2\bullet^-$, thus preventing its reaction with other reactor components. This line of reasoning was, admittedly, compromised from the start, inasmuch as the reactivity of reduced benzoquinone species with CT and CT transformation intermediates was not known. Nevertheless, experiments with benzoquinone were conducted, primarily because a more suitable superoxide radical scavenger could not be identified.

Benzoquinone addition decreased the rate of CT degradation relative to the Fenton system with IP and no benzoquinone (Figure 35 versus Figure 34). Even at the relatively high concentrations used, however, benzoquinone addition did not entirely quench CT transformation. Although results of these experiments tend to confirm the importance of IP oxidation to the kinetics of CT transformation, they provide little of the anticipated mechanistic insight. If benzoquinone does in fact react with superoxide radical to produce the corresponding semiquinone, that species must be as reactive or nearly as reactive with CT as is the superoxide radical. The mechanism of IP participation, although only modestly affected by benzoquinone, is no less uncertain as a consequence of these experiments.

Results of these experiments with benzoquinone are in stark contrast with those in previously reported work involving benzoquinone with PCE as the target compound. That work indicated clearly that benzoquinone addition initially accelerated PCE transformation rates, an effect that was subsequently reversed due to quinone destruction, presumably by hydroxyl radicals (see previous section, this report). Seemingly, Fenton-driven CT and PCE transformations proceed via different radical mediated pathways.

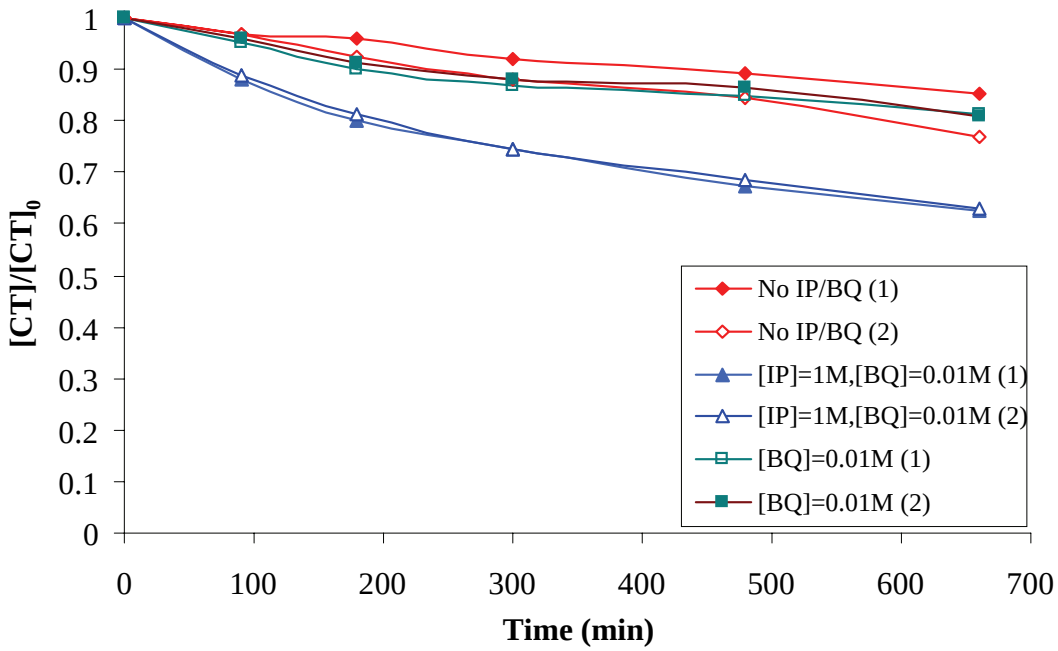

Figure 35. Effect of benzoquinone (an $O_2^{\bullet -}$ radical scavenger) on CT degradation rates in Fenton's reaction. Initial conditions: $[Fe(III)]_T$ = 0.11 mM, $[H_2O_2]_o$ = 0.21 M, $[CT]_o$=0.33 mM , pH= 2.1, T=31±1°C.

One additional observation is perhaps worth noting. Reactors containing both IP and benzoquinone experienced no color change during the course of the experiments. Those that contained only benzoquinone became dark, perhaps because the quinone was maintained in an oxidized state.

Homogeneous, Bench-Scale Experiments-Summary and Conclusions

- Fenton-dependent tetrachloroethylene (PCE) degradation followed first order kinetics with a rate constant that was about proportional to total soluble iron. The reaction proceeded with essentially no lag following the addition of H_2O_2, indicating that near steady concentrations of iron species and hydroxyl radical were established quickly.
- The initial rate of PCE degradation was increased by over an order of magnitude by the addition of hydroxylamine hydrochloride, a strong reductant. The rate enhancement could not be sustained, however, indicating that hydroxylamine was consumed in the reaction. The result supports the research consensus that Fe(III) reduction to Fe(II) via H_2O_2 consumption is the rate limiting step in the Fenton system as hydroxylamine can rapidly, directly reduce Fe(III) to Fe(II).
- Quinones are known electron shuttles that may facilitate iron reduction. 1,4-Hydroquinone (HQ), 1,4-benzoquinone (BQ) and 9,10-anthraquinone-2,6-disulfonic acid all initially increased PCE degradation in Fenton's system. The increase was proportional to the quinone concentration. However, as with hydroxylamine addition, the rate enhancement was not sustained, suggesting that the quinones were gradually destroyed. The PCE degradation rate stabilized at a rate that was slower than that of the unamended Fenton's system suggesting that the by-products of quinone degradation may themselves retard the contaminant degradation rate.
- PCE degradation was negligible when Fe(III) was replaced with Cu(II) in the Fenton system. However, when both copper and iron were present at a Cu:Fe ratio of 2, the first order rate constant for PCE degradation increased by a factor of 4.3. Analysis of potential chemical mechanisms for this outcome suggest that Cu(II) is reduced to Cu(I) by H_2O_2 after which Cu(I) reduces Fe(III) to Fe(II). This sequence of reactions may provide a more rapid pathway for iron reduction than direct reaction with H_2O_2. Although the ability of copper to accelerate PCE degradation is modest, Cu(II) is more soluble than Fe(III), so copper may provide kinetic benefits in the pH range where the iron concentration in Fenton's system is limited by solubility considerations.
- The pseudo-first-order rate constant for PCE degradation increases more rapidly with increasing temperature in the copper:iron system than when iron alone is provided. Thus, the kinetic benefit of copper addition is increased in Fenton systems operated above ambient temperature.
- A homogeneous phase, kinetic model was formulated based on earlier work by De Laat and Gallard (1999) in which the rate constant for disproportionation of the Fe(III)-hydroperoxy complex (the rate limitation for radical production kinetics) was fitter to H_2O_2 utilization data.
- As chlorinated VOCs are degraded in Fenton systems, chloride anions will build up in the regenerant solution. The rate constants for the reaction of hydroxyl radical with chloride ion indicates that chloride

accumulation through repeated carbon bed regenerations will retard VOC degradation rates. However, model simulations using the literature rate constant for the •OH/Cl^- reaction overestimated chloride ion effects in experimental trials. A revised •OH/Cl^- rate constant was fitted on the basis of these data. Our second-order rate constant was lower than the previously reported value by a factor of 3.

- The rate of PCE degradation by Fenton's reaction increases with increasing pH in the range $1 \leq pH \leq 3$. Above pH 3, iron solubility limits free iron concentration availability lowering the rate of PCE degradation. Observed PCE degradation rates at $0.9 \leq pH \leq 3$ were compared to the results of mathematical simulations. There was considerable difference between experiment and simulation although general effects of pH were in agreement. At every pH (except pH = 0.9), the model over-predicted the PCE transformation rate.
- The rate of Fenton-dependent carbon tetrachloride (CT) degradation was increased in the presence of isopropanol (IP), a •OH scavenger. The work suggests that the mechanism of CT degradation involves direct reaction with superoxide radical (O_2•$^-$). A more complete mechanism is under investigation. The increase in rate may be due to an IP co-solvent effect that increases O_2•$^-$ activity.
- PCE degradation by Fenton's reagents is negligible in the presence of IP, an •OH scavenger, indicating that PCE destruction is initiated by hydroxyl radical (•OH) attack. No chlorinated intermediates were detected in this experiment. PCE degradation diminished modestly at the highest concentration of chloride addition (0.0288 M). A concentration near 1 mM, Cl^- had a negligible effect on PCE transformation kinetics.

Bench-scale, Heterogeneous, Column Experiments

Adsorption Isotherms

Freundlich isotherm parameters for GAC (URV-MOD 1) adsorption of all compounds tested are summarized in Table II (repeated below). The data for adsorption of methylene chloride, a representative contaminant, is provided as Figure 36.

Table II. (Repeated from earlier section.) Chemical Properties of the Organic Compounds Studied

Name	Formula	Log K_{ow} [a]	$k_{M,OH}$ (M^{-1} s^{-1}) [b]	Diffusivity (cm^2/s) [c]	Adsorbed concentration (mg/g) [d]	Freundlich Parameters [e]	
						K (mg/g) $(L/mg)^{1/n}$	1/n
Methylene Chloride (MC)	CH_2Cl_2	1.15	9.00E+07	1.21E-05	275	0.07	1.06
1,2-DCA	$C_2H_4Cl_2$	1.47	7.90E+08	1.01E-05	146	0.04	1.33
1,1,1-TCA	$C_2H_3Cl_3$	2.48	1.00E+08	9.24E-06	20	0.65	0.87
Chloroform (CF)	$CHCl_3$	1.93	5.00E+07	1.04E-05	188	1.48	0.77
Carbon Tetrachloride (CT)	CCl_4	2.73	2.00E+06	9.27E-06	N/A	12.30	0.59
TCE	C_2HCl_3	2.42	2.90E+09	9.45E-06	103	5.82	0.70
PCE	C_2Cl_4	2.88	2.00E+09	8.54E-06	11	45.66	0.56

Note: $k_{M,OH}$ is the second-order rate constant for the reaction of hydroxyl radical with the target organic compound.

Source: [a]Swarzenbach et al., 1993; [b]www.rcdc.nd.edu, except carbon tetrachloride (Haag and Yao, 1992); [c]calculated from Wilke-Chang equation (Logan, 1999); [d]From analysis of initial carbon concentration for carbon recovery experiments (data at 32ºC). [e]From isotherm data obtained in this lab at 32ºC.

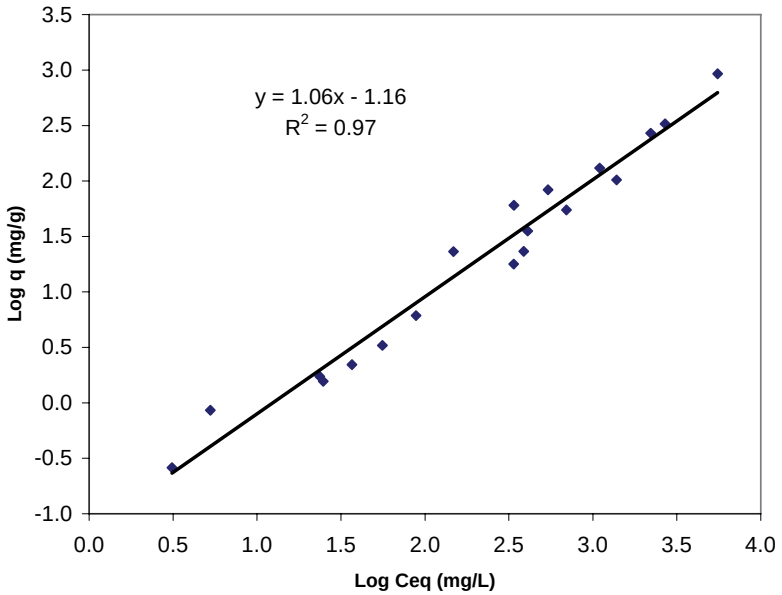

Figure 36. Isotherm data for methylene chloride on URV-MOD 1 (32°C).

Bench-scale Column Experiments

Recovery using Fenton's Reagents

Contaminants with a range of compound hydrophobicities and reactivities with •OH (Table I) were selected for Fenton-driven regeneration experiments in which spent GAC was regenerated in columns. Preliminary carbon recovery experiments were run at 24 ± 2°C for seven chlorinated VOCs: (methylene chloride (MC), 1,2-dichloroethane (DCA), chloroform (CF), 1,1,1-trichloroethane (TCA), carbon tetrachloride (CT), TCE and PCE). The same experiments were repeated at 32º C. Carbon recovery data for MC, CF and TCE at 32ºC are summarized in Figure 37. Recovery kinetics followed the order MC>CF>TCE. The transformed data are shown on a semi-log plot in Figure 38. After an initial period of rapid recovery that lasted 1-3 hours, further reductions in the sorbed concentration conformed to first-order kinetics. TCE removal from GAC was only 50% complete after 14 hours. This was unexpected since the second-order rate constant ($k_{M,OH}$, Table II) for the reaction of hydroxyl radical with TCE (2.9E+09 $M^{-1}s^{-1}$) is near the molecular-collision diffusion limit (www.rcdc.nd.edu) and is higher than the rate constants for reaction of •OH with MC and CF. Lack of dependence of recovery kinetics on reaction rate with •OH suggests that the kinetics of Fenton-driven recovery of GAC is controlled by mass transport, as opposed to the rates of hydroxyl radical generation or radical reaction with contaminant targets.

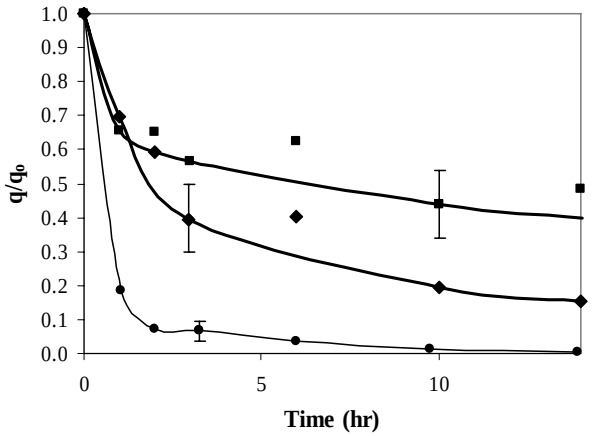

Figure 37. Fractional removal of adsorbate from GAC for MC (●), CF (♦) and TCE (■). Fractional q/q_o represents the mass of contaminant remaining in the carbon. The regenerant solution contained 10 mM iron, pH = 2.0, and 0.15 M H_2O_2 average concentration throughout the experiment. Temperature was controlled in the reservoir at 32°C. The lines are a smoothed fit to the data. Average error bars are indicated for each curve. n=2 for each data point (average between top and bottom samples).

The shapes of the recovery curves (Figure 37) are consistent with an intraparticle diffusion limitation: at short times, target concentrations in most of the GAC pores were nearly uniform, until concentration profiles developed along particle radii. With time the concentration gradient penetrated further into the particle increasing the apparent diffusion length and leading to slower, nearly first-order contaminant removal kinetics. The apparent first-order rate constants derived from the latter portion of each experiment are summarized in Table XVIII.

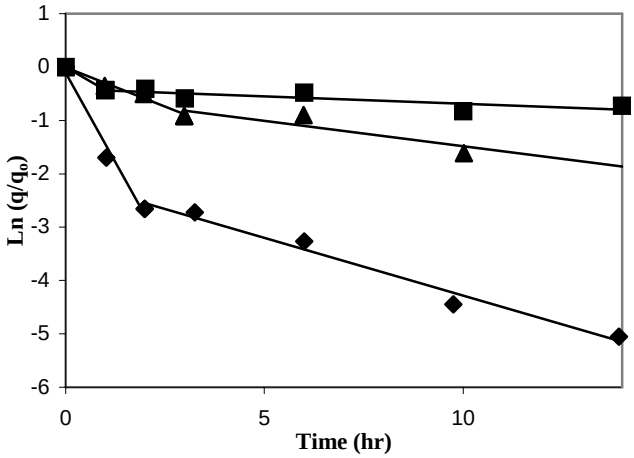

Figure 38. Semi-log plot of the data in Figure 37 for MC (♦), CF (▲) and TCE (■). The slopes of lines from about t= 2 h to the end of the experiment were used to calculate the observed rates (k_{obs}).

Experimental results (Figure 38 and related discussion) suggest that mass transfer rates limit the slow recovery stage in GAC regeneration under the conditions employed in this work. If intraparticle diffusion controls the overall recovery rate, the concentration of the target compound in the bulk liquid should be low due to rapid consumption via Fenton's reaction in the bulk liquid phase. In that case, it can be shown that the flux of contaminant from the particle surface (J) follows a relation like

$$J = k_m \overline{C_p} \tag{47}$$

where k_m is a hybrid, conditional coefficient and $\overline{C_p}$ is the average concentration of the target compound in the liquid that fills the pores of the particles. If adsorption and desorption rates are fast, the local aqueous- and solid-phase concentrations of the adsorbate are in equilibrium so that:

$$C_p = \left(\frac{q}{K} \right)^n \tag{48}$$

When the Freundlich isotherm is linear (n=1), equation 48 can be expressed in terms of average concentrations so that:

$$\overline{C_p} = \frac{\overline{q}}{K} \tag{49}$$

without error. For the analysis that follows, it was assumed that average concentrations could be inserted in the non-linear isotherm (equation 48) without generating excessive error, so that

$$\overline{C_p} = \left(\frac{\overline{q}}{K} \right)^n \tag{50}$$

Table XVIII. Summary Table for Rates Observed (k_{obs}) at 24°C and 32°C, and Cost Estimates at the Bench and Field Scales

Compound	k_{obs} (hr^{-1})				Cost ($/kg GAC)[e]	
	Bench-scale[a] T=24°C	Bench-scale[b] T= 32°C	Bench-scale Desorption[c] T= 32°C	Field-scale[d]	Bench- Scale T= 32°C	Field-scale
MC	0.17	0.25	0.19	0.12	4.6	6.63 (100%) 3.57 (97%)
1,2-DCA	0.10	0.24	N/A	N/A	N/A	N/A
1,1,1-TCA	0.075	0.058	N/A	N/A	N/A	N/A
CF	0.066	0.11	0.11	0.059	3.50 (93%)	6.63 (93%)
CT	0.052, 0.060	N/A	N/A	N/A	N/A	N/A
TCE	0.045	0.027, 0.060	0.043	0.015 0.033 0.068	5.14 (52%)	2.55(73%) 4.53(82%) 6.54(95%)
PCE	0.037, 0.062	0.042	N/A	0.011	2.63(35%)	6.54(50%)

Note: [a]Bench-scale regeneration column experiments at 24°C (Figure 38), and [b] T= 32°C (Figure 37).
[c]Bench-scale desorption experiments (clean water, no Fenton reagents as eluant – Figure 39).
[d]Field-scale regeneration column experiments. [e]Cost is based on hydrogen peroxide consumption for spent GAC regeneration. The number in parenthesis indicates the percentage GAC recovery for each trial.

We recognize, however that the magnitude of error introduced by this approximation increases with the degree of non-linearity in respective isotherms.

A mass balance on the adsorbate in the carbon particles, assuming that aqueous-phase mass can be neglected, then yields:

$$M\frac{d\bar{q}}{dt} = -JA_s \tag{51}$$

where M and A_s are the total carbon mass and total external surface area of GAC, respectively, and $\bar{q}$ is the average concentration of the adsorbate on the carbon surface.

The preceding equation can be solved with the initial condition

$$\bar{q} = \bar{q}_o \text{, at t=0} \tag{52}$$

Substituting equations (47) and (50), equation (51) becomes

$$M\frac{d\bar{q}}{dt} = -A_s k_m \left(\frac{\bar{q}}{K}\right)^n \tag{53}$$

This equation implies that the initial rate of decrease of the average target concentration in the solid, $\frac{d\bar{q}}{dt}\Big/(q_o)^n$ at t = 0, should be directly proportional to $(1/K^n)$ for all target compounds, assuming that k_m does not vary appreciably among the various targets. A rigorous analysis would show that k_m is equal to the observed pseudo-first order rate constant for target removal (k_{obs}).

The preceding analysis motivated us to plot the observed pseudo-first order rate constant for target removal (k_{obs}) vs. $1/K^n$ for all target compounds (Figure 39). The fact that most compounds follow the expected trend (positive correlation between $1/K^n$ and initial rate of adsorbate loss) is consistent with the hypothesis that intraparticle mass transfer controls the overall carbon recovery process.

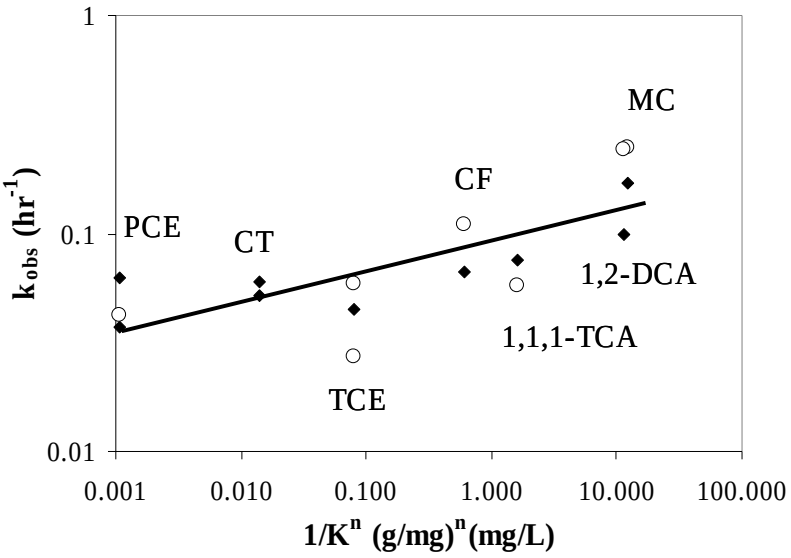

Figure 39. Correlation between first-order observed rate constant (k_{obs}) and compound-specific $(1/K)^n$. Rates for a 14-hour regeneration period with 10 mM iron, 0.1-0.15 M H_2O_2, pH = 2.0. Experiments were conducted at room temperature (24°C) – closed symbols and 32°C – open symbols. The line is a linear fit of the log- transformed data.

Clean Water and Fenton-Driven Recovery Experiments

Comparison of clean water (no Fenton's reagents present) and Fenton-driven recovery experiments (Figure 40) indicate that carbon recovery trajectories for the Fenton-driven and no-reaction (clean-water elution) cases matched for MC and TCE. For those contaminants, it seems evident that contaminant reaction did not limit recovery kinetics. For CF, however, degradation in the presence of Fenton's reagents was slower than in the clean water circulation experiments. This occurred because the bulk aqueous-phase concentration was maintained near zero in the latter experiments by continuously feeding clean influent to the column reactor. Since the reaction of •OH with CF is relatively slow (Table II), CF accumulated to some extent in the bulk liquid when Fenton's reaction was relied upon to eliminate CF from the recirculated fluid. This diminished the driving force for CF transport from the GAC and protracted the recovery period. This interpretation is supported by liquid-phase CF measurements during GAC

recovery using Fenton's reagents (Figure 41). It is apparent that recovery kinetics were limited, at least in part, by the rate of reaction of bulk liquid phase CF.

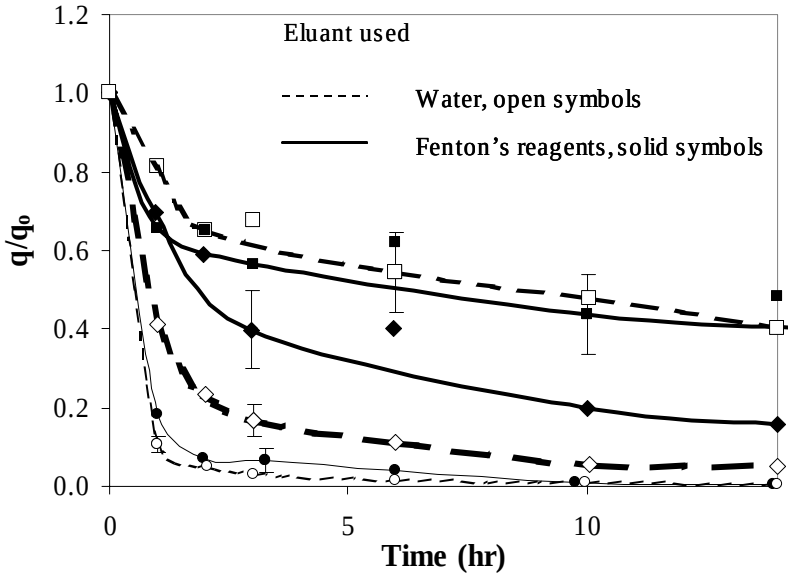

Figure 40. Comparison of recovery rates using eluant solutions with and without Fenton's reagents. When eluant consisted of water, bulk aqueous phase contaminants were near zero. Target compounds were MC (●), CF (♦), and TCE (■). Regenerant solutions contained 10 mM iron, 0.15 M average H_2O_2, pH = 2.0, T = 32°C. Concentrations are normalized by the initial contaminant concentration on the carbon (q/q_o). Data points represent the average value between carbon extractions of GAC samples from the top and bottom of the GAC bed. An average error bar is indicated for one data point for each curve.

As indicated previously, the Fenton solution was replaced with a pure water eluant for selected trials. That is, the external (bulk aqueous-phase) concentration of adsorbate was maintained near zero by passing water through the expanded carbon bed rapidly and discarding the once-used eluant. In these trials, 10-gram samples of carbon were preloaded with MC (CH_2Cl_2) or TCE. Initial contaminant loadings were 291 and 69 mg VOC/g GAC, respectively. Carbon was transferred into the regeneration column, where tap water was flushed through at 950 mL/min to expand the carbon bed. Figure 42 shows the solid's time-dependent concentration profiles for MC and TCE.

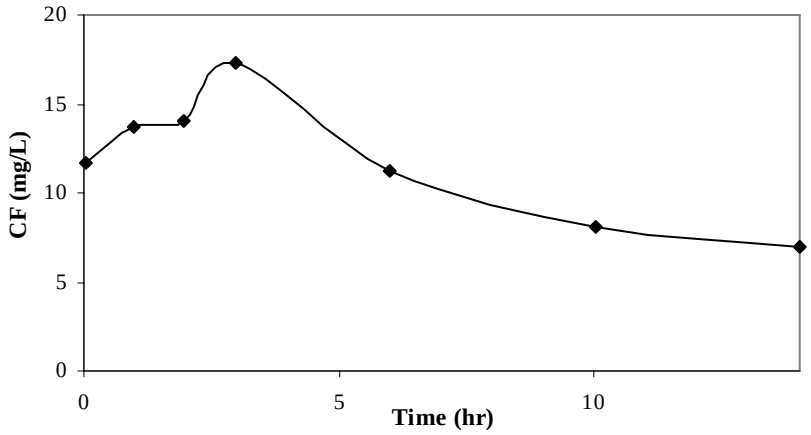

Figure 41. Liquid phase reservoir concentrations for CF-loaded GAC recovery. Times of data points correspond to those in Figure 40.

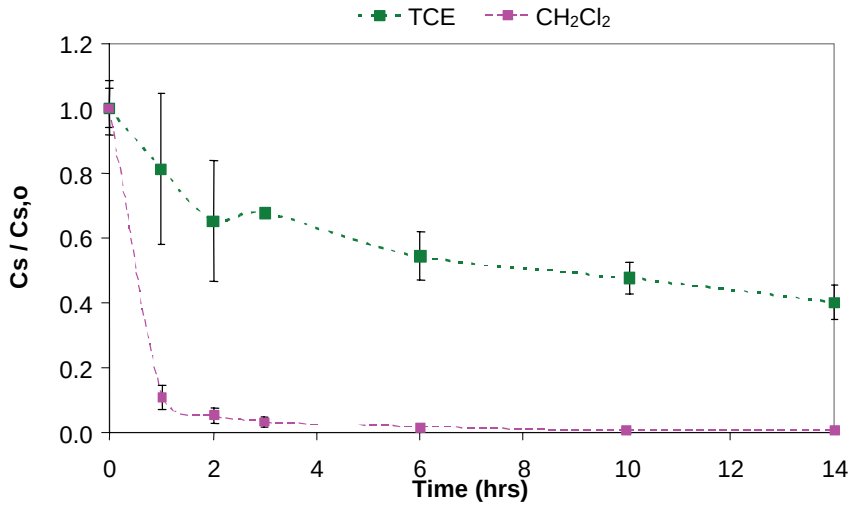

Figure 42. 14-hour carbon recovery profiles for CH_2Cl_2 and TCE in expanded-bed columns using fresh water (29°C) flushing to remove the VOC from the bulk liquid. n=2 for each data point (average between top and bottom samples).

Again, pseudo-first-order kinetics were observed. Respective first-order recovery constants for CH_2Cl_2 and TCE removals were 0.219 and 0.043 hr^{-1} (Table XIX).

As in the Fenton-dependent trials, a correlation between carbon recovery and compound solubility (see Log K_{ow}, Table II) was evident. Recovery of the more soluble compound (MC) was 98% over a 14-hour period, versus 51% recovery of TCE.

Table XIX. Expanded-Bed Recovery Data

Compound	Reaction k_{obs} (hr^{-1})	% Mass Destroyed*	Flushing k_{obs} (hr^{-1})	% Mass Removed	$k_{\bullet OH,R}$ ($M^{-1}s^{-1}$)#
Methylene Chloride (MC)	0.242	97	0.219	98	9.0×10^{7}
1,1,1-Trichloroethane (TCA)	0.291	67	0.223	48	1.0×10^{8}
Trichloroethylene (TCE)	0.041	52	0.043	51	2.9×10^{9}

* - For 14-hour exposure to 10 mM iron and 7500 mg/L H_2O_2
\# - From Buxton (1988)

Recovery profiles for the Fenton-dependent trials and those in which fresh water was flushed through (without recirculation) are superimposed in Figure 43. Recovery kinetics were similar (independent of eluent composition) for both compounds. This suggests that desorption or mass transfer, as opposed to aqueous-phase reaction kinetics, limited overall GAC recovery rates for both MC and TCE.

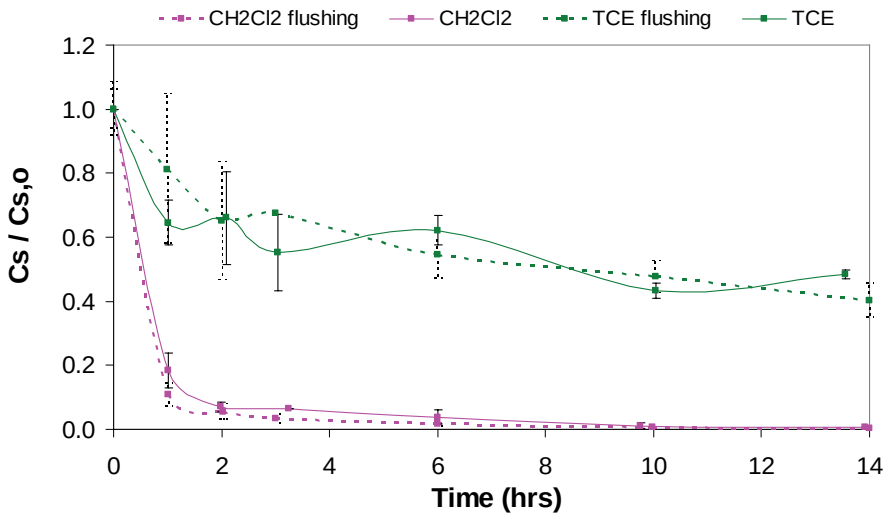

Figure 43. 14-hour carbon recovery profile comparison for CH_2Cl_2 and TCA in expanded bed columns. Fenton-dependent and water flushing trials are presented.

Fixed-Bed Recovery Trials—Effect of Particle Size

To verify the importance of diffusive transport to overall recovery kinetics, the effect of particle size on recovery rate was examined. Recovery data were collected over a 250-minute flushing period (with clean water) for GAC preloaded with chloroform. Chloroform is relatively soluble in water with a moderately non-linear adsorption isotherm (Table II). Despite operating at a significantly lower flow rate than the expanded-bed design (200 mL/hr versus 950 mL/hr) the assumption of fast convective mixing in the bulk was maintained, and diffusion limitations through the hydrodynamic boundary layer surrounding carbon particles were neglected. Dependence of carbon recovery rate on particle size (other being factors equivalent) was taken as an indication that pore-volume or surface diffusion limits the carbon recovery process. That is, decreasing pore length/particle diameter would result in faster contaminant removal only if the recovery process were limited by intra-particle mass transfer.

Time dependent residual mass loadings on sieved GAC are represented for each particle size range tested (Figure 44). The smallest particle range (1.0-1.18 mm diameter) yielded the fastest carbon recovery rate (apparent ***k***: 0.226 hr^{-1}). Recovery rates decreased as particle size increased (1.4-1.7 mm: 0.204 hr^{-1}; 2.0-2.38 mm: 0.129 hr^{-1}). Results suggest that pore or surface diffusion has an effect on chloroform removal kinetics from Calgon URV-MOD 1 carbon in Fenton driven recovery systems.

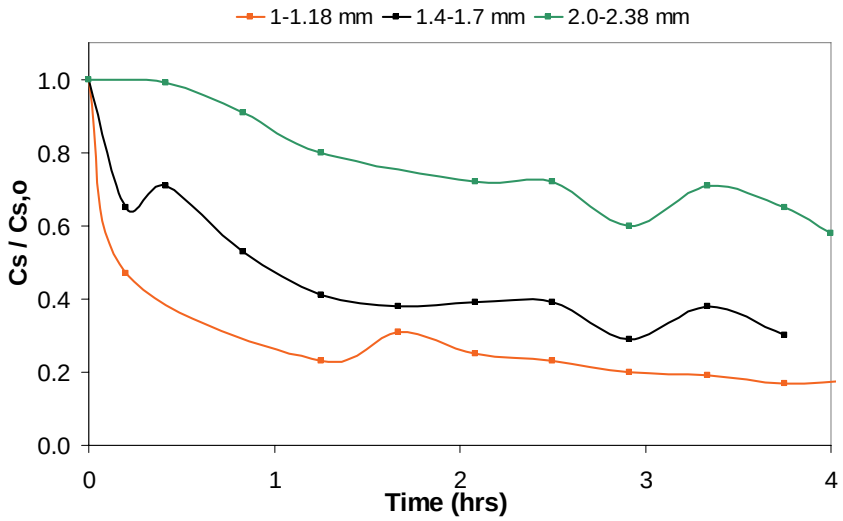

Figure 44. Fixed-bed carbon recovery kinetics for three discrete size distributions of GAC, preloaded with chloroform and normalized to the respective loading concentration.

Theoretical Considerations - Modeling

In aqueous-phase GAC applications, effects due to Knudsen diffusion are generally considered negligible as it is assumed that surface tension limits the availability of micro-pores that approach the molecular size of the contaminant. Pore-volume diffusion is an intrinsic property of the GAC-adsorbate system and is often the rate-limiting step in the sorption mechanism (Furuya ***et al***., 1996). However, it has been established by several researchers (Snoeyink, 1990; Weber 1972; DiGiano and Weber, 1973) that a parallel transport mechanism (surface diffusion) is often needed to characterize the complicated adsorption process (Furuya ***et al.,*** 1996). The relative contribution of each mechanism to the overall effective diffusivity is a function of several factors. For example, unlike pore-volume diffusion, which is always present, the importance of surface diffusion depends on the affinity of the adsorbate to the adsorbent (Furuya ***et al***., 1996). It has been shown (Suzuki, 1990) that although surface diffusivities are often two orders of magnitude smaller than pore volume diffusivities, a large surface concentration gradient, such as those experienced with high-affinity solutes, can result in a surface flux that is much greater than the contribution of pore diffusion to overall mass transfer (Ma ***et al***., 1996). Therefore, a general transport function in which pore and surface diffusion are individually characterized is generally employed.

In both aqueous-phase and surface diffusion, transient contaminant fluxes obey Fick's second law:

$$\frac{\partial \boldsymbol{C}}{\partial \boldsymbol{t}} = \boldsymbol{D}\nabla^2 \boldsymbol{C} \tag{54}$$

where C is the concentration of diffusing substance, and $\boldsymbol{D}$ is the diffusion coefficient (Crank, 1975). Here we approximate a GAC particle to a sphere. The following equation results from a mole balance of contaminant in the pore space of the GAC particle:

$$\frac{\partial \boldsymbol{C_p}}{\partial \boldsymbol{t}} = \frac{\boldsymbol{D_{ef,p}}}{\boldsymbol{r}^2} \frac{\partial}{\partial \boldsymbol{r}} (\boldsymbol{r}^2 \frac{\partial \boldsymbol{C_p}}{\partial \boldsymbol{r}}) - \boldsymbol{a_i} \cdot \boldsymbol{J_s} \tag{55}$$

where $\boldsymbol{C_p}$ is the local concentration of contaminant in the liquid within the pores, $\boldsymbol{D_{ef,p}}$ is its effective (aqueous-phase) diffusivity in the pores, $\boldsymbol{a_i}$ is the surface area of solid per unit volume of pore space, and $\boldsymbol{J_s}$ is the interfacial flux of contaminant, expressed as moles of contaminant transferred to the solid phase per unit time and per unit solid surface area.

Analogous to pore-volume diffusion, a spherical GAC particle is assumed for the characterization of surface diffusion. For adsorbed contaminant a similar mass balance results in

$$\frac{\partial \hat{\boldsymbol{C}}_s}{\partial \boldsymbol{t}} = \frac{\boldsymbol{D_{ef,s}}}{\boldsymbol{r}^2} \frac{\partial}{\partial \boldsymbol{r}} (\boldsymbol{r}^2 \frac{\partial \hat{\boldsymbol{C}}_s}{\partial \boldsymbol{r}}) + \boldsymbol{J_s} \tag{56}$$

where $\hat{\boldsymbol{C}}_s$ represents the concentration of contaminant adsorbed on the solid surface in moles per unit solid surface area, $\boldsymbol{D_{ef,s}}$ is the effective surface diffusivity, and the interfacial flux of contaminant is again represented as $\boldsymbol{J_s}$.

Here, we will make the assumption that adsorption and desorption processes are much faster than diffusive transport. Under these conditions, we can assume that the solid and the liquid in the pore space are at equilibrium (Figure 45). Therefore, the interfacial flux of contaminant, $\boldsymbol{J_s}$, is governed by the Freundlich isotherm, and represented as follows:

$$\hat{\boldsymbol{C}}_s = \boldsymbol{K} \cdot \boldsymbol{C_p}^{\frac{1}{\boldsymbol{n}}} \tag{57}$$

where $\boldsymbol{K}$ is often interpreted as the adsorbent capacity ((mg/g)(L/mg)$^{1/n}$), and 1/n the relative strength of adsorption. A smaller value of 1/n, suggests a stronger adsorption bond (Letterman, 1999). The Freundlich parameters $\boldsymbol{K}$ and 1/n have no theoretically derived physical significance, however, and must be determined empirically. Compound-specific Freundlich parameters were experimentally determined on URV-MOD 1 carbon, as presented earlier.

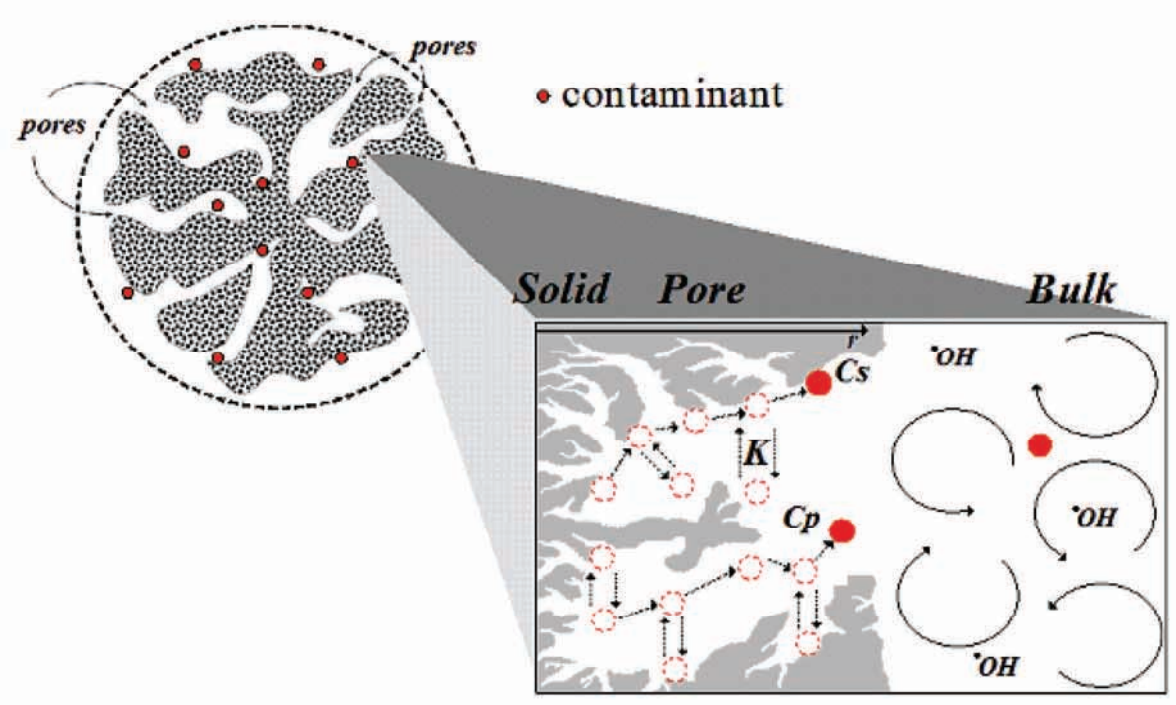

Figure 45. GAC particle cross section. Empirical Freundlich parameter (K) characterizes interfacial contaminant flux based on local equilibrium between the sorbed and aqueous concentrations.

A mass transfer equation that assimilates the effects of pore and surface diffusion into a single diffusivity is derived by manipulating (55), (56), and (57). The interfacial contaminant flux is adjusted to represent moles of contaminant transferred to the solid phase per unit time and per unit solid volume by multiplying (56) by the surface area to solid volume ratio, a_i. Adding the resulting solid mass transfer equation with the aqueous mass transfer equation (55), and then using the isotherm relationship (57) to eliminate the solid concentration leads to the following:

$$\frac{\partial C_p}{\partial t} = \frac{1}{1+\frac{a_i}{n}\cdot K\cdot C_p^{\left(\frac{1}{n}-1\right)}}\frac{1}{r^2}\frac{\partial}{\partial r}\left[r^2\left(D_{ef,p}+\frac{a_i}{n}\cdot K\cdot C_s^{\left(\frac{1}{n}-1\right)}\cdot D_{ef,s}\right)\frac{\partial C_p}{\partial r}\right] \tag{58}$$

which is equivalent to an intraparticle aqueous-phase diffusion equation with variable coefficients. However, for the case of a linear isotherm (1/n=1), the differential equation can be written as,

$$\frac{\partial C_p}{\partial t} = \frac{D}{r^2}\frac{\partial}{\partial r}\left(r^2\frac{\partial C_p}{\partial r}\right) \tag{59}$$

where

$$D = \frac{D_{ef,p}+a_i\cdot D_{ef,s}\cdot K}{1+a_i\cdot K} \tag{60}$$

In this case, the effects of pore volume and surface diffusion are combined into a single fitting parameter, the apparent diffusivity D. It is clear from equation (60) that the effects of pore and surface diffusion can be considered

individually based on the fitting parameter, $\boldsymbol{D}$. For example, assuming pore diffusion is the dominant transport mechanism, (60) may be interpreted as,

$$\boldsymbol{D} = \frac{\boldsymbol{D_{ef,p}}}{1 + \boldsymbol{a_i} \cdot \boldsymbol{K}} \tag{61}$$

However, when surface diffusion cannot be ignored, equation (60) can also be simplified to the following equation by assuming a similar tortuosity, τ, for both pore and surface diffusion,

$$\boldsymbol{D} = \frac{\boldsymbol{D_{mol}}}{\tau} \tag{62}$$

The initial and boundary conditions are derived in part from the experimental setup, which typically provides fast convective mixing in the bulk liquid phase (negligible film resistance), a negligible bulk liquid-phase concentration (rapid consumption of desorbing contaminant in the bulk liquid-phase) and negligible contaminant concentration on the GAC particle exterior surface (for maintenance of equilibrium with the bulk liquid-phase concentration). That is,

$$\boldsymbol{C_p}(\boldsymbol{r},0) = \left(\frac{\hat{\boldsymbol{C}}\boldsymbol{s},\boldsymbol{o}}{\boldsymbol{K}}\right)^{\frac{1}{\boldsymbol{n}}} \qquad \boldsymbol{r} = \in [0,\boldsymbol{R}] \qquad \boldsymbol{t} = 0 \tag{63}$$

$$\boldsymbol{C_p}(\boldsymbol{r},\boldsymbol{t}) = 0 \qquad \boldsymbol{r} = \boldsymbol{R} \qquad \boldsymbol{t} = \in [0,\infty] \tag{64}$$

$$\frac{\partial \boldsymbol{C_p}}{\partial \boldsymbol{r}} = 0 \qquad \boldsymbol{r} = 0 \qquad \boldsymbol{t} = \in [0,\infty] \tag{65}$$

where $\hat{\boldsymbol{C}}_{\boldsymbol{s,o}}$ is the initial solid contaminant concentration (mg/m^2), $\boldsymbol{C_p}$ the aqueous-phase intraparticle contaminant concentration (mg/L), and $\boldsymbol{K}$ and 1/n the empirical Freundlich parameters.

An analytical solution is available for equations (59-65, for n=1 only), which yields the aqueous bulk concentration. The intraparticle liquid-phase concentration profile (generated by (55)) can be translated to a solid loading by assuming that equilibrium exists throughout the particle and integrating over the particle volume. The loading so obtained can be represented in terms of a volume-averaged effective liquid-phase concentration in a single GAC particle. Following a contaminant mass balance on the system, solution for the bulk aqueous-phase contaminant concentration yields,

$$\boldsymbol{C_l} = \sum_{\boldsymbol{j}=1}^{7} \frac{\boldsymbol{P_j}}{\boldsymbol{R_j}^2} \sum_{\boldsymbol{n}=1}^{\infty} \boldsymbol{A_{n,j}} \cdot \left(\boldsymbol{e}^{-\frac{\boldsymbol{n}^2 \cdot \pi^2 \cdot \boldsymbol{D} \cdot \boldsymbol{t}}{\boldsymbol{R_j}^2}} - \boldsymbol{e}^{-\frac{\boldsymbol{Q} \cdot \boldsymbol{t}}{\boldsymbol{V_l}}} \right) \tag{66}$$

where C_l is the bulk aqueous-phase concentration (mg/L), $\boldsymbol{P_j}$ is the particle population fraction, $\boldsymbol{R_j}$ the population of particles with radius $\boldsymbol{R}$, $\boldsymbol{Q}$ the aqueous flow rate (m^3/min), $\boldsymbol{V_l}$ the reactor liquid volume (m^3), and $\boldsymbol{A_n}$ the consolidated constant represented as

$$A_{n,j} = \frac{\dfrac{6 \cdot \overline{\hat{C}}_{s,o} \cdot D \cdot a_i \cdot \phi \cdot M}{V_l \cdot \rho_{ap}}}{\dfrac{Q}{V_l} - \dfrac{n^2 \cdot \pi^2 \cdot D}{R_j^2}} \tag{67}$$

The consolidated term includes the previously determined average solid concentration $\overline{\hat{C}}_{s,o}$, M the mass of GAC (g), the particle porosity Φ, ρ_{ap} the particle density (g/m^3), and D the fitting parameter. It was determined from experimental data that it was advantageous to periodically sample the liquid effluent from the reactor instead of the residual contaminant mass on the solids, as a greater sampling frequency could be achieved while introducing less experimental error due to depletion of carbon mass in the bench-scale reactor. It is important to note that although the liquid-phase contaminant was measurable, the bulk liquid-phase concentration remained very small compared to the contemporary intra-particle concentrations, validating (approximately) the selection of the bulk liquid-phase boundary condition (equation (62)).

Model calibration was based on fitting τ using experimental data for CH_2Cl_2 and TCA desorption. That is, τ was selected to minimize the sum of squared error between model output and experimental results (time-dependent liquid-phase concentration of contaminant in the reactor effluent). If the effective diffusivity is dominated by pore and surface diffusion, then τ can be deduced from the effective diffusivity by (22) (assuming a similar τ for pore and surface diffusion). τ should remain constant (independent of sorbate identity) if pore-volume and surface diffusion are the dominant transport mechanisms for all sorbates. Furthermore, a single τ should be experienced independent of the residual contaminant concentration on the solid if an energetically homogeneous (no range of binding energies) surface exists.

Pore Diffusion Modeling

For compounds with a near-linear isotherm on URV-MOD 1 carbon (i.e., CH_2Cl_2, 1/n=1.0; TCA 1/n=0.93; Table II), an analytical solution (64) to the apparent diffusion model (57) is available. Tortuosity (τ)-dependent curves are compared to experimental recovery data by partial differential analysis using MathCad software. The physical properties of Calgon URV-MOD 1 carbon are considered uniform with respect to porosity and internal surface area (Table III) throughout the diameter range 0.6-2.38 mm (the range of particle sizes used in experiments). The actual pore volume is approximated as the sum of all pore volumes, 0.643 mL/gGAC, and includes the volume of micropores (Table III). The result is a constant surface area to pore-volume ratio, a_i (2×10^9 m^{-1}), across all particle sizes. As a result, an error in D is anticipated, as a potentially significant fraction of the micro-sized pores may be unoccupied because of surface tension effects in liquid-phase application (Knudsen effects).

A series of contaminant recovery simulations was developed for desorbed CH_2Cl_2 by varying the single fitting parameter, τ (Figure 46).

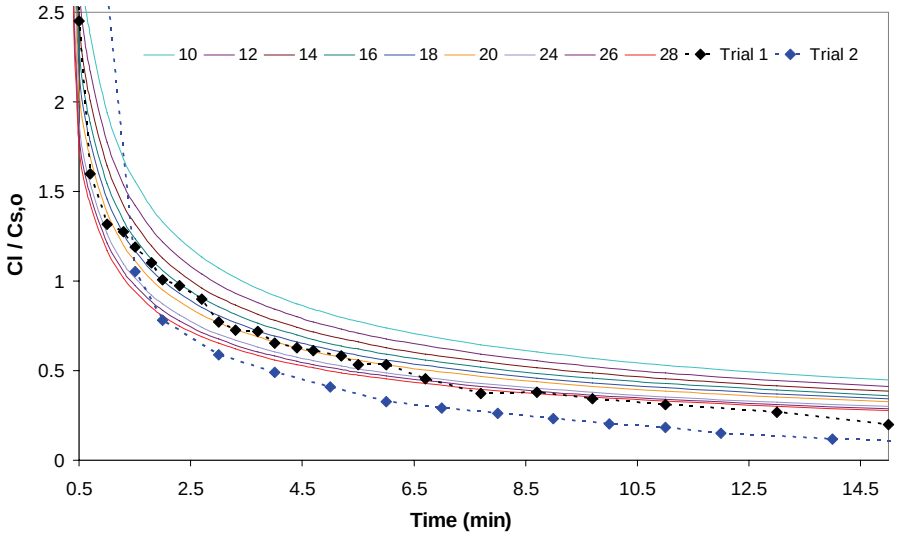

Figure 46. A comparison of experimental and modeled, bulk aqueous-phase concentration profiles for CH_2Cl_2 where the single fitting parameter, τ, was varied.

For CH_2Cl_2, model predictions are compared to the two experimental data sets obtained using modestly different loading concentrations. Although initial surface loading concentrations differ slightly, transport effects associated with initial concentration differences are considered negligible. Therefore, the difference in recovery rates between the data sets is probably due to experimental error, and a minimized sum-of-squares method was applied to select an appropriate simulation curve (τ = 26) using the experimental average. Notice that selection of this value depends on an assumption that surface diffusion can be neglected (equation 61). Any appreciable role for surface diffusion would result in a larger fitted tortuosity value. Column washout due to liquid loading and contaminant flux by non-diffusive mechanisms was accounted for by fitting modeled profiles to data obtained after a few liquid retention periods had passed. Based on a column residence time of approximately 4 seconds, it is assumed that a uniformly distributed flow and complete mixing will occur within five bed volumes. However, a more accurate determination of the physical characteristics of column washout, and the hydraulic detention time is desirable. Figure 47 shows the normalized bulk-phase concentration profiles for the two CH_2Cl_2 data sets against the model prediction over a 15-minute flushing period.

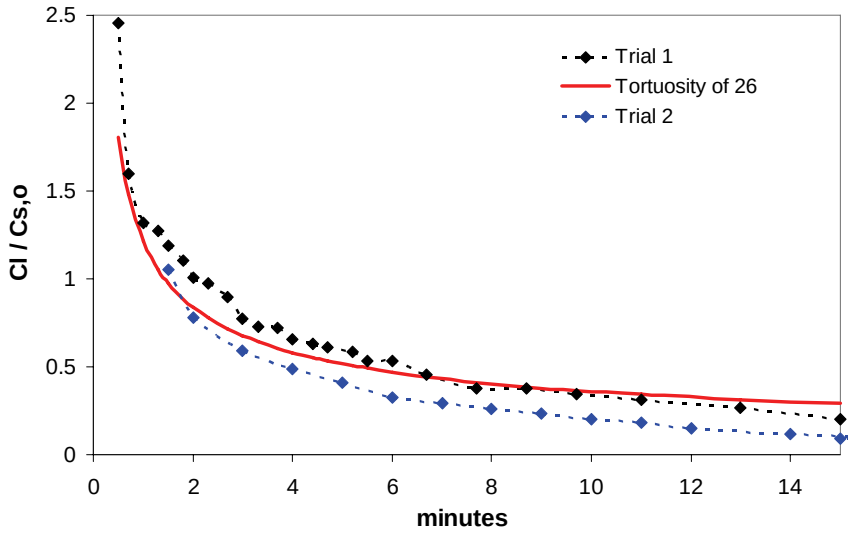

Figure 47. The normalized, bulk aqueous-phase contaminant concentration versus time-comparison for experimental CH_2Cl_2 data and results of the pore diffusion model.

A τ of 26 minimized the squared error between experimental and modeled recovery profiles, although the pore diffusion model predicted contaminant removal slightly after approximately seven minutes.

For TCA, the isotherm was approximated as linear (1/n=0.93), and only a single experimental data set was available. Carbon properties and a column flow rate consistent with the CH_2Cl_2 simulations were used in the model. A value of 0.65 L/g is used for the isotherm fitting parameter, ***K***, (Table II) and a series of τ-dependent recovery curves was again developed for the pore diffusion model. Here, a τ of 129 minimized the relative error between experimental data and the pore diffusion model (Figure 48). Again, this value is based on an assumption that surface diffusion does not contribute to intra-particle mass transfer (equation 61). A similar washout period (30 seconds) was used to justify rejection of the first few data points based on residence time, and the recovery process was modeled over a 250-minute flushing period.

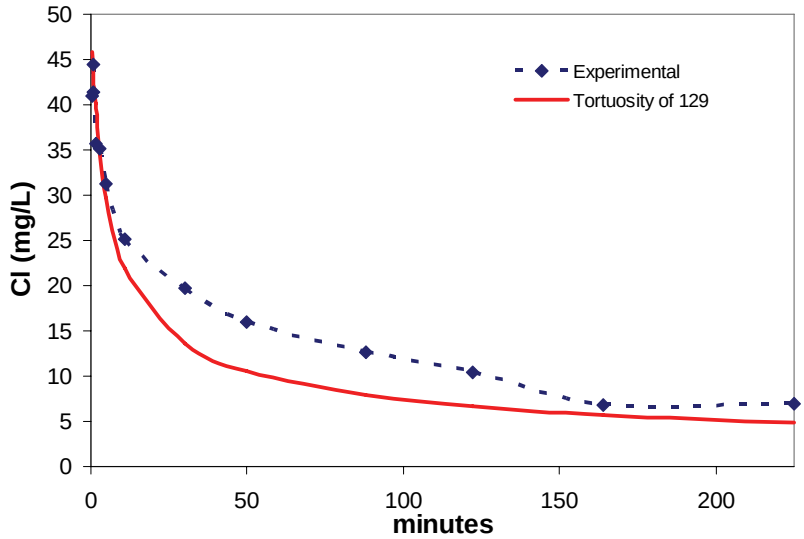

Figure 48. A comparison of bulk aqueous phase contaminant concentrations between experimental TCA data and a pore diffusion model.

Initially, a large discrepancy exists between the measured and simulated TCA profiles with the model over-predicting contaminant removal rate over the first 30 minutes, and under-predicting thereafter. Like the profile experienced with CH_2Cl_2, the fitted curve for TCA does not provide an adequate physical representation of contaminant loss over the entire removal period, suggesting that contaminant removal cannot be accurately predicted with a pore diffusion model of the form used here. Also, it is evident that a single τ cannot be utilized to account for transport-limited recovery of both compounds ($\tau_{opt.}$=26 for CH_2Cl_2; $\tau_{opt.}$=129 for TCA).

A remarkably broad range of τ has been reported for activated carbon macropores, ranging from 5-65 (Yang, 1987). From equation (58) it is apparent that the accuracy of fitted τ values can be no greater than the accuracy with which $\boldsymbol{K}$ (the capacity parameter in the Freundlich isotherm) is estimated from equilibrium data. Based on a linear regression for the CH_2Cl_2 isotherm data, a 95% confidence interval corresponds to a range of adsorbent capacities of $0.036 \leq \boldsymbol{K} \leq 0.151$ $^{L}/g$ (Figure 49a). From the inverse relationship that exists between $\boldsymbol{K}$ and τ, varying $\boldsymbol{K}$ within the confidence interval led to a corresponding range for τ of 13-54 (CH_2Cl_2 recovery experiments). A similar error analysis (Figure 49b) on TCA led to a range of τ values from 89-491. Thus, it is unlikely that CH_2Cl_2 and TCA recovery rates are limited by the same physical constraint. It is probable that the lower solubility of TCA (Table II) accounts for the apparent difference in mechanism of rate limitation.

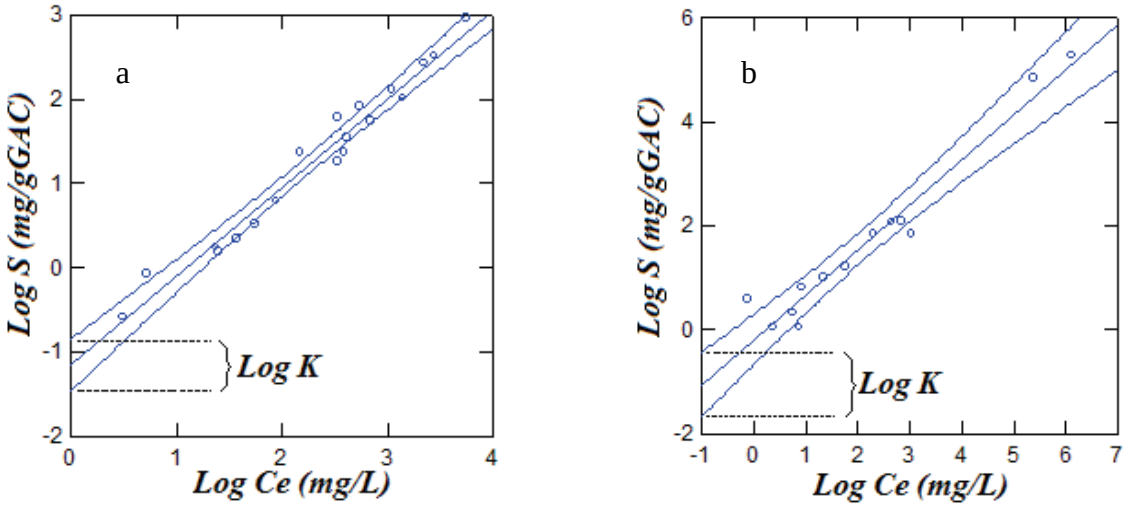

Figures 49(a)(b). A 95% confidence interval on log-transformed isotherm data for CH_2Cl_2 (a) and TCA (b). Isotherm adsorbent capacity, K, is obtained from the intercept of the log-transformed isotherm.

Pore and Surface Diffusion Modeling

In evaluating the effectiveness of a pore and surface diffusion model, the minimized sum-of-squares recovery profiles for CH_2Cl_2 and TCA (Figure 47, 48) are considered. Although surface diffusion is now accounted for, it is assumed that a similar tortuosity is experienced for both pore and surface diffusion. As a result, the model fitting parameter is given by equation (60). Applying (54), a τ of 1920 corresponded to the minimized sum-of-squares recovery profile for CH_2Cl_2 (Figure 50).

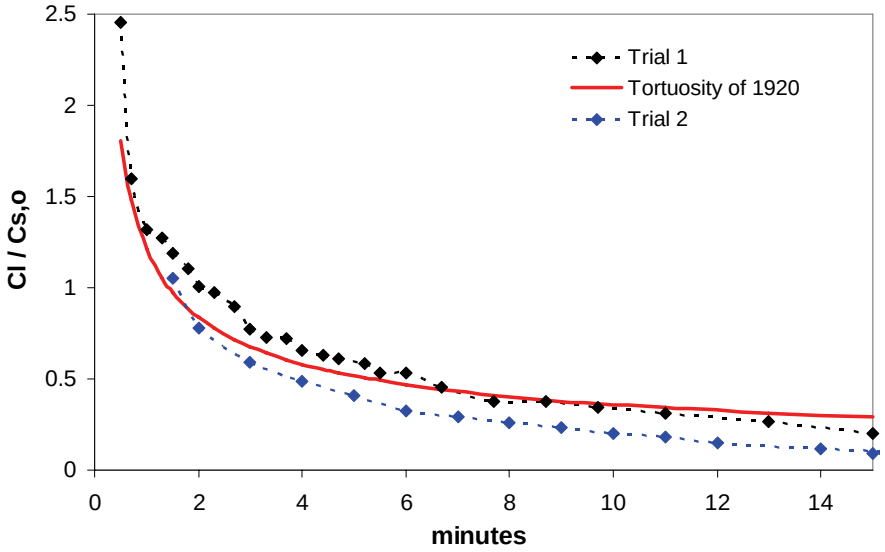

Figure 50(a). A normalized, bulk aqueous-phase contaminant concentration comparison between experimental CH_2Cl_2 data and a pore and surface diffusion model.

A similar analysis applied to the minimized sum-of-squares recovery profile for TCA resulted in a τ of 129,530 (Figure 50b).

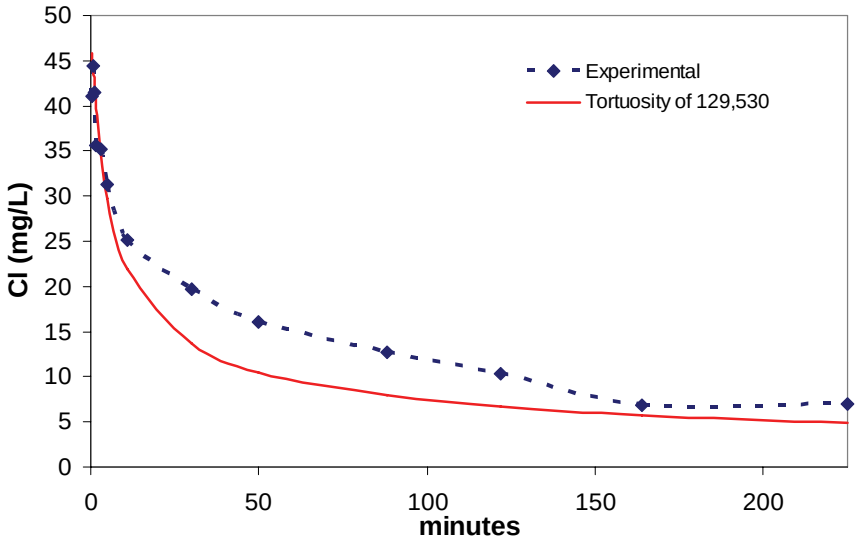

Figure 50(b). A comparison of bulk aqueous-phase contaminant concentrations between experimental TCA data and a pore and surface diffusion model.

Like the pore diffusion model, it is evident that a single τ cannot be utilized to account for transport-limited recovery of both compounds ($\tau_{opt.}$=1920 for CH_2Cl_2; $\tau_{opt.}$=129,530 for TCA). On this basis, it seems likely that an intraparticle diffusion model cannot adequately account for observed transport kinetics during carbon recovery in the desorption experiments. This conclusion is based on the inability to model linear isothermal contaminants for CH_2Cl_2 and TCA with a single τ using the pore and surface diffusion model described. Transport limitations other than those arising from intraparticle diffusion, such as adsorption/desorption kinetics, may produce the deviations between the

experimental and predicted curves. Although an assumption of local equilibrium (fast sorption kinetics) is often employed in intraparticle transport mechanisms, the validity of this assumption is seldom validated. For example, comparison of surface diffusion and desorption energy barriers has not been adequately considered for systems such as these. Furthermore, it seems unlikely that an energetically homogenous surface exists with a uniform heat of adsorption. A reasonable view is that variation in $\boldsymbol{D_{ef,s}}$ is an outcome of variation in heats of adsorption, and that $\boldsymbol{D_{ef,s}}$ is in fact a sensitive indicator of energetic surface heterogeneity (Carman, 1956).

In addition, although accounting for both pore and surface diffusion, an apparent diffusion model may be insufficient for predicting concentration effects over a broad range of experimental conditions. The apparent diffusivity determined at a particular temperature and concentration has very limited applications for other conditions (Furuya ***et al***., 1996). This may result from the fact that the pore and surface diffusion mechanisms require different values of τ due to an energetically heterogeneous surface. When surface flux is relatively high (high affinity solutes), a diffusion model would then be inadequate for characterizing removal kinetics. For compounds with limited solubility, for example, intraparticle aqueous concentrations of the sorbate may be much lower than their equilibrium levels. Under these circumstances, surface diffusion may be the predominant mechanism of sorbate transport to the particle exterior. Surface effects resulting from pore volume distribution may prove to be significant as well. As pore dimensions approach the molecular size of the contaminant, it is anticipated that surface diffusion mechanisms limit transport kinetics. It is known from literature that in micropores found in zeolites (Ruthven, 1984), surface diffusion is the dominant transport mechanism, while pore diffusion dominates in macropores (Ma ***et al***., 1996).

Results presented in this section lead the investigators to conclude that mass transport mechanisms limit the effectiveness of Fenton's reaction for carbon recovery, at least for slightly soluble compounds that are reactive with Fenton's reagents. Therefore, optimal design for this type of treatment would maximize contaminant flux from the sorbent while minimizing the use of H_2O_2, the primary contributor to process cost. Just how this is done will probably be compound specific.

Role of Iron Phase (Precipitated vs. Dissolved)

The following section evaluates the effectiveness of loading iron onto the surface of GAC prior to the Fenton treatment. Localizing the reaction on the carbon surface was considered as a means to increase contaminant destruction efficiency and minimize reagent use. That is, it was hypothesized that radical production in the immediate vicinity of adsorbed contaminants would allow a higher proportion of radicals to react with the target compounds as opposed to H_2O_2 and other competitors. In addition, the eluant reservoir size was reduced to decrease non-productive (outside the column) H_2O_2 consumption.

To test this hypothesis, native and iron-amended GAC were used in parallel column regeneration trials. Both types of GAC (15 g each) were loaded with TCE and regenerated. Results were compared with previous column experiments with iron in solution. After 14 hours, TCE recovery was essentially the same in all three situations

(Figure 51). Table XX summarizes the results, as well as column iron content, and volume of H_2O_2 used in each trial. Precipitating the iron on the surface of the GAC lowers the use of H_2O_2, which is the primary cost associated with the GAC regeneration process (see later section on process cost estimation). Iron addition to the carbon surface, however, provided little advantage in terms of carbon recovery kinetics.

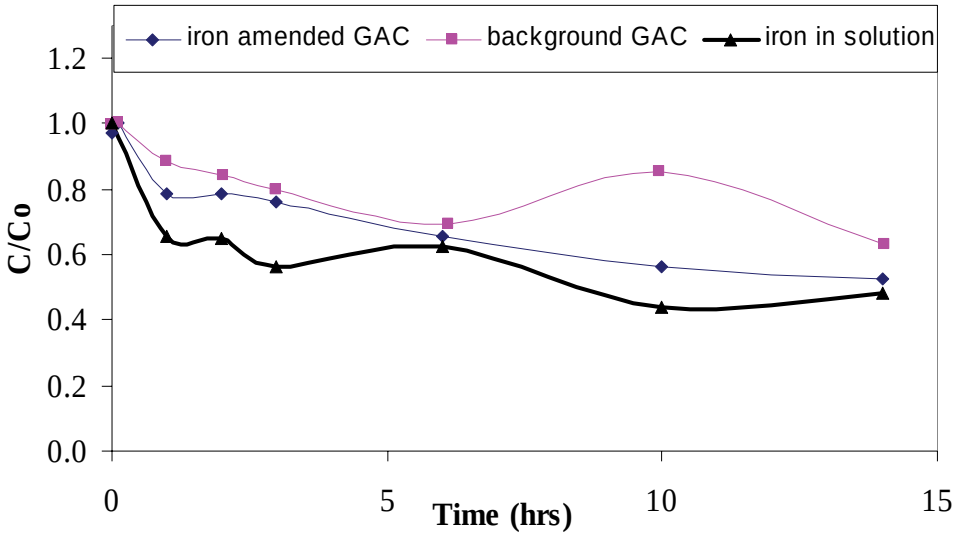

Figure 51. TCE Recovery with background GAC, iron amended GAC and iron in solution.

Bench-scale PCE regeneration column experiments (Table XXI) were conducted using a lower iron loading than in the TCE trials (Table XX). In this set of experiments, the effect of pH for PCE recovery was established. Iron-amended GAC was loaded with PCE and regenerated at pH 2 and 3 (Figure 52). As in the TCE trials, PCE destruction efficiencies with iron-amended GAC and with iron in solution (pH 2) were very similar, however H_2O_2 use was reduced by almost a factor of three (Table XXI). Results also suggest that pH is not an important process parameter in the range $2.0 \leq pH \leq 3.0$.

Table XX. Characteristics of GAC and Results after 14 hours of Iron-Amended Regeneration Trials

GAC type	Iron Content	C/Co (TCE)	H_2O_2 (mL)
Background GAC, pH 4.67	2 mgFe/gGAC (1.4mM)	37%	9
Iron-amended GAC, pH 2	7.4mgFe/gGAC (5 mM)	47%	25.8
Iron in Solution, pH 2	10 mM	50%	160-224

Results indicate that iron and H_2O_2 additions for the degradation of chlorinated solvents can be reduced significantly below the levels used in earlier experiments without significant deterioration of carbon recovery kinetics. It seems clear that engineering the reaction site for GAC regeneration can significantly reduce the process costs.

Unfortunately, enhancement of degradation rates for compounds that are diffusion or desorption limited has not yet been achieved. Alternative methods, such as use of alternative solvents and GAC with a greater proportion of surface area in macropores, should be explored to overcome the kinetic limitations arising from mass transport.

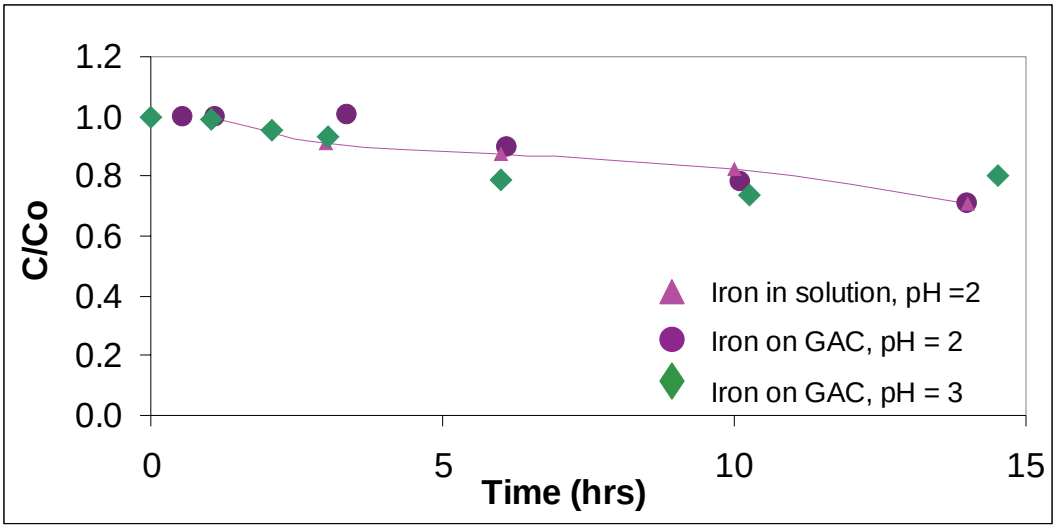

Figure 52. pH effect on iron-amended GAC loaded with PCE in column regeneration trials.

Table XXI. Observed Degradation Rate Constant and Average Hydrogen Peroxide Use for PCE-Laden GAC Regeneration With and Without Iron-Amended to the Carbon

pH/Iron	k_{obs} (hr^{-1})	H_2O_2 added (mls/hr)
2/Iron in solution	0.024	16
2/Iron-amended GAC	0.025	5.6
3/Iron-amended GAC	0.034	5.6

Note: *Uncertainty about Iron content (not accurately measured)

Heterogeneous, Bench-Scale Experiments - Conclusions

- Ethyl acetate was the best solvent tested for solid: liquid extraction of PCE from GAC. An extraction period of 12 hours provided nearly complete recovery of adsorbed PCE.
- Degradation of adsorbed chlorinated VOCs in heterogeneous Fenton's systems indicated that carbon recovery kinetics was bi-phasic. A fast initial degradation phase was followed (after 1-3 hours) by a slower second phase. The fraction of contaminant degraded in the initial rapid phase increased as the aqueous-phase solubility and $(1/K)^n$ value of the contaminants increased. Results suggest that intraparticle diffusion of the

contaminant limits recovery kinetics during the slow phase treatment, for at least a subset of the compounds tested.

- When GAC was loaded with CF and recovery was accomplished by rapidly flushing the carbon with clean water, the rate of CF recovery was inversely related to the size of carbon particles. Results suggest that pore and/or surface diffusion, and thus particle size, affect the overall removal kinetics for chloroform from Calgon URV-MOD 1 carbon in Fenton driven systems.
- A mass transfer model in which local solid: liquid equilibrium is assumed between the carbon surface and proximate pore was formulated to simulate mass transfer and recovery of carbon adsorption capacity. An analytical solution was developed for the special case in which contaminant adsorption was governed by a linear Freundlich isotherm ($n \approx 1$). A single fitting parameter (tortuosity) brought recovery simulations and data into reasonable agreement. However, a common tortuosity could not be obtained for all compounds, suggesting that surface diffusion and/or desorption effects can also limit GAC recovery kinetics.
- Based on the combined experimental and model results, it is concluded that mass transport mechanisms can limit the effectiveness of Fenton's reaction for carbon recovery, at least for slightly soluble compounds that are reactive with Fenton's reagents. Therefore, optimal design for this type of treatment would maximize contaminant flux from the sorbent while minimizing the use of H_2O_2, the primary contributor to process cost.
- Trials were conducted using Calgon URV-MOD 1 carbon on which iron had been precipitated onto the pore and outer surfaces. No iron was added to the bulk regenerant (Fenton's solution). It was hypothesized that this would localize the Fenton-driven radical generation near the GAC surface, in the vicinity of target compounds, and potentially avoid rate limitations due to pore and surface diffusion and/or compound desorption from the carbon surface. Improvement in the rate of carbon recovery due to the iron amendment was negligible, however. However, iron amendment to the carbon surface did decrease by about 3-fold the rate of H_2O_2 usage, which is the primary driver in operating cost of the system.

Field-Scale Regeneration Trials

Equipment Testing - Methylene Chloride and Chloroform Recovery Tests

Initial field regeneration trials were carried out using a larger column (I.D. = 5 cm, L = 30 cm, V = 600 mL, residence time = 2 s) containing 100 g URV-MOD 1 GAC that was pre-loaded with MC or CF (under lab conditions). Contaminant selection was based on hydrophobicity and reactivity with hydroxyl radicals (Table I).

Regenerant solution was recirculated continuously during each 30-hour experiment. Hydrogen peroxide was added at 1-hour intervals during hours 0-6 and 23-28 (Figure 53). At each point of addition, 150 mL of a 50% H_2O_2 stock solution was added to the 7 L recirculation reservoir. Since H_2O_2 was essentially exhausted at each addition point, the H_2O_2 concentration immediately after addition was about 0.38 M.

Carbon was periodically withdrawn from the top and bottom of the reactor for extraction and measurement of residual contaminants. Methylene chloride was essentially gone (full recovery) after 6-7 hours of operation. After 30 hours, just 6% of the original CF loading (125 mg CF/g carbon) remained on the GAC. The cost of recovery ranged from $2.5/kg to $6.6/kg GAC treated for the target contaminants studied. When multiple contaminants are simultaneously adsorbed to GAC, the compound with slowest recovery would determine the overall cost. Little was done in these experiments to limit the non-productive consumption of H_2O_2. That is, neither the configuration of the recovery system nor the schedule of H_2O_2 additions was designed to reduce H_2O_2 consumption/radical production that did not result in MC or CF destruction. Further discussion of this point is provided below.

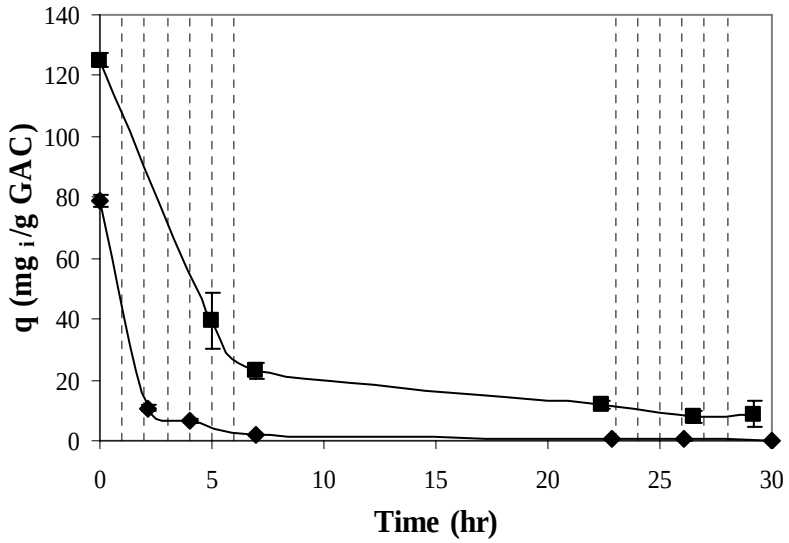

Figure 53. Carbon regeneration for (♦) MC and (■) CF in field experiments. Units in the y-axis are "mg VOC/g GAC". Degradation to below detection limit and 93% for MC and CF, respectively, was achieved after a 30-hour regeneration period. Reservoir concentrations: 10 mM iron, 0.15 M average H_2O_2, pH = 2.0. Dotted lines indicate times of 150 mL hydrogen peroxide additions. Error bars indicate difference in concentrations measured for samples taken from the top and bottom of the carbon bed.

Sequential Adsorption/Regeneration Experiments

The feasibility of carbon regeneration depends on both the acceptability of regeneration costs (primarily H_2O_2 consumption) and maintenance of carbon adsorption capacity through multiple degradation steps. Here, carbon adsorption capacity was tested before and after each of three surface regenerations. The work discussed in this section is part of a paper accepted for publication (De Las Casas et al., 2006).

Carbon was loaded with 100-110 mg TCE/g GAC in a batch reactor in the lab, then transferred to the field site for regeneration in the field column. GAC (100 g, dry weight) was suspended in 1 L of pure water that was pre-saturated with TCE at room temperature (initial TCE concentration ≈ 1100 mg/L). After 3 days, the distribution of TCE between carbon and liquid was near equilibrium with more than 99% of the contaminant on the carbon surface. The process was repeated twice, after field regeneration, using the same carbon sample to determine whether TCE adsorption was adversely affected by Fenton-driven regeneration. During regeneration periods, 0.7±0.2 g carbon samples were periodically withdrawn from the top and bottom of the column and extracted in ethyl acetate for determination of residual TCE. The regenerant solution containing 10 mM total Fe (pH 2) was recirculated at a rate that produced 50% GAC bed expansion. To initiate regeneration, 150 mL of 50% H_2O_2 was added to the 7 L regenerant volume to produce an initial H_2O_2 concentration of 0.38 M. Thereafter, the schedule of H_2O_2 additions was as indicated in Figure 54. At each point, an additional 150 mL of the 50% H_2O_2 stock solution was added to the regenerant reservoir.

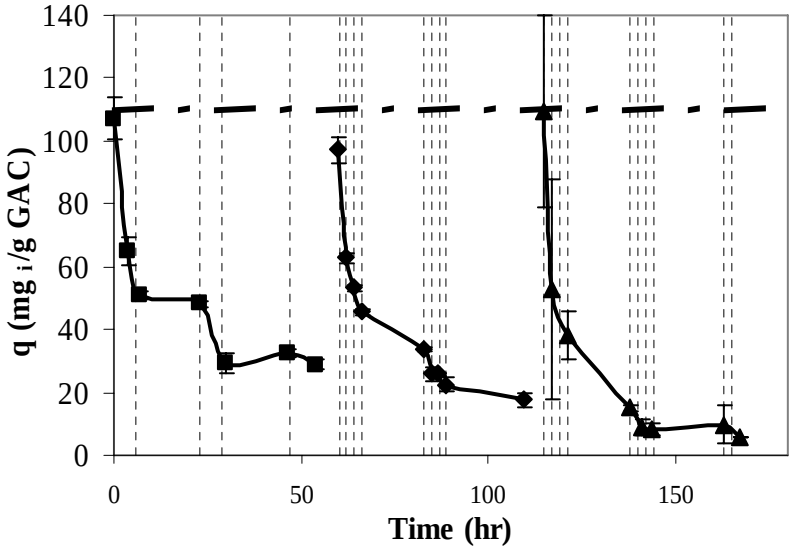

Figure 54. TCE carbon recovery during three sequential regeneration cycles. Vertical dotted lines indicate points of hydrogen peroxide addition. The horizontal dashed line represents the TCE load (107 mg/g GAC) at the start of the first carbon recovery procedure. TCE degradation of 73% (■), 82% (♦), and 95% (▲) was obtained for the three, consecutive, regeneration cycles. Error bars indicate the difference between the carbon extraction values from top and bottom of the column.

In each phase of the experiment, carbon recovery was initially fast with 50% TCE loss from the carbon surface in 4 hours or less. Thereafter, recovery was much slower so that final (60-hour) TCE recoveries were 73, 82 and 95% during the sequential regenerations. Improvement in the later regeneration cycles was probably a consequence of

more frequent H_2O_2 addition rather than a treatment-derived change in the physical characteristics of the URV-MOD1 carbon. Most important was the maintenance of TCE adsorption capacity after the 180-hour experiment (Figure 54). This finding is supported by previous investigations involving ***N***-nitrosodimethylamine (Kommineni ***et al.***, 2003) and methyl ***tert***-butyl ether (Huling ***et al***., 2005a) adsorption/regeneration on GAC.

Huling et al. (2005a) discussed two mechanisms that could adversely affect the performance of the activated carbon regenerated via an aggressive oxidative treatment such as the Fenton's reaction. In the study, the authors discussed possible chemical and physical alterations to GAC due to oxidative treatment. In a previous study, Huling et al. (2005b) reported reduction in surface area, microporosity, total porosity and sorptive capacity as a result of repeated (10-15) regeneration treatments to the GAC. In addition, incomplete transformation of the target compound(s) may affect the performance of the GAC by accumulating reaction intermediates on sorption sites and in this way diminishing the availability of sites for the target compounds. Other studies have also reported no loss of carbon sorption capacity under aggressive oxidative conditions (Toledo et al., 2003).

TCE was measured periodically in the regenerant reservoir to gauge the adequacy of the H_2O_2 addition schedule. Comparison of regenerant TCE concentrations with (calculated) aqueous-phase concentrations in equilibrium with residual sorbed TCE concentrations (Figure 55) suggests that less frequent H_2O_2 could have produced similar recovery kinetics while reducing H_2O_2 consumption.

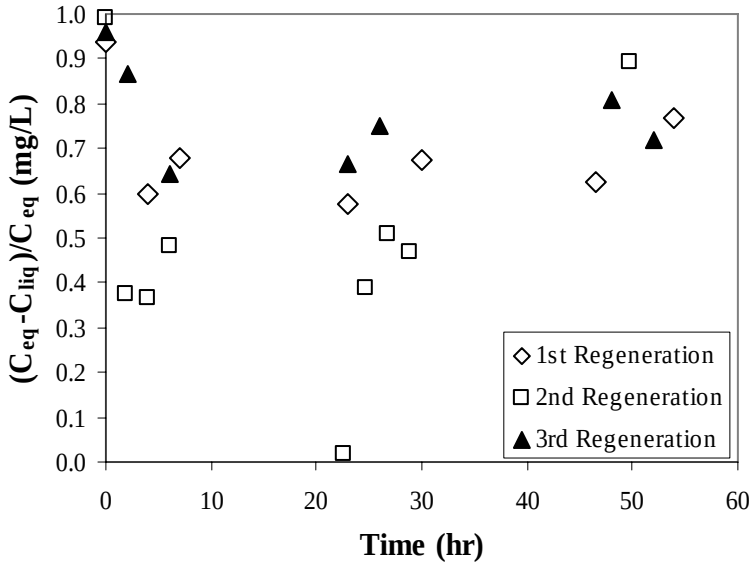

Figure 55. Ratio of ΔC_l ($C_{eq} - C_{liq}$) to C_{eq}, where C_{eq} is the aqueous-phase TCE concentration in equilibrium with the residual adsorbed concentration (q) and C_{liq} is the measured, liquid phase concentration. Results for three consecutive regeneration periods are superimposed. Equilibrium concentrations were calculated using measurements of residual adsorbed TCE (Figure 53) and TCE isotherm parameters (Table II). Note: t = 0 marks the beginning of each recovery cycle.

Were liquid levels to approach equilibrium with residual adsorbed TCE between peroxide additions, reactor performance could be improved significantly by increasing the frequency of H_2O_2 additions. Conversely, if aqueous-phase concentrations remain low relative to equilibrium levels calculated on the basis of adsorbed mass, then the

period of H_2O_2 addition could be extended to lower operational costs. The data (Figure 56) suggest that dissolved TCE was quickly destroyed following each H_2O_2 addition to the regenerant. However, aqueous-phase TCE concentrations also recovered quickly after H_2O_2 was exhausted. There was apparently little to gain by decreasing the frequency of H_2O_2 addition in this experiment.

Temperature was measured in the regenerant solution during the experiment. Overall, temperature increased from ambient (~30°C) to 55-60°C during the 180-hour procedure. This is consistent with the exothermic nature of the Fenton's reaction. Temperature decreased slowly following H_2O_2 exhaustion (1-2°C/hr). Greater temperature increases might be expected in larger reactors although more judicious application of H_2O_2 or reduction in regenerant iron levels would tend to mitigate temperature rise. Because TCE mass transport and reaction kinetics are favorably affected by higher temperature, the exothermic decomposition of H_2O_2 via reaction with iron might, if handled carefully, increase carbon recovery rates and lower overall costs for carbon surface regeneration.

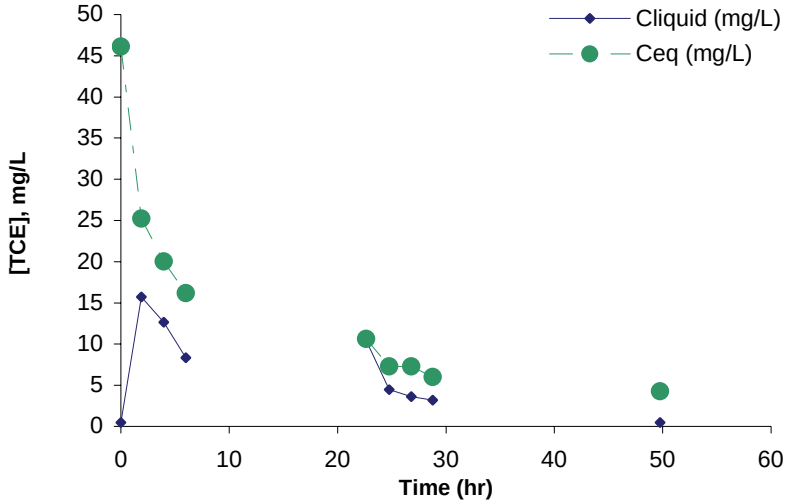

Figure 56. Comparison between Ceq (aqueous-phase TCE concentrations in equilibrium with the residual adsorbed concentration (q)) and Cliq (measured, liquid phase concentration). Original data from Figure 54. Equilibrium concentrations were calculated using measurements of residual adsorbed TCE (Figure 54) and TCE isotherm parameters (Table II). Note: t = 0 marks the beginning of the recovery cycle.

Loading Carbon with SVE Gases

Vadose zone gases from the soil vapor extraction system at the Park-Euclid (Arizona) state Superfund site containing primarily PCE, TCE and light diesel components as contaminants were used to load URV-MOD 1 GAC in a final set of field experiments.

It is likely that gas-phase contaminants experience more facile access to adsorption sites in carbon micropores, so that the contaminant mass removed prior to apparent breakthrough may be greater in gas-phase applications. Nevertheless, a water film is almost always present on the carbon surface in such situations, so that, ultimately, the adsorption capacity is dictated by the heterogeneous equilibrium between the adsorbed and liquid-phase chemical. If

Henry's Law limits the liquid-phase chemical concentration, the carbon load at breakthrough should be indifferent to the form in which the contaminant is applied. That is, gas-phase treatment should yield the same loading as treatment of a liquid that is in Henry's Law equilibrium with that gas. Crittenden et al. (1988) suggested that 45% relative humidity represents a critical cutoff point, in that a liquid film is fully developed on the carbon at sustained relative humidity greater than 45%. Gas removed from surface solids should be near saturation levels with water vapor (at the soil temperature). For this reason, a moisture knockout box is usually included in SVE designs.

The GAC was loaded for approximately 72 hours using a 4-cfm SVE side-stream. Effluent gases were pumped back into the system of extraction wells. To determine the carbon loading, GAC samples were taken from the top and bottom of the column, extracted in ethyl acetate and analyzed with GC-ECD. Initial, 6-hour regeneration trials produced 80% reduction in the adsorbed TCE concentrations, but only a 30% loss of adsorbed PCE (Figure 57). As in the previous field trials, degradation was initiated by adding 150 mL of the 50% H_2O_2 stock to the regenerant solution (total volume 7 L). Subsequently, 50 mL of the stock H_2O_2 solution was added every 15-30 minutes to replenish the initial H_2O_2 concentrations throughout the regeneration period. This procedure led to excessive H_2O_2 utilization and attendant cost.

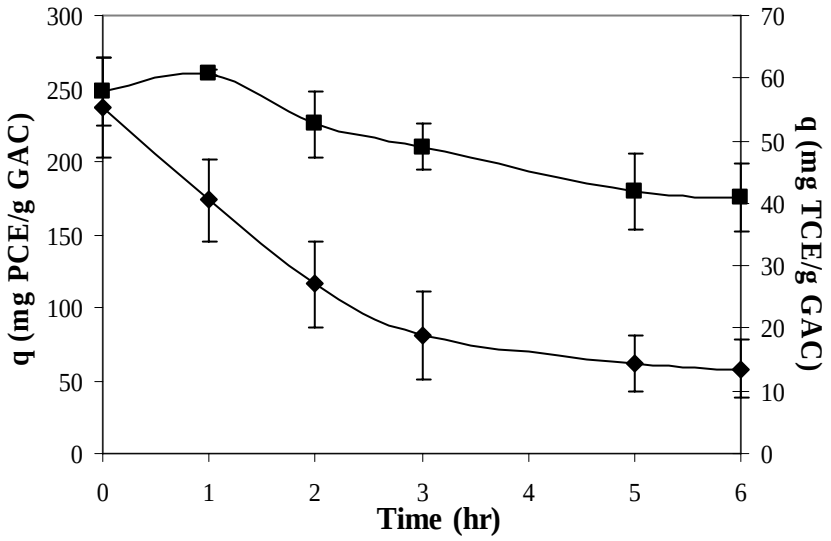

Figure 57. Carbon regeneration for SVE-loaded GAC. The two primary pollutants at the site are PCE and TCE. Overall, 30% and 80% degradation for PCE (■) and TCE (♦) were achieved during the 6-hour regeneration period. Reagent concentrations were 10 mM iron, 0.15 M H_2O_2 (average), at pH = 2.0. Error bars indicate the difference between the carbon samples from top and bottom of the column.

A total of 1.1 L of 50% H_2O_2 was consumed to destroy 7.0 g of PCE and 4.0 g TCE. This gives a molar yield of $2.2x10^{-3}$ and $1.6x10^{-3}$ for PCE and TCE, respectively. Pulsed addition of H_2O_2 with intervening periods in which H_2O_2 was exhausted (for contaminant transport to the bulk regenerant phase) might have produced comparable recoveries using a fraction of the oxidant. Peroxide costs could also be lowered significantly by reducing the volume of regenerant in the system. In the presence of Fenton's reagents, aqueous-phase concentrations of contaminants were generally near zero. Because the rate of H_2O_2 consumption is independent of the contaminant concentration, however,

H_2O_2 use continued during such periods without affecting contaminant transport out of the carbon particles. Under all circumstances, H_2O_2 consumption was proportional to the total regenerant volume, including the volume in the recirculation tank, where little or no contaminant was consumed under conditions of the field test. Consequently, future field experiments using similar conditions could further reduce the recirculation tank volume to lower reagent costs.

Economic Analysis

The cost of an in-place GAC recovery system based on Fenton's mechanism would include reagent (H_2O_2) consumption, power requirements to circulate regenerant, replacement of carbon that is lost due to abrasion and chemical (treatment) inactivation/destruction, capital expenses associated with the regeneration system itself (pumps, pipes and tanks) and the additional capacity necessary for temporary column retirement for regeneration. Here, it is assumed that H_2O_2 costs dominate the additional cost for an in-place Fenton carbon recovery system (see subsequent, detailed GAC Economic Analysis for a more complete cost estimate supporting this assumption). The primary sinks for •OH are H_2O_2 itself, due to concentration effects (Table II) and possibly (as regeneration cycles progress) free chloride ion. Thus, free radical concentrations (and H_2O_2 consumption rates necessary to maintain those levels) are essentially independent of the identity or concentration of the target compounds. This is not to say, however, that H_2O_2 costs are independent of contaminant identity. Compounds that desorb slowly from GAC require significantly greater time to achieve comparable degrees of recovery and, hence, greater recovery costs.

When multiple contaminants are present simultaneously, the compound most resistant to Fenton-driven recovery, in this case PCE, is likely to dominate recovery costs. Consequently, PCE degradation was used to estimate overall carbon regeneration costs. Other assumptions and economic or operational factors were:

Unit cost of H_2O_2 (50% solution, 1.18 g/mL)	\$0.34/L (Kommineni ***et al.***, 2003) (transportation cost not included)
H_2O_2 utilization for carbon recovery	95-232 mL (bench-scale column) 1-2 L (field column)
Carbon in experimental columns	10-16 g (bench-scale column) 78-100 g (field column)
Carbon purchase cost (EPA, 2000)	\$1.54-2.64/kg virgin coal carbon \$1.10-1.72/kg regenerated carbon
Carbon change out/disposal	\$0.66/kg (soiltherm.com, 2006)

Costs for carbon recovery/replacement alternatives are compared in Table XXII. The comparison is necessarily simplistic. The mechanism, rate limitation and kinetics of PCE recovery on GAC are poorly known, certainly not well enough to produce a most refined economic analysis. In-place oxidations of all other contaminants tested were

significantly faster than that of PCE and, therefore, more economically attractive. Nevertheless, PCE was among the important contaminants in this application and should be considered when assessing the utility of the technology locally.

Table XXII. Comparison of GAC Replacement vs. Regeneration Costs

Option	***Cost/kg***	***Critical assumptions/parameters***
1. Replacement	$3.30	$2.64/kg purchase cost
		$0.66/kg disposal of spent carbon
2. Thermal Regeneration	$2.64	$1.65/kg regeneration cost
		$0.66/kg transportation
		$0.33/kg carbon replacement
3. Fenton-based, in-place recovery		Peroxide costs dominate (0.34/L)
		PCE recovery dictates treatment time
a. Lab column	$2.69	95 mL H_2O_2/12 g GAC
b. Field column	$6.54	1.5 L H_2O_2/78 g GAC

Methods for increasing the efficiency of H_2O_2 use have been discussed to some extent. The mixing reservoir allowed the Fenton reaction to take place and H_2O_2 to be consumed without oxidation of the target contaminants. Based on the dimensions of the pilot-scale column, and assuming a porosity of 0.5 of the GAC, the pore volume within the column is approximately 0.3 L. The total liquid volume of the reactor system was 7 L. This suggests that more than 95% of the H_2O_2 applied to this system was consumed outside of the column (i.e. 0.3 L/7 L). Although we assume that the Fenton reaction (in our system) occurred predominantly in the reservoir, limiting the H_2O_2 reaction outside the mixing reservoir would economize H_2O_2. It may be possible to immobilize iron on the carbon surface and run regenerations in a pH range to avoid iron dissolution during recovery operations. The feasibility of such a scheme depends on selection of iron loadings that allow degradation reactions to proceed without blocking the carbon surface or interfering with contaminant access to carbon pores. Preliminary tests of Fenton-driven recovery in such iron-mounted systems have been discussed in a previous section. The potential advantage lies in localization of H_2O_2-consuming reactions and radical generation in the vicinity of the carbon surface. Bulk-aqueous-phase Fenton reactions can be minimized (i.e. sizing down reservoir) so that non-productive H_2O_2 consumption (that which destroys no contaminants) is greatly diminished.

Cost Estimation Based on Iron-Amended GAC Regeneration

The cost of carbon recovery in the field-scale reactors using iron-mounted on the surface of the GAC is discussed here by considering the scale-up factors and issues for going from bench to field scale. The field-scale set-up is approximately seven times bigger than the bench-scale, in which experiments with iron-amended carbon were

actually run (based on g GAC and reservoir size). This factor was used to roughly scale costs to the field-scale. Table XXIII summarizes the results from the bench-scale trials, discussed previously (see bench-scale section). The last column shows the estimated demand for H_2O_2, scaled-up to field dimensions. If the iron-amended GAC were employed in field trials, attendant costs will be significantly lower than those actually encountered. For example, if we regenerate 100 g GAC, it is estimated that 181 mL H_2O_2 will be consumed. Actual field trials utilized 1-2 L H_2O_2 when iron was provided. That is at least 8 times higher than the amount to be used if an iron-amended GAC system were implemented. In the field site studied, the SVE stream contains mainly TCE and PCE. However, the presence of other organic compounds can increase the demand for H_2O_2. Nevertheless, for ease of calculations it is assumed that the same amount of H_2O_2 will be applied in the recovery of the spent GAC when both TCE and PCE are present. Consequently, the cost of GAC regeneration for SVE-loaded GAC will be the same for both compounds, and estimations based on TCE regeneration will be applied to estimate the field-scale cost. If the iron-mounted GAC is 10 times more efficient than the soluble iron system, then the peroxide cost would be $0.62/kg GAC ($0.28/lb GAC). Under these circumstances, the iron-amended GAC regeneration is probably less expensive than replacement of spent GAC (Table XXIII). A more complete economic analysis follows.

Table XXIII. Cost Evaluation Based on Bench-Scale Results Using TCE-Loaded and Iron-Amended GAC.

GAC type	Iron Content	C/Co (TCE)	H_2O_2 (mL)	H_2O_2 (mL) scaled-up to field dimensions (estimate)
Iron-amended GAC	7.4mgFe/gGAC (5 mM)	47%	25.8	181 ($0.62/kg GAC)[+]
Iron in Solution, pH 2	10 mM	50%	160-224	1.6*

* Actual field scale trials employed 1-2 L H_2O_2 for experiments using iron in solution. Field-scale is approximately 7x bigger than bench-scale experiments. Costs can be easily calculated using the cost of H_2O_2 ($0.34/L). Field scale reservoir can be reduced in size as it was done with the bench-scale trials, reducing costs by half.

[+] Costs calculated for 181 mls H_2O_2 to regenerate 100 g GAC. Both background GAC and iron-amended GAC trials employed a 400 ml-size reservoir (less than half the size of the iron in solution experiment (1 L reservoir).

GAC Economic Analysis

The economic analysis conducted here was designed to compare alternative carbon replacement/regeneration strategies in processes using activated carbon for contaminant adsorption. In scenario #1, spent carbon is replaced with new activated carbon, and the waste carbon is disposed of as a hazardous waste. Scenario #2 differs in that carbon is periodically regenerated or, at least, partially regenerated using Fenton's reagents to destroy the adsorbed contaminants. The economic analysis was carried out by comparing costs that are unique to each scenario on both a present worth and an annual cost basis. Most of the costs from activated carbon adsorption for treatment of gas-phase streams derived from SVE (the basic scheme for both scenarios) are common to both alternatives. As such they are omitted from the analysis. These include energy costs for the SVE system, capital costs for the carbon adsorption unit, initial carbon costs and some maintenance and other labor activities. A description of the costs that are unique to each alternative follows:

	Scenario #1	Scenario #2
Carbon costs	GAC replacement cost GAC cost = $1.60/lb Disposal cost = $1.00/lb	5% loss/regeneration cycle GAC cost = $1.60/lb No disposal costs
H_2O_2 consumption	Not Applicable	$0.345/lb H_2O_2 plus transportation from Houston $3.50/mi, 1067 miles
Incremental capital for chemical dosing/storage	Not Applicable	Dosing pumps, H_2O_2 storage tanks

The scenarios were built in part from field experience in this project (H_2O_2 dosing and time to recovery) and in part based on engineering rules of thumb or professional judgment. Cost comparisons were carried out for carbon recovery when (i) PCE and (ii) methylene chloride were the target contaminants. The behaviors of these compounds during carbon regeneration were diametrically opposed. PCE provides a challenging recovery problem, presumably because of its affinity for the carbon surface and consequent slow desorption rate. Carbon recovery following methylene chloride breakthrough is remarkably fast, probably due to its low affinity for the carbon surface.

Other assumptions or data used to support the economic comparison were:

- bulk GAC density = 0.5 kg/L
- gas-flow rates during SVE = 10, 100 cfm (2 distinct analyses)
- equilibrium is assumed to exist among gas, liquid and solid phases at breakthrough during SVE
- T = 25°C
- The concentration of contaminant (PCE or MC) in the gas treated by SVE is 100 ppmv.
- GAC column diameter = 1 m
- The mass of carbon in the column is irrelevant since carbon wastage rates are calculated on the same basis for each scenario investigated
- The pump efficiency during recirculation of Fenton's reagents is 0.70.
- The economic discount operator of 0.08 was assumed
- Equipment for H_2O_2 dosing and storage has a service life of 20 years
- GAC disposal cost ($1.00/lb) is an engineering estimate
- All GAC costs are in year 2000 dollars and all other cost are in 2006 dollars

Details for the analysis, including calculations, are provided in Appendix B. Additional assumptions are exposed in the appendix. The following summary represents the annualized costs that are unique to each alternative (Table XXIV). Annual costs are provided for hypothetical SVE systems treating gas flows of 10 and 100 cfm for removal of

PCE or methylene chloride. Alternative #2 consists of in-place recovery using the Fenton-driven method investigated here.

The analysis shows that the chemical costs are in fact the dominant expense in Scenario #2 (Appendix B). The following analysis was added to this section and to Appendix B to highlight the importance of H_2O_2 purchase to the total cost in Scenario #2.

Table XXIV. Cost Estimates Comparing Hazardous Waste Disposal of Spent GAC (#1) and Virgin Carbon Replacement versus Fenton's Reagent Regeneration of GAC (#2)

Target Contaminant / **SVE Flow**	**PCE**	**MC**
10 cfm	#1: $2,545 / #2: $25,212	#1: $1.1M / #2: $0.83M
100 cfm	#1: $25,416 / #2: $239,745	#1: $11.1 M / #2: $8.2M

Note: Option 1: GAC cost = $2.60/lb. Option 2: GAC cost = $1.60/lb (no disposal), H_2O_2 cost (purchase and transportation), additional process energy, labor, and capital (recirculation pumps, chemical storage tanks).

Cost of H_2O_2 Consumption in Fenton's System

The following table (XXV) contains both total costs for each treatment alternative and the associated H_2O_2 cost in order to illustrate the importance of reagent costs to overall process economics.

Table XXV. Summary of Estimated H_2O_2 Cost Contribution to Total Cost of Fenton's Regeneration

Compound	Total H_2O_2 Cost for GAC regeneration ($/yr)		Total Annual Cost ($/yr)		Fraction of H_2O_2 Cost for GAC regeneration ($/yr)	
	Q_{air} =10 cfm	Q_{air} =100 cfm	Q_{air} =10 cfm	Q_{air} =100 cfm	Q_{air} =10 cfm	Q_{air} =100 cfm
PCE	17,966	179,495	25,212	239,745	71%	75%
MC	0.75M	7.4M	0.83M	8.2M	90%	90%

Note: All values were obtained from Appendix F.

Engineering Considerations

A number of practical considerations that may affect operation of a Fenton-driven carbon recovery system have been neglected to this point. Chief among these is (i) the generation of molecular oxygen from the decomposition reactions of H_2O_2 in the presence of iron and (ii) the exothermic character of the same reactions. In this section, each of these is analyzed using engineering tools in order to gain perspective on the magnitude of related operational difficulties.

In the case of gas-phase O_2 generation, field data on H_2O_2 consumption are combined with operational flow rates and hydrogen peroxide decomposition stoichiometry to determine the probable oxygen volume rate of flow during regeneration. For perspective, this is compared to the volume rate of flow of the regenerant stream that is necessary to expand the carbon bed during regeneration. The analysis can go only so far, however, since the effects of oxygen generation in carbon pores cannot be adequately addressed without much more study.

The engineering analysis of heat generation/transport is again based on the H_2O_2 consumption data and regenerant flow using the (known) heat of hydrogen peroxide decomposition. In this case, the regenerant flow and specific heat of water allow us to calculate the regenerant temperature rise necessary to balance the rate of heat liberation due to reaction during one pass of regenerant through the reactor during recovery. Then, based on the volume of regenerant in the storage tank and regenerant flow rate it is possible to predict the rate and extent of fluid temperature rise during recovery operations.

The methods and calculations are fully explained below.

Hydrogen Peroxide Stability

The primary factors contributing to H_2O_2 decomposition during storage include: increasing temperature (2.2 factor increase in first-order reaction rate constant for each 10°C); increasing pH (especially at pH > 6-8); increasing contamination (especially transition metals such as copper, manganese or iron); and to a lesser degree, exposure to ultraviolet light. In most cases, pH and contamination work in tandem as the dominant factors (US Peroxide, 2006). [http://www.h2o2.com/intro/faq.html]. Generally, 50% hydrogen peroxide loses less than 1% per year when stored properly (according to manufacturer's specifications.) [http://www.h2o2.com/h2o2update/volume2/hypochlorite.html] During Fenton based reactions, of course, H_2O_2 decomposition is exactly what is to be promoted.

Hydrogen peroxide often decomposes exothermically into water and oxygen gas spontaneously:

$$2H_2O_2 \rightarrow 2H_2O + O_2 + \text{Energy} \qquad (68)$$

This process is very energetically favorable; it has a $\Delta H°$ of –98.2 KJ/mol, a $\Delta G°$ of -19.2 KJ/mol and a ΔS of 70.5 J/mol °K. The rate of decomposition is dependent on the temperature, concentration of hydrogen peroxide, pH and the presence of impurities (transition metals) and stabilizers.
[Wikipedia, http://en.wikipedia.org/wiki/Hydrogen_peroxide#Decomposition].

Although pure hydrogen peroxide is fairly stable, it decomposes into water and oxygen when heated above about 80°C. [http://www.infoplease.com/ce6/sci/A0824724.html]

The Heat of H_2O_2 Decomposition

Accumulation of heat in the regenerant and, as a consequence, in the carbon bed from the exothermic decomposition of H_2O_2 could be beneficial within manageable limits, but would be a problem if excessive. However, moderate heat generation and consequent temperature increases could aid the recovery process by increasing radical generation rates and the rates of temperature dependent mass transfer processes. An energy balance was used to estimate the temperature increase in the regenerant. In the balance, the average rate of heat generation by hydrogen peroxide decomposition was exactly balanced by the rate of heat loss in advective flow through the column. That is

$$\Delta H^{\circ}_{rxn}\,\dot{m}_{H_2O_2} = \rho Q C_p \Delta T \qquad \text{where}$$

$\Delta H^{\circ}_{rxn}\,\dot{m}_{H_2O_2}$ = average rate of heat generation from the H_2O_2 decomposition (J/min)

ρ = density of the solution (g/mL)

Q= flowrate through the column (mL/min)

C_p = specific heat (cal/g $^{\circ}$C)

ΔT = temperature change = $T_f - T_i$ ($^{\circ}$C)

It should be noted that $\dot{m}_{H_2O_2}$ is taken here as the average rate of H_2O_2 use during experiments that comprised the field demonstration project. H_2O_2 was unevenly applied and consumed during those experiments, however. Consequently, there will be periods in which heat is generated more rapidly and more slowly than estimated here. The average rate of heat generation provides an adequate estimate of temperature rise as long as that rate is not so rapid as to become dangerous during particularly fast reaction periods (immediately following addition of H_2O_2 to the regenerant). In fact, predicted and (field) observed rates of regenerant temperature rise proved to be modest (see below).

Furthermore, it was assumed that:

The heat capacity of the carbon and column materials could be ignored;

Radiative heat losses were comparatively small;

1. There was no cumulative heat energy in the regenerant or carbon bed (one-pass analysis);
2. Excursions from the average rate of H_2O_2 consumption and heat generation could be ignored for convenience; and
3. All reactions involving H_2O_2 other than its breakdown to water and molecular oxygen could be ignored.

Heat production:

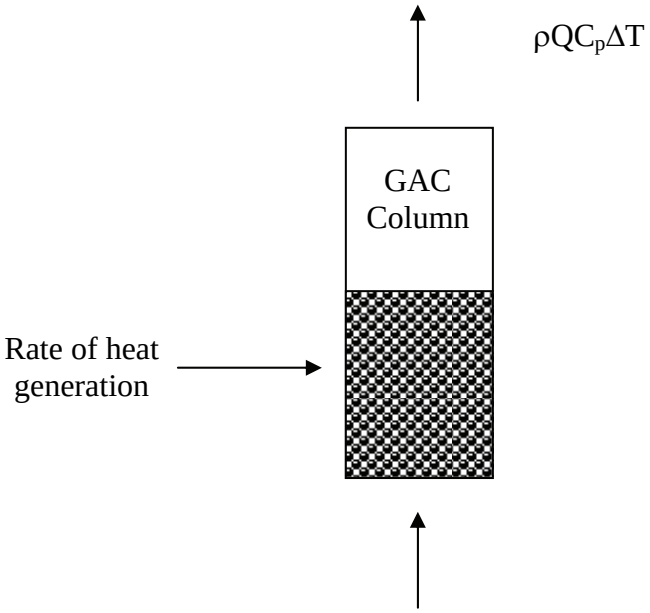

ΔH°_{rxn} is the heat of reaction at constant pressure and standard conditions

C_p=1.00 cal/g $^{\circ}$C and $\rho_{solution}$ = 1 kg/L

1 cal=4.184 J

For the reaction: $2H_2O_{2\,(l)} \rightarrow 2H_2O_{\,(l)} + O_{2\,(g)}$ ΔH_{rxn}° (KJ/mol) = 2(-286)+0-2(-187.8)= -196.4

	ΔH_f° (KJ/mol)
H_2O_2 (l)	-187.8
H_2O (l)	-286
O_2 (g)	0

Source: Fundamentals of Chemistry. Brady, J. and Holum, J. 3rd ed. John Wiley & Sons. NY:1988.

Since 2L of 50% wt/wt H_2O_2 in water (ρ = 1.2 g/ml) were used to regenerate the pilot column over a 54-hour period, the mass of H_2O_2 consumed was

$$\frac{0.50g}{g_{solution}} \times \frac{1.2g_{solution}}{mL_{solution}} \times \frac{1000mLs}{1L} \times \frac{1mol}{34g_{H2O2}} = 17.65\frac{mol}{L}$$

$$17.65\frac{mol}{L} \times 2L = 35.30molH_2O_2$$

Thus, the average rate of H_2O_2 consumption was

$$\frac{35.30 moles H_2O_2}{54 hrs} \times \frac{1 hr}{60 \min} = 1.09 x 10^{-2} moles H_2O_2 / \min$$

and the average rate of heat generation from the reaction was:

$$\frac{1.09 x 10^{-2} moles H_2O_2}{\min} \times \frac{196.4 KJ}{2 mol H_2O_2} \times \frac{1000 J}{1 KJ} = 1.07 x 10^3 J / \min$$

The rate of regenerant flow through the column was estimated at 8 L/min (field data), so that the average increase in regenerant temperature to balance the rate of heat generation was:

$$\frac{1.07 x 10^3 J}{\min} \times \frac{1 \min}{8000 mL} \times \frac{1 cal}{4.184 J} \times \frac{1 mL}{1 g} \times \frac{g^\circ C}{1 cal} = 0.032^\circ C$$

This is the temperature increment in regenerant fluid per single pass through the carbon column due to the regeneration reaction. The average detention time in the regenerant tank was about 1 minute, so that there were opportunities for heat energy to accumulate in the regenerant, immediately after one of the H_2O_2 pulses, when the decomposition reaction was most rapid. In fact, however, the reservoir temperature never exceeded 52°C, after an overnight low of 36°C, suggesting that the regeneration system can be conveniently regulated through management of the H_2O_2 addition rate.

In an hour, without any regenerant cooling, the temperature rise would be

$$\Delta T_{1hr} = \frac{60 \min}{hr} \times \frac{8 L / \min}{7 L} \times 0.032^\circ C = 2.2^\circ C$$

The field reaction was operated for 7-hour periods with consequent temperature changes of about 16°C, or 2.2°C/hr, suggesting that the analysis is valid. However, the rate of H_2O_2 use during the 7-hr daylight periods was about 3x the average daily rate, so that perhaps two-thirds of the heat generated is unaccounted for in the regenerant fluid.

Oxygen Formation via Fenton's Reactions:

The mechanism proposed by De Laat and Gallard (1999) describes in detail the reactions that result in oxygen formation. Depending on the pH of the solution, $HO_2\bullet$/ $O_2\bullet^-$ will react with iron to generate oxygen.

$$Fe(III) + HO_2\bullet \rightarrow Fe^{2+} + O_2 + H^+ \qquad k_{11a} < 2 \times 10^3\ M^{-1}\ s^{-1}$$

$$Fe(III) + O_2\bullet^- \rightarrow Fe^{2+} + O_2 \qquad k_{11b} = 5 \times 10^7\ M^{-1}\ s^{-1}$$

$HO_2\bullet + HO_2\bullet \rightarrow H_2O_2 + O_2$	$k_{13a} = 8.3 \times 10^5\ M^{-1}\ s^{-1}$
$HO_2\bullet + O_2\bullet^- + H_2O \rightarrow H_2O_2 + O_2 + OH^-$	$k_{13b} = 9.7 \times 10^7\ M^{-1}\ s^{-1}$
$\bullet OH + HO_2\bullet \rightarrow H_2O + O_2$	$k_{14a} = 0.71 \times 10^{10}\ M^{-1}\ s^{-1}$
$\bullet OH + O_2\bullet^- \rightarrow OH^- + O_2$	$k_{14b} = 1.01 \times 10^{10}\ M^{-1}\ s^{-1}$

Given the typical conditions under which these reactions occur, however, radical-radical recombination reactions are not a significant source of oxygen. Consequently, oxygen production is estimated according to the overall hydrogen peroxide decomposition reaction (above) resulting in liquid water and oxygen gas formation. This analysis ignores

1. Compressibility effects
2. Dissolved oxygen transport in the regenerant
3. Temperature effects

Stoichiometrically, $2H_2O_2$ molecules generate one molecule of oxygen during decomposition:

$$2H_2O_{2\,(l)} \rightarrow 2H_2O_{\,(l)} + O_{2\,(g)}$$

From previous calculations based on the average rate of H_2O_2 decomposition, 2L of 50% wt/wt H_2O_2 in water were used to regenerate the pilot column over each 54-hour period. The average rate of O_2 production was therefore

$$\frac{35.30 moles H_2O_2}{54 hrs} \times \frac{1 mol O_2}{2 mol H_2O_2} \times \frac{1 hr}{60 \min} = 5.45 x 10^{-3} moles O_2 / \min$$

Normalized to the rate of flow of water:

$$\frac{5.45 x 10^{-3} moles O_2}{\min} \times \frac{32000 mg O_2}{mol O_2} \times \frac{\min}{8 L} = 21.8 mg O_2 / L$$

Now, the solubility of oxygen in water can be calculated as follows:

$$P_{O2} = 1 atm$$

Using Henry's law, the concentration of oxygen dissolved in water is

$$[O_2] = K_H P_{O2}$$

where K_H = Henry's law constant =0.0012630 M·atm (From Table 2.4 at T=25°C. Introduction to Environmental Engineering and Science. 2nd Ed. Masters, G. Prentice Hall. New Jersey, 1998.)

$$[O_2] = 0.0012630\,M \cdot atm \times 1atm = 0.0012630\,M \times \frac{32000\,mg}{mol} = 40.4mg/L$$

$[O_2] = 40.4mg/L$ (at equilibrium with pure O_2 gas at a total pressure of 1 atm.).

The concentration of oxygen for a pure oxygen saturated solution at 25°C is about 40 mg/L, which means that the oxygen concentration produced from the decomposition of hydrogen peroxide does not exceed (21.8mg/L < 40 mg/L) the solubility of oxygen in water.

The oxygen concentration was calculated for the 54-hour period of regeneration. In general, the hydrogen peroxide was added over short periods (30 min) followed by longer periods (6 hours) in which hydrogen peroxide was exhausted and the target compound was allowed to desorb from the GAC. Thus, oxygen formation rates were considerably higher during those short periods. The likely formation of O_2 gas bubbles, which was actually observed in the lab and field experiments, indicates that course media should be used and that the GAC bed should be expanded during regeneration to aid in the release of gas bubbles from the column.

Field-Scale Regeneration Trials-Summary

- The data and analysis suggest that intraparticle diffusion or desorption from the solid phase of the contaminant is a limiting factor in the second, slow phase of degradation.
- The following table contains bench- and field-scale recovery data that reflect the ease or speed of column recovery when respective compounds have initially saturated carbon adsorption sites. The consensus of the study group regarding the source of rate limitation during the recovery process is as indicated (Table XXVI).

Table XXVI. Summary of Efficiency Results for Fenton's Reagent Regeneration of GAC in Bench and Field Trials

Compound	Percentage Removed from GAC (%)		Controlling Mechanism
	Bench-scale (14 hrs @ 32C)	Field scale (7-54 hours)	
Methylene Chloride (MC)	99	98 (7 hrs) 99 (30 hrs)	Radical Reaction rate
1,2-DCA	98	N/A	Radical Reaction rate
1,1,1-TCA	67	N/A	Desorption or pore diffusion
Chloroform (CF)	93	82 (7 hrs) 93 (29 hrs)	Radical Reaction rate
Carbon Tetrachloride (CT)	73 @25C	N/A	Desorption or pore diffusion
Trichloroethylene (TCE)	52	73-95 (50-54 hrs)*	Desorption or pore diffusion
Perchloroethylene (PCE)	35	50 (52 hrs)	Desorption or pore diffusion

*depending on H_2O_2 application frequency (see Field-scale Results Section).

- GAC was preloaded with methylene chloride (MC) and chloroform (CF) for field-scale regeneration experiments. H_2O_2 was added hourly between hours 0-6 and 23-28. The reduction of solid-phase CF was 93% after 30 hours. Residual MC could not be detected.
- GAC was loaded with trichloroethylene (TCE) in the laboratory and regenerated in the field in three successive loading/regeneration cycles. In each cycle, the solid-phase TCE concentration decreased by >50% in the first 4 hours. After 60 hours, however, carbon recoveries ranged from 73-95%. No loss of adsorption capacity was observed during the overall period of the experiment. H_2O_2 was added intermittently during regeneration. By allowing the bulk aqueous-phase contaminant concentration to approach equilibrium levels prior to H_2O_2 addition, it may be possible to minimize H_2O_2 costs. Since recovery appears to be limited by compound desorption at least in some cases, accumulation of the target in the aqueous phase prior to H_2O_2 addition is likely to minimize chemical costs.
- Temperature in the field reactor was observed to increase from an ambient value of about 30°C to 55-60°C during a 60-hour regeneration period. Because VOC mass transport and reaction kinetics are favorably affected by higher temperatures, the exothermic decomposition of H_2O_2 could, if handled carefully, increase carbon recovery rates and lower overall costs for carbon surface regeneration.
- PCE, TCE and light diesel contaminants from the field site soil vapor extraction system were used to load URV-MOD 1 GAC in a final set of field experiments. A 6-hour regeneration trial reduced the adsorbed TCE concentration by 80%, but PCE by only 30%. H_2O_2 was added periodically but without any attempt to minimize chemical consumption.
- A scoping-level economic analysis was conducted, based on regeneration of PCE-loaded GAC. PCE presents the most challenging recovery situation in terms of recovery kinetics. The cost for Fenton-based regeneration, determined from results of bench-scale studies (~$2.70/lb), was comparable to that of conventional thermal regeneration (~$2.60/lb) and new carbon replacement (~$3.30/lb). The cost of Fenton regeneration based on the field trials was higher (~$6.50/lb), but this cost may not represent operational cost following optimization of chemical addition frequency. There was no attempt to minimize H_2O_2 consumption, the primary cost-driver, in the field trial. Further study in this are is recommended.
- It may be possible to both minimize unproductive H_2O_2 consumption and to shift the operational pH range for carbon recovery by precipitating iron on the carbon surface prior to use in adsorption/recovery operations. The feasibility of such a scheme depends on selection of iron loadings that allow degradation reactions to proceed without blocking carbon pores, interfering with contaminant access. Bench-scale trials were carried out. Although field-scale trials using iron-amended GAC were not conducted, a first-cut, estimate of H_2O_2 cost ($0.34/L) was undertaken. The analysis suggests that iron-amended GAC regeneration costs would be ~$0.28/lb GAC, or about 10-fold lower than the cost of thermal carbon regeneration or GAC replacement.

Summary and Recommendations for Additional Study

General Observations

Data suggest that a single mechanism does not control the rate of VOC-loaded carbon regeneration by Fenton's mechanism for all contaminants. Weakly adsorbed compounds with relatively low reactivity with •OH, like chloroform, can be limited by reaction in the bulk aqueous phase. Less soluble, more reactive compounds like TCE are limited by intraparticle transport, and the desorption reaction rate may also play a role in the most strongly bound compounds (e.g., PCE). For compounds with limited solubility, for example, intraparticle aqueous concentrations of the sorbate may be much lower than their equilibrium levels. Under these circumstances, surface diffusion may be the predominant mechanism of sorbate transport to the particle exterior. Surface effects resulting from pore volume distribution may prove to be significant as well. As pore dimensions approach the molecular size of the contaminant, it is anticipated that surface diffusion mechanisms limit transport kinetics. It is known from literature that in micropores found in zeolites (Ruthven, 1984), surface diffusion is the dominant transport mechanism, while pore diffusion dominates in macropores (Ma *et al.*, 1996). Results lead the investigators to conclude that mass transport mechanisms limit the effectiveness of Fenton's reaction for carbon recovery, at least for slightly soluble compounds that are reactive with Fenton's reagents. Therefore, optimal design of this type of treatment would maximize contaminant flux from the sorbent while minimizing the use of H_2O_2, the primary contributor to process cost. Just how this is done will probably be compound specific. Pulsed addition of H_2O_2 probably offers advantages over continuous maintenance of a target H_2O_2 concentration when mass transport governs the carbon recovery rate. Temperature management may be an essential issue inasmuch as the kinetics of physico-chemical processes that determine recovery rate are temperature dependent and the Fenton reactions are exothermic. Fenton-based carbon regeneration was shown to be cost competitive for VOCs of modest binding strength on GAC but was not clearly cost effective for strongly binding VOCs. However, the cost efficiency can be improved substantially by implementing the design/operational changes discussed. Additional cost saving may be possible by directing radical-generating reactants to the carbon surface. Selection of carbon (or other sorbents) with a pore size distribution that minimizes mass transfer limitations should also be considered.

The specific project findings on which this summary discussion is based follow.

Homogeneous, Bench-Scale Experiments

- Tetrachloroethylene (PCE) degradation followed first order kinetics in which the rate constant was a function of total iron in the Fenton system. The reaction proceeds with essentially no lag following the addition of H_2O_2, indicating that near steady concentrations of iron species and hydroxyl radical are established quickly.
- The initial rate of PCE degradation was increased by more than an order of magnitude by the addition of hydroxylamine hydrochloride, a strong reductant. However, the rate enhancement could not be sustained, indicating that hydroxylamine was consumed in the reaction. The result supports the research consensus that Fe(III) reduction to Fe(II) via H_2O_2 consumption limits the radical production rate in the Fenton system.
- Quinones are known electron shuttles that can facilitate iron reduction. 1,4-hydroquinone (HQ), 1,4-benzoquinone (BQ) and 9,10-anthraquinone-2,6-disulfonic acid all initially increased PCE degradation in Fenton's system. The increase was proportional to quinone concentration. However, as with hydroxylamine addition, the rate enhancement was not sustained, probably reflecting the gradual destruction of the quinone. After quinine addition, the PCE degradation rate eventually stabilized at a rate that was slower than that of the unamended Fenton's system, suggesting that the by-products of quinone degradation retarded the contaminant degradation rate.
- PCE degradation ceases if Cu(II) replaces Fe(III) in the Fenton's system. However, if both copper and iron are present in a Cu:Fe ratio of 2, the rate of PCE degradation increases by a factor of 4.3. This accelerated rate was steady over the course of the experiments. Among the possible mechanistic explanations, Cu(II) may be reduced to Cu(I) via H_2O_2 consumption after which the conversion of Cu(I) to Cu(II), Cu(I) reduces Fe(III) to Fe(II). The hypothesized mechanism may provide a more rapid pathway for iron reduction than reaction of Fe(III) with H_2O_2 in the Fenton system. Although the ability of copper to accelerate PCE degradation is modest, Cu(II) solubility is greater than that of iron, and copper may provide greater benefit in the pH range where the iron concentration solubility in Fenton's system is limited.
- The first-order rate constant for PCE degradation increased more rapidly with temperature in the copper:iron system than in the Fe-only Fenton system. Thus, the benefit of copper addition will be increased for Fenton's reactor systems operating above ambient temperature.
- A homogeneous-phase kinetic model was formulated based on earlier work by De Laat and Gallard (1999), in which the rate constant for Fe(III)-hydroperoxy complex reduction is the sole fitted parameter. Although model simulations were in qualitative agreement with results generated here, there were several noteworthy quantitative departures between model and experiment. It is suspected that the fitted rate constant requires revision based on the substantially lower ionic strength in the present work and the insensitivity of the fitted rate constant to pH in the De Laat and Gallard case.
- As chlorinated VOCs are degraded in a Fenton's system, chloride anions build up in the regenerant solution. Literature rate constants for the reaction of the hydroxyl radical and chloride indicate that chloride

accumulation should significantly retard VOC degradation rates. However, model simulations using the literature rate constant overestimate the chloride impact observed in the experimental trials. Additional modeling efforts using a fitted rate constant for the •OH/Cl^- reaction are in progress.

- The rate of PCE degradation by Fenton's system increases with increasing pH in the range 1 to 3. Above pH 3, decreased iron solubility limits free iron availability and, consequently, limits the rate of degradation. Measured PCE degradation rates at $0.9 < pH < 3.0$ were not in good agreement with the model results although predicted and observed trends in pH-dependent data are similar. At every pH (except pH = 0.9), the model over-predicts the PCE transformation rate.
- The rate of carbon tetrachloride (CT) degradation was increased by the addition of isopropanol (IP), a •OH scavenger. The work strongly suggests CT degradation occurs via superoxide radical ($O_2•^-$) attack in Fenton's system. Literature studies suggest the increase in rate may be due to a co-solvency effect due to IP addition that increases $O_2•^-$ activity.
- PCE degradation by Fenton's reagents was negligible in the presence of IP, which indicates PCE destruction occurs via hydroxyl radical (•OH) attack. No chlorinated intermediate or final products were detected. PCE degradation diminished modestly at the highest concentration of chloride added (0.0288 M). However, at a concentration near 1 mM, Cl^- had essentially no effect on PCE transformation kinetics.

Heterogeneous, Bench-Scale Experiments

- Ethyl acetate was the best solvent tested for solid:liquid extraction of PCE from GAC. An extraction duration of 12 hours provided practically complete extraction.
- Contaminant degradation kinetics in a heterogeneous Fenton's system (VOC loaded on GAC) follow bi-phasic, first-order kinetics. A fast initial phase was followed (after 1-3 hours) by a slower second phase. The fraction of total contaminant degraded in the rapid initial phase increased with the aqueous-phase solubility of the contaminants. The data and analysis suggest intraparticle diffusion or desorption of the contaminant is a limiting factor in the second, slow phase of degradation.
- When chloroform (CF) -loaded GAC was rapidly flushed with fresh water, the rate of CF loss increased as the size of the GAC particles on which it was adsorbed decreased. These results suggest that pore and/or surface diffusion, affect the overall removal kinetics.
- A mass transfer model in which it was assumed that solid:liquid equilibrium exists throughout the porous carbon particles (kinetics are not limited by the desorption reaction rate) was formulated to simulate mass transfer of contaminants in the heterogeneous system. Analytical solutions were developed when contaminant adsorption was governed by a linear isotherm. A single fitting parameter (tortuosity) brought simulations and data into reasonable agreement. However, a common tortuosity could not be obtained for all compounds, suggesting that desorption effects limit GAC recovery kinetics for some contaminants.

- Based on experimental and model results, it is concluded that mass transport mechanisms limit the effectiveness of Fenton's reaction for carbon recovery, at least for slightly soluble compounds (e.g., PCE) that are reactive with Fenton's reagents. Therefore, optimal design for this type of treatment would maximize contaminant flux from the sorbent while minimizing the use of H_2O_2, the primary contributor to process cost.
- Trials were conducted using Calgon URV-MOD 1 carbon on which iron had been precipitated onto the pore and outer surfaces. No iron was added to the bulk regenerant (Fenton's solution). This was to localize the Fenton's-driven radical generation near the GAC surface and the desorbing VOC targets, to minimize the rate limitation due to desorption or pore and surface diffusion. However, negligible improvement in the rate of carbon recovery was observed compared to the rate observed using non-iron-amended carbon. The rate of H_2O_2 usage, the primary driver in operating cost of the system, was decreased by about three-fold in the iron-amended system.

Field-Scale Regeneration Trials

- GAC was preloaded with methylene chloride (MC) and chloroform (CF) for field-scale regeneration experiments. H_2O_2 was added hourly between hours 0-6 and 23-28. The reduction of solid-phase CF was 93% after 30 hours. Residual MC could not be detected.
- GAC was loaded with trichloroethylene (TCE) in the laboratory and regenerated in the field using Fenton's reagents through three loading/regeneration cycles. In each regeneration cycle, an initial loss of over 50% of the TCE occurred in the first 4 hours, and after 60 hours TCE recovery was 73-95%. No loss of adsorption capacity was observed after three GAC regenerations. H_2O_2 was added intermittently during regeneration. Analysis indicates H_2O_2 additions timed to allow the bulk aqueous contaminant concentration to reach near-equilibrium levels would minimize H_2O_2 cost.
- Temperature in the field reactor increased from an ambient value of about 30°C to 55-60°C during a 60-hour regeneration period. Because VOC mass transport and reaction kinetics are favorably affected by higher temperatures, the exothermic decomposition of H_2O_2 could increase carbon recovery rates and lower overall costs for carbon surface regeneration.
- PCE, TCE and light diesel contaminants from the field site soil vapor extraction system were used to load URV-MOD 1 GAC in a final set of field experiments. A 6-hour regeneration trial reduced adsorbed TCE by 80%, but PCE recovery was only 30%.
- A scoping-level economic analysis was conducted, based on regeneration of PCE-loaded GAC (the most challenging case investigated). The cost for Fenton Reagent regeneration based on the bench-scale studies (~$2.70/lb) was comparable to that for conventional thermal regeneration (~$2.60/lb) and new carbon replacement (~$3.30/lb). The cost of Fenton regeneration based on the field trials was higher (~$6.50/lb), but this

may be a considerable overestimate since the primary cost driver, H_2O_2 consumption, was not optimized to any extent in the field trial. Further tests in this regard are needed.

- It may be possible to immobilize iron on the carbon surface and regenerate in a pH range to avoid iron dissolution during recovery operations. The feasibility of such a scheme depends on selection of iron loadings that allow degradation reactions to proceed without blocking the carbon surface or interfering with contaminant access to carbon pores. Field-scale trials using iron-amended GAC were not conducted. The results of bench-scale experiments were used to estimate recovery costs in the iron-amended carbon systems. Projected regeneration costs, ~$0.28/lb GAC, were approximately 10-fold lower than the cost of thermal regeneration or GAC replacement.

Data Quality and Limitations

The data presented in this report was gathered using the procedures and tools detailed in the Quality Assurance Project Plan (QAPP) submitted prior to project initiation. None of the procedures detailed in the QAPP were required to be modified during the subsequent execution of the project. Consequently, there are no limitations on the use of the data related to its original intended application beyond the following specific instances considerations.

- Using isopropanol as a hydroxyl radical scavenger, the experimental work was able to establish that tetrachloroethylene was degraded in the Fenton's system by hydroxyl radical attack. However, because no specific superoxide radical scavenger could be identified that itself was not subject to hydroxyl radical attack, the work was not able to conclusively indicate that other halogenated VOCs, such as carbon tetrachloride, are degraded by superoxide attack. The experimental results suggest that this is the case, but other possible mechanisms cannot be completely ruled out.
- Considerable work was undertaken in modeling both the homogeneous and heterogeneous system degradation of VOCs by Fenton's reagents. This work is largely beyond the original scope of the project and was undertaken as a no cost extension of benefit to the project. Quality control and assurance for the modeling approach was not detailed in the QAPP. Details of the approach, computer code, mathematical algorithms, model assumptions and sources of input data are provided in Appendix A. In an effort to validate the homogeneous model functioning, the project model was used to simulate the data and model fit from the study by De Laat and Gallard (1999). The De Laat and Gallard study was conducted in a much higher ionic strength and lower iron environment than the current work. The project model was successful in simulating the literature study data, yet when the model was used to simulate data generated in the conditions of interest in this project, the agreement was not nearly as good. Several efforts that were made to reconcile the issue are detailed earlier, including temperature corrections, ionic strength corrections and chloride concentration adjustments. Although the fit improved with these revisions, the model is still not considered ready for use as a predictive tool and should not be applied unless first

validated for a data set with the appropriate water composition conditions as will be used in the model. Recommendations for addressing this shortcoming are given later in this section.

- The economic analysis reported was based (unless otherwise specified) on the results from the pilot-scale treatment unit deployed in the field. Only very limited efforts were made to optimize this system, particularly with respect to H_2O_2 use, which is the primary driver of the technology's cost. This fact coupled with the observation that H_2O_2 use in the field was greater than 5-fold higher (per mass of carbon regenerated) than in the lab trials, suggests that the cost estimates for the Fenton's based system over-estimate the real cost of the technology deployment.

Research Recommendations

Based on this work and the perspective provided by other investigators it is possible to recommend additional, follow-on research in a number of areas. These are:

1. Despite the contributions of De Laat and co-workers, uncertainties remain in details of both the Fenton mechanism itself and its application for destruction of organic contaminants. The primary uncertainties from the perspective of advanced oxidation processes include (i) the respective roles of hydroxyl and superoxide radicals in transforming specific halogenated contaminants (e.g. CCl_4 and PCE) and (ii) matrix effects on process kinetics and efficiency – that is, those imposed by non-target organics, partial degradation products and reactive anions like Cl^- and SO_4^{2-}. Extension of the De Laat kinetic model to more chemically complex waters depends on reasonable representation of radical reaction kinetics with a variety of chemical species that are usually omitted for simplicity. Difficulty in matching chloride-dependent reaction kinetics with model predictions using published rate constants is apparent in this work. This is unfortunate in light of the obvious importance of chloride ion concentrations in the context of our investigation.
2. A reinforced De Laat chemical model can be used to help understand the accelerating effects of copper and isopropanol additions that were observed in this work. In neither case are we able to offer a convincing mechanism for compound-dependent changes in reaction kinetics, and explanations remain speculative. Without additional work, the potential benefits of copper and cosolvent addition in Fenton-based advanced oxidation systems are unlikely to be realized.
3. Certain other minor additions to the homogeneous Fenton model would be helpful. In particular, an easy way to incorporate effects due to solution ionic strength and temperature could be important.
4. A great deal remains to be learned in the heterogeneous application of Fenton chemistry for carbon recovery. That is, the roles of transport and reaction on overall recovery kinetics have not been fully sorted out, as indicated by the inability to model recovery kinetics using the simplified approach adopted to date. Pore diffusion is an unlikely controlling process for tightly held contaminants like PCE and the relative

roles of pore diffusion and surface diffusion on intraparticle transport have not been sorted out. Desorption kinetics need to be considered for such compounds (PCE, TCE) in the next modeling attempts.

5. Field operations provide yet another level of uncertainty that has not yet been fully evaluated. It is evident that process economic feasibility depends on the efficient use of H_2O_2 for contaminant destruction, but additional work is necessary to find a target-dependent H_2O_2 feed rate to promote such efficiency. A systems approach to H_2O_2 scheduling and additional verifying experiments seem warranted.
6. Provision of Fe on the carbon surface provides operational possibilities (pH>3.0, soluble Cu(II) provision to enhance kinetics, cosolvent effects) that have not yet been investigated. Much more effort here is warranted.
7. The full breadth of compounds that can be destroyed in place following carbon adsorption has not yet been identified. Reactivity with •OH seems not to be the most important issue, as indicated by the relative success in previous NDMA experiments and the apparent stubbornness of PCE to Fenton-based recovery. A through examination of compound parameters that affect the recovery kinetics for specific compounds would be useful.
8. The presence of reactive co-contaminants on carbon to be regenerated using the propanol Fenton-based technology may have consequences that have not yet been investigated.

References

Adams, J.Q. and R.M. Clark. (1989) Cost estimates for GAC treatment systems. *J. AWWA*, 35-41.

Arnold, S., Hickey, W. and Harris, R. (1995). Degradation of Atrazine by Fenton's Reagent: Condition Optimization and Product Quantification. *Environ. Sci. Technol*., *29*, 2083-2089.

ATSDR Information Center (last updated on June 22, 2001), ATSDR-Public Health Statements: Tetrachloroethylene, URL http://atsdr1.atsdr.cdc.gov/ToxProfiles/phs8822.html.

Bansal, R., Donnet J. and Stoeckli F. (1988). *Active Carbon*, New York: Marcel Dekker, Inc.

Bercik, L., (2003). "Heterogeneous Degradation of Chlorinated Solvents via Fenton's Reaction". Masters Thesis, University of Arizona.

Betterton, E., Hollan, N., Arnold, R., Gogosha, S., Mckim, K. and Liu, Z. (2000). Acetone-Photosensitized Reduction of Carbon Tetrachloride by 2-Propanol in Aqueous Solution. *Environ. Sci. Technol.*, *34*, 1229-1233.

Boltz, D. and Holwell, J. (1978). *Colorimetric Determination of Nonmetals*, 2nd. Edition, Chemical Analysis 8; John Wiley and Sons, Inc.: New York, p 543.

Burbano, A., Dionysiou, D., Suidan, M., and Richardson, T. (2005). Oxidation kinetics and effect of pH on the degradation of MTBE with Fenton reagent. *Water Research*, 39, 107-118.

Buxton, G., Greenstock, C., Helman, P. and Ross, A. (1988). Critical Review of Rate Constants for Reactions of Hydrated Electrons, Hydrogen Atoms and Hydroxyl Radicals (OH/O). *J. Phys. Chem. Ref. Data*, Vol. 17, No. 2, p 513.

Carman, P., (1956). *Flow of Gases through Porous Media*, Academic Press, New York, N.Y.

Casero, I., Sicilia, D., Rubio, S. and Pérez-Bendito, D. (1997). Chemical Degradation of Aromatic Amines by Fenton's Reagent. *Wat. Res.* Vol. 31, No. 8, pp. 1985-1995.

Chen R. and Pignatello JJ. (1997). Role of quinone intermediate as electron shuttles in Fenton and Photoassisted Fenton Oxidations of Aromatic compounds. *Environ. Sci. Technol*., 31, 2399-2406.

Chen, G., Hoagb, G., Chedda, P., Nadim, F., Woody, B. and Dobbs, G.(2001). The mechanism and applicability of in situ oxidation of trichloroethylene with Fenton's reagent. *J. Haz. Mat.* 171-186.

Clark, J. (2002) (December, 2005). The Electrochemical Series, URL http://www.chemguide.co.uk/physical/redoxeqia/ecs.html#top.

Clean Harbors Environmental (2004). Clean Harbors Environmental Services, Inc. 1 Hill Avenue, PO Box 859048, Braintree, MA 02185-9048, ph: 781-792-5000. Personal (email) communications to procure hazardous waste disposal costs.

Cotton, F., Wilkinson, G., Murillo, C. and Bochmann, M. (1999). *Advanced Inorganic Chemistry*, 6th Edition, John Wiley & Sons, Inc. New York.

Crank, J. (1975). *The Mathematics of Diffusion*, Oxford University Press, New York, N.Y.

Crittenden, J., Hutzler, N., Geyer, D., Oravitz, J. and Friedman, G. (March 1986). Transport of Organic Compounds with Saturated Groundwater Flow: Model Development and Parameter Sensitivity, *J. Water Resources Research*, Vol. 22, No. 3, pp. 271-284.

Crittenden, J.C., Hand, D.W., Arora, H. and Lykins, B.W. (1987). Design Considerations for GAC Treatment of Organic Chemicals. *J. AWWA. 79*, No. 1, 74-82.

Crittenden, J.C., Cortright, R.D., Rick, B., Tang, S.R. and Perram, D. (1988). Using GAC to Remove VOCs From Air Stripper Off-Gas. *J. AWWA.* 80, 73-84.

De Laat, J. and Gallard, H. (1999). Catalytic Decomposition of Hydrogen Peroxide by Fe(III) in Homogeneous Aqueous Solution: Mechanism and Kinetic Modeling, *Environ. Sci. Technol.* 33, 2726-2732.

De Laat, J. and Giang Le, T. (2005). Kinetics and Modeling of the Fe(III)/H_2O_2 System in the Presence of Sulfate in Acidic Aqueous Solutions. *Environ. Sci. Technol*., *39*, 1811-1818.

De Laat, J. and Giang Le, T (2006). Effects of Chloride Ions on the Iron(III)-Catalyzed Decomposition of Hydrogen Peroxide and on the Efficiency of the Fenton-Like Oxidation Process. *Appl. Cat. B: Environ.*, 66, 137-146.

De Laat, J., G.T. Le and B. Legube. (2004) A comparative study of the effects of chloride, sulfate and nitrate ions on the rates of decomposition of H2O2 and organic compounds by Fe(II)/H2O2 and Fe(III)/H2O2. *Chemosphere*, 55: 715-723.

De Las Casas, C., Bishop, K., Bercik, L., Johnson, M., Potzler, M., Ela, W., Sáez, A.E., Huling, S. and Arnold, R. In-Place Regeneration of GAC using Fenton's Reagents. In Clark, C. and Lindner, A. (eds), "Innovative Approaches for the Remediation of Subsurface-Contaminated Hazardous Waste Sites: Bridging Flask and Field Scales." ACS Symposium Series, accepted for publication, Feb. 2006.

DiGiano, F.A. and Weber, W. J., Jr. (1973). Sorption Kinetics in Infinite-Batch Experiments. *JWPCF*, 45, 713-725.

Duesterberg, C., Cooper, W. and Waite, T. (2005). Fenton-Mediated Oxidation in the Presence and Absence of Oxygen. *Environ. Sci. Technol*., *39*, 5052-5058.

Eaton, A., Clesceri, L. and Greenberg, A. (1995). *Standard Methods for the Examination of Water and Wastewater*; 19th Edition, Publication Office, American Public Health Association: Maryland.

Environmental and Remediation Equipment (August, 2005). URL http://www.soiltherm.com/GAC_Comparison/gac_comparison.html.

EPA (2000). *Granular Activated Carbon Adsorption and Regeneration,*EPA-832-F-00-017.

Fredrickson, J., Kostandarithes H., Li S., Plymale A. and Daly, M. (2000). Reduction of Fe(III), Cr(VI), U(VI), and Tc(VII) by Deinococcus radiodurans R1., *Appl. Environ. Microbiol.*, 66, 2006-2011.

Furuya, E., Ikeda, H., and Takeuchi, Y. (1987). *Fundamentals of Adsorption*. Engineering Foundation, New York, N.Y., 235.

Furuya, E., Chang, H., Miura, Y., Yokomura, H., Tajima, S., Yamashita, S. and Noll, K. (1996). Intraparticle Mass Transport Mechanism in Activated Carbon Adsorption of Phenols. *J. Environ. Eng*., Vol. 122, No. 10, pp. 909-916.

Gallard, H., De Laat, J. and Legube, B. (1999). Spectrophotometric Study of the Formation of Iron (III)-Hydroperoxy Complexes in Homogeneous Aqueous Solutions, *Wat. Res.*, Vol. 33, No. 13, pp. 2929-2936.

Gallard, H. and De Laat, J. (2000). Kinetic Modeling of Fe(III)/H_2O_2 Oxidation Reactions in Dilute Aqueous Solution Using Atrazine as a Model Organic Compound, *Wat. Res*. Vol. 34, No. 12, pp. 3107-3116.

Glaze, W., Kenneke, J. and Ferry, J. (1993). Chlorinated byproducts from the titanium oxide-mediated photodegradation of trichloroethylene and tetrachloroethylene in water. *Environ. Sci. Technol*., *27*, 177-184.

Grigor'ev, A., Makarov, I. and Pikaev, A. (1987). Formation of Cl_2^- in the Bulk Solution During the Radiolysis of Concentrated Aqueous Solutions of Chlorides. *High Energy Chem*., *21*, 99-102.

Haag, W.R. and Yao, C.C.D. (1992). Rate constants for reaction of hydroxyl radicals with several drinking water contaminants. *Environ. Sci. Technol., 26,*1005-1013.

Heslop, R. and Robinson, P. (1967). *Inorganic Chemistry. A Guide to Advanced Study*, 3rd Ed., Elsevier Publishing Company, Amsterdam.

Holleman, A. and Wiberg, E. (2001). *Inorganic Chemistry*, Academic Press, San Diego.

Huling, S., Arnold, R., Sierka, R. and Miller, M. (1998). Measurement of Hydroxyl Radical Activity in a Soil Slurry Using the Spin Trap -(4-Pyridyl-1-oxide)- *N-tert*-butylnitrone. *Environ. Sci. Technol*., *32*, 3436-3441.

Huling, S., Arnold, R., Jones, P. and Sierka, R. (2000a). Predicting Fenton-driven degradation using contaminant analog. *J. Environ. Eng*., pp. 348-353.

Huling, S., Arnold, R., Sierka, R., Jones, P. and Fine, D. (2000b). Contaminant Adsorption and Oxidation via Fenton Reaction, *J. Environ. Eng.*, pp. 595-600.

Huling, S., Jones, P., Ela, W. and Arnold, R. (2005a). Fenton-driven chemical regeneration of MTBE-spent GAC, *Wat. Res*. Vol. 39, No. 10, pp. 2145-2153.

Huling, S.G., Jones, P.K., Ela, W.P., Arnold, R.G. (2005b). Repeated reductive and oxidative treatments on granular activated carbon. *J. Environ. Eng*. Vol. 131, No. 2, pp. 287–297.

Huling, S., Jones, P. and Lee, T. (In Press 2007). Iron Optimization for Fenton-Driven Oxidation of MTBE-Spent Granular Activated Carbon. *Environ. Sci. Technol*.

King, RB. (2006). *Encyclopedia of Inorganic Chemistry*, 2nd. Edition, Copper: Inorganic and Coordination Chemistry; John Wiley and Sons, Inc.(online service); Chichester; Hoboken: New Jersey, p. 14.

Kommineni, S., Ela, W., Arnold, R., Huling, S., Hester, B. and Betterton, E. (2003). NDMA Treatment by Sequential GAC Adsorption and Fenton-Driven Destruction. *Environ. Eng. Sci.* Vol. 20, pp. 361-373.

Kremer, M.L. (2003) The Fenton reaction. Dependence of the rate on pH. *J. Phys. Chem. A.* 107(11): 1734-1741.

LaGrega, M., Buckingham, P., Evans, J. and Environmental Resources Management (2001). *Hazardous Waste Management*, 2nd edition. San Francisco: McGraw Hill.

Letterman, RD. (1999). *Water Quality and Treatment. A Handbook of Community Water Supplies.* Fifth Edition, Adsorption of Organic Compounds; McGraw-Hill, Inc.:New York, p. 13.3.

Liu, Z., Betterton, E. and Arnold, R. (2000). Electrolytic Reduction of Low Molecular Weight Chlorinated Aliphatic Compounds: Structural and Thermodynamic Effects on Process Kinetics. *Environ. Sci. Technol*., *34*, 804-811.

Logan, B. (1999). *Environmental Transport Processes;* John Wiley & Sons, Inc.: New York, p 654.

Lowry, G. and Reinhard, M. (2000). Pd-Catalyzed TCE Dechlorination in Groundwater: Solute Effects, Biological Control, and Oxidative Catalyst Regeneration. *Environ. Sci. Technol.,* Vol. 34, pp. 3217-3223.

Ma Z., Whitley, R. D. and Wang, N.-H. L. (May 1996). Pore and surface diffusion in multicomponent adsorption and liquid chromatography systems. *AIChE J*., Vol. 42, No. 5, pp.1244-1262.

Masarwa, M., Cohen, H., Meyerstein, D., Hickman, DL., Bakac, A. and Espenson, JH (1988). Reactions of Low-Valent Transition-Metal Complexes with Hydrogen Peroxide, Are They "Fenton-like" or Not? 1. The Case of Cu^{+}_{aq} and Cr^{2+}_{aq}., *J. Am. Chem. Soc.110*, 2493-4297.

Miller Brooks Environmental Inc. (2004). *Final Draft Park-Euclid Remedial Investigation Report,* Arizona Department of Environmental Quality, Project No. 365-0011-01, Phoenix, AZ, 707.

Morel, F. and Hering, J. (1993) *Principles and Applications of Aquatic Chemistry*, Wiley-Interscience, New York.

National Research Council (1994). Alternatives for Ground Water Cleanup, National Academy Press, Washington, DC, 315.

Noll, K. E, Gounaris, V. and Hou, W. (1992). *Adsorption Technology for Air and Water Pollution Control*, Lewis Publishers, Michigan.

Petlicki, J. and van de Ven, T. (1998). The equilibrium between the oxidation of hydrogen peroxide by oxygen and the dismutation of peroxyl or superoxide radicals in aqueous solutions in contact with oxygen. *Faraday Trans., 94*, 2763-2767.

Peyton, G., Bell, O., Girin, E. and Lefaivre, M. (1995). Reductive Destruction of Water Contaminants during Treatment with Hydroxyl Radical Processes. *Environ. Sci. Technol*., *29*, 1710-1712.

Poppe, MA. (2001). Analysis of MTBE and MTBE By-product Degradation Using Fenton-Type Reactions in a Homogeneous System. Master's Thesis, Unpublished. University of Arizona.

Prousek, J. (1995). Fenton Reaction after a Century, *Chem. Lisy,* Vol. 89, pp. 11-21.

Radiation Chemistry Data Center of the Notre Dame Radiation Laboratory (May, 2003). URL http://www.rcdc.nd.edu/.

Radiation Chemistry Data Center of the Notre Dame Radiation Laboratory (August, 2005). URL http://www.rcdc.nd.edu/.

Roberts, J. and Sawyer, D. (1981). Facile Degradation by Superoxide Ion of Carbon Tetrachloride, Chloroform, Methylene Chloride, and p,p'-DDT in Aprotic Media. *J. Am. Chem. Soc*., *103*, 712-714.

Ruthven, D. M. (1984). *Principles of Adsorption and Adsorption Processes*, Wiley-Interscience, New York.

Sedlak, D. and Andren, A. (1991). Aqueous-phase oxidation of polychlorinated biphenyls by hydroxyl radicals. *Environ. Sci. Technol*., *25*, 1419-1427.

Smith, B., Teel, A. and Watts, J. (2004). Identification of the Reactive Oxygen Species Responsible for Carbon Tetrachloride Degradation in Modified Fenton's Systems. *Environ. Sci. Technol*., *38*, 5465-5469.

Snoeyink, V. L. (1990). Adsorption of Organic Compounds, *Water Quality and Treatment*, 4th Ed., McGraw Hill, New York, N.Y., 781-875.

Stark, J. and Rabani, J. (1999). Photocatalytic Dechlorination of Aqueous Carbon Tetrachloride Solutions in TiO2 Layer Systems: A Chain Reaction Mechanism. *J. Phys. Chem. B*, *103*, 8524-8531.

Stumm, W. and Morgan, J. (1981). *Aquatic Chemistry: An Introduction Emphasizing Chemical Equilibria in Natural Waters*. 2nd ed. Wiley-Interscience, New York.

Sudo, Y., Misic, M., and Suzuki, M. (1978). Concentration dependence of effective surface diffusion coefficient in aqueous phase adsorption on activated carbon. *Chem. Eng. Sci*., 33, 1287-1290.

Suzuki, M., and Fujii, T. (1982). Concentration dependence of surface diffusion coefficient of propionic acid in activated carbon particles. *AIChE J*., 28, 380-385.

Suzuki, M., (1990). *Adsorption Engineering*, Elsevier, Amsterdam.

Swarzenbach, R., Gschwend, P. and Imboden, D. (1993). *Environmental Organic Chemistry*, John Wiley & Sons, Inc., New York, p 681.

Teel, A., Warberg, C., Atkinson, D. and Watts, R. (2001). Comparison of Mineral and Soluble Iron Fenton's Catalysts for the Treatment of Trichloroethylene. *Wat. Res*., Vol. 35, No. 4, pp. 977-984.

Teel, A. and Watts, R. (2002). Degradation of carbon tetrachloride by modified Fenton's reagent. *J. Haz. Mat*. 179-189.

Toledo, L.C., Silva, A.C.B., Augusti, R., Lago, R.M., 2003. Application of Fenton reagent to regenerate activated carbon saturated with organochloro compounds. *Chemosphere*, Vol. 50, pp. 1049–1054.

Teruya, E. (2000). Potential Regeneration of Activated Carbon Using Fenton's Reaction after MTBE Adsorption, Master's Thesis, Unpublished, University of Arizona.

U.S.EPA. Wastewater Technology Fact Sheet (2000). Granular Activated Carbon Absorption and Regeneration, U.S.EPA-Office of Water: Washington, DC, EPA 832-F-00-017.

Walling, C. (1975). Fenton's Reagent Revisited, *Acc. Chem. Res*., Vol. 8.

Walling C. and Kato S. (1971). The Oxidation of Alcohols, by Fenton's Reagent, The Effect of Copper Ion., *J. Am. Chem. Soc*., 93, pp. 4275-4280.

Watts, R., Bottenberg, B., Hess, T., Jensen, M. and Teel, A. (1999). Role of Reductants in the Enhanced Desorption and Transformation of Chloroaliphatic Compounds by Modified Fenton's Reactions. *Environ. Sci. Technol., 33*, 3432-3437.

Weber, W. J. Jr., (1972). *Physiochemical Processes*, John Wiley, New York, N.Y., 199-259.

Yang, T. Ralph (1987). *Gas Separation by Adsorption Processes*, Massachusetts, Butterworth Publishers.

Yoshida, M., Lee, B-D. and Hosomi, M. (2000). Decomposition of aqueous tetrachloroethylene by Fenton oxidation treatment, *Wat. Sci. Technol*. Vol. 42, pp. 203-208.

Zoh, K. and Stenstrom, M. (2002). Fenton oxidation of hexahydro-1,3,5-trinitro-1,3,5-triazine (RDX) and octahydro-1,3,5,7-tetranitro-1,3,5,7-tetrazocoine (HMX), *Wat. Res*., Vol. 36, pp. 1331-1341.

Appendices

Appendix A. Computer Simulation of Homogeneous System

Appendix A.1 Variable's Identification and Significance

Variables and their significance in the homogeneous model

Q1=Q(1)= [·OH]

Q2=Q(2)= [HO_2·]

Q3=Q(3)= [O_2·$^-$]

x1 = W1 = [Fe^{2+}]

x2 = W2 = [H_2O_2]

W3 = [PCE]

W4 = [Cl^-]

W5 = [CT]

x6 = Fe_{TOTAL}

x7 = [Fe^{3+}]

x9 = [$FeOH^{2+}$]

x10 = [$Fe(OH)_2^+$]

x11 = [$Fe_2(OH)_2^{4+}$]

x12 = [I_1] = [$Fe^{III}(HO_2)^{2+}$]

x13 = [I_2] = [$Fe^{III}(OH)(HO_2)^+$]

x14 = [H^+]

x15 = [SO_4^{2-}]

F1 = d [Fe^{2+}]/dt

F2 = d[H_2O_2]/dt

F3 = d[PCE]/dt

F4 = d[Cl^-]/dt

F5 = d[CT]/dt

Equilibrium constants are used to calculate the Fe(III) species. The constants were obtained directly from De Laat and Gallard (1999). The value of the equilibrium constants was employed directly without substitution of the variables.

Rate constants named as XK6 through XK15 correspond to k6 to k15 as defined by De Laat and Gallard (1999) and included in this report (Table IV).

Additional rate constants XK20 – XK25 are included to simulate reactions of organic targets with the radicals as follows:

XK20 = $k_{OH,PCE}$ PCE + OH $\rightarrow$

XK21 = $k_{OH,Cl}$ Cl^- + OH $\rightarrow$

XK22 = $k_{OH,SO4}$ $SO_4^{2-} + OH \rightarrow$

XK23 = $k_{O2,CT}$ $CT + O_2^{\cdot -} \rightarrow$

XK24 = $k_{O2,Cl}$ $Cl^- + O_2^{\cdot -} \rightarrow$

XK25 = $k_{O2,SO4}$ $SO_4^{2-} + O_2^{\cdot -} \rightarrow$

Grouping of variables to solve the Newton´s method for the steady state concentration of the radicals was employed. The terms ALPHA, BETA, GAMMA, DELTA, EPS and their equivalence are included in the coding. For example, ALPHA = W1*W2*XK7.

In this model, the concentration of Fe^{3+} was calculated by solving a quadratic equation of the total iron. AFE, BFE, CFE correspond to the a,b,c coefficients in the quadratic equation. The term DFE groups the terms inside the square root.

The terms DISC, DI1, DI2, DI3 are used in solving the matrices in the Newton´s method and Z11 – Z 45 in the Runge Kutta method.

Appendix A.2 Fortran Code for Non-Chlorinated Compounds

```
C*********************************************************************
*
C
*
C   RUNGE-KUTTA FOR SYSTEMS OF DIFFERENTIAL EQUATIONS ALGORITHM 5.7
*
C
*
C*********************************************************************
*
C
C
C
C     TO APPROXIMATE THE SOLUTION OF THE MTH-ORDER SYSTEM OF FIRST-
C     ORDER INITIAL-VALUE PROBLEMS
C              UJ' = FJ(T,U1,U2,...,UM), J=1,2,...,M
C           A <= T <= B, UJ(A)=ALPHAJ, J=1,2,...,M
C     AT (N+1) EQUALLY SPACED NUMBERS IN THE INTERVAL [A,B].
C
C     INPUT ENDPOINTS A,B; NUMBER OF EQUATIONS M; INTIAL
C           CONDITIONS ALPHA1,...,ALPHAM; INTEGER N.
C
C     OUTPUT APPROXIMATIONS WJ TO UJ(T) AT THE (N+1) VALUES OF T.
C
      DOUBLE PRECISION, DIMENSION(3,4) :: AA
      DOUBLE PRECISION, DIMENSION(3) :: Y
      DOUBLE PRECISION, DIMENSION(3) :: Q
      CHARACTER NAME1*30,BB*1
      INTEGER OUP,FLAG
      LOGICAL OK

      DOUBLE PRECISION X1,X2,X6,X7,X9,X10,X11,X12,X13,X14,X15
      DOUBLE PRECISION XK6,XK7,XK8,XK9,XK10A,XK10B,XK11A,XK11B,XK12A
      DOUBLE PRECISION XK12B,XK13A,XK13B,XK14A,XK14B,XK15,XK20
      DOUBLE PRECISION W1,W2,W3,TOL,ALPHA,BETA,GAMMA,DELTA,EPS,R,U
      DOUBLE PRECISION AFE,BFE,CFE,DFE,DISC,DI1,DI2,DI3
      DOUBLE PRECISION Z11,Z12,Z13,Z21,Z22,Z23,Z31,Z32,Z33,Z41,Z42,Z43


C     CHANGE FUNCTION F1 THROUGH F5 FOR A NEW PROBLEM
C     NOTE: THIS VERSION IS TO BE USED FOR NON-CHLORINATED COMPOUNDS.
C           HCOOH REACTS ONLY WITH OH AND NO BY-PRODUCT REACTIONS ARE
CONSIDERED.
C     F1=Fe2+, F2=H2O2, F3=HCOOH OR ANY OTHER ORGANIC COMPOUND
      F1(T,X1,X2,Q1,Q2,Q3,X7,X9,X10,X11,X12,X13) = 2.7d-03*(X12+
      *X13)-63.d0*X1*X2-3.2d08*X1*Q1-1.2d06*X1*Q2-1.0d07*X1*Q3+
     *1.0d03*(X7+X9+X10+2*X11)*Q2+5.0d07*(X7+X9+X10+2*X11)*Q3
      F2(T,X1,X2,Q1,Q2,Q3) = -63.d0*X1*X2-3.3d7*X2*Q1+
      *8.3d5*Q2*Q2+9.7d7*Q3*Q2+5.2d9*Q1*Q1
      F3(T,W3,Q1)= -XK20*W3*Q1

      OPEN(UNIT=5,FILE='CON',ACCESS='SEQUENTIAL')
      OPEN(UNIT=6,FILE='CON',ACCESS='SEQUENTIAL')
C     DEFINE FUNCTIONS F1,...,FM
      WRITE(6,*) 'This is the Runge-Kutta Method for systems with m=2.'
      WRITE(6,*) 'Remember to modify the function according to the
rxns'
```

```
      WRITE(6,*) 'Enter Y or N '
      WRITE(6,*) ' '
      READ(5,*)  BB
      IF(( BB .EQ. 'Y' ) .OR. ( BB .EQ. 'y' )) THEN
         OK = .FALSE.
10       IF (OK) GOTO 11
            WRITE(6,*) 'Input left and right endpoints separated by'
            WRITE(6,*) 'blank'
            WRITE(6,*) ' '
            READ(5,*) A, B
            IF (A.GE.B) THEN
               WRITE(6,*) 'Left endpoint must be less'
               WRITE(6,*) 'than right endpoint'
            ELSE
               OK = .TRUE.
            ENDIF
         GOTO 10
11       OK = .FALSE.
c         WRITE(6,*) 'Input the TWO initial conditions.'
c        WRITE(6,*) ' '
c         READ(5,*) W1, W2
12       IF (OK) GOTO 13
            WRITE(6,*) 'Input a positive integer for the number'
            WRITE(6,*) 'of subintervals '
            WRITE(6,*) ' '
            READ(5,*) N
            IF ( N .LE. 0 ) THEN
              WRITE(6,*) 'Must be positive integer '
            ELSE
              OK = .TRUE.
            ENDIF
         GOTO 12
13       CONTINUE
      ELSE
         WRITE(6,*) 'The program will end so that the functions'
         WRITE(6,*) 'F1-F5 can be created '
         OK = .FALSE.
      ENDIF
      IF(.NOT.OK) GOTO 400
      WRITE(6,*) 'Select output destination: '
      WRITE(6,*) '1. Screen '
      WRITE(6,*) '2. Text file '
      WRITE(6,*) 'Enter 1 or 2 '
      WRITE(6,*) ' '
      READ(5,*) FLAG
      IF ( FLAG .EQ. 2 ) THEN
         WRITE(6,*) 'Input the file name in the form - '
         WRITE(6,*) 'drive:name.ext'
         WRITE(6,*) 'with the name contained within quotes'
         WRITE(6,*) 'as example:   ''A:OUTPUT.DTA'' '
         WRITE(6,*) ' '
         READ(5,*) NAME1
         OUP = 3
         OPEN(UNIT=OUP,FILE=NAME1,STATUS='NEW')
      ELSE
         OUP = 6
      ENDIF
      WRITE(OUP,*) 'RUNGE-KUTTA AND NEWTON METHODS FOR SYSTEMS'
      WRITE(OUP,6)
```

```
6     FORMAT(5X,'T(i)',9X,'W1(i)',8X,'W2(i)',8X,'W3(i)',8X,
     *'Q1(i)',8X,'Q2(i)',8X,'Q3(i)',8X,'X6(i)',8X,'X7(i)',8X,'X9(i)',
     *8X,'X10(i)',8X,'X11(i)',8X,'X12(i)',8X,'X13(i)',8X,'X14(i)')
C     STEP 1
      H=(B-A)/N
      T=A
C     STEP 2 INITIAL CONDITIONS
      TOL=1.d-5
      NN=10000
      Q1=1.d-40
      Q2=1.d-40
      Q3=1.d-40
      Q(1)=Q1
      Q(2)=Q2
      Q(3)=Q3
C     W1=FE2+,W2=H2O2,W3=HCOOH,X15=SO4
      W1=2.d-4
      W2=2.2d-03
      W3=2.d-07
      X15=0.d0
C     REACTION RATE CONSTANTS FROM GALLARD AND DE LAAT 1999
      XK6=2.7d-3
      XK7=63.d0
      XK8=3.2d08
      XK9=3.3d07
      XK10A=1.2d06
      XK10B=1.d07
      XK11A=1.d3
      XK11B=5.d07
      XK12A=1.58d05
      XK12B=1.d10
      XK13A=8.3d05
      XK13B=9.7d07
      XK14A=0.71d10
      XK14B=1.01d10
      XK15=5.2d09
C     OH RXNS W/HCCOH
      XK20=6.5d08
C     IRON SPECIES. INITIAL CONDITIONS CALCULATED WITH EXCELL SOLVER
      X6=2.d-04
      X7=1.d-40
      X9=2.9000d-40
      X10=7.6200d-41
      X11=8.0000d-78
      X12=0.d0
      X13=0.d0
      X14=1.0000d-03
      NJUMP=10000
      XM=1
      U=1
C     STEP 3
      WRITE(OUP,1) T,W1,W2,W3,Q1,Q2,Q3,X6,X7,X9,X10,X11,X12,X13,X14
C     STEP 4
      NJ1=0

C     WRITE(OUP,*) '1',Q1,Q2,Q3,Q(1),Q(2),Q(3)

      DO 110 I=1,N
C        STEP 5
```

```
          ALPHA=W1*W2*XK7
          BETA=XK8*W1+XK9*W2+XK20*W3
          GAMMA=XK6*(X12+X13)
          DELTA=XK10A*W1+XK11A*(X7+X9+X10+2*X11)+XK12A
          EPS=XK10B*W1+XK11B*(X7+X9+X10+2*X11)+XK12B*X14

          AFE=2*.8d-3/(X14**2)
          BFE=1+2.9d-3/X14+7.62d-7/(X14**2)+3.1d-3*W2/X14+
         *2.0d-4*2.9d-3*W2/(X14**2)
          CFE=W1-X6
          DFE=BFE**2-4*AFE*CFE
2200      IF(DFE.GT.0) GOTO 2100
          WRITE(oup,*) 'WARNING: quadratic eqn is negative'
2100      X7=(-BFE+SQRT(DFE))/(2*AFE)
          IF(X7.LT.0) X7=0
          X9=2.9d-03*X7/X14
          IF(X9.LT.0) X9=0
          X10=7.62d-07*X7/(X14**2)
          IF(X10.LT.0) X10=0
          X11=8.0d-04*(X7**2)/(X14**2)
          IF(X11.LT.0) X11=0
          X12=3.1d-03*X7*W2/X14
          IF(X12.LT.0) X12=0
          X13=2.0d-04*2.9d-03*W2*X7/(X14**2)
          IF(X13.LT.0) X13=0
          X6=W1+X7+X9+X10+2*X11+X12+X13
          IF(X6.LT.0) X6=0


C         STEP 11
          K=1
C         STEP 12
100       IF (K.GT.NN) GOTO 200
C           STEP13
C           COMPUTE J(Q)
            AA(1,1)=-BETA-XK14A*Q(2)-XK14B*Q(3)-4*XK15*Q(1)
            AA(1,2)=-XK14A*Q(1)
            AA(1,3)=-XK14B*Q(1)
            AA(2,1)=XK9*W2-XK14A*Q(2)
            AA(2,2)=-DELTA-4*XK13A*Q(2)-XK13B*Q(3)-XK14A*Q(1)
            AA(2,3)=XK12B*X14-XK13B*Q(2)
            AA(3,1)=-XK14B*Q(3)
            AA(3,2)=XK12A-XK13B*Q(3)
            AA(3,3)=-EPS-XK13B*Q(2)-XK14B*Q(1)
C           COMPUTE -F(Q)
            AA(1,4)=-ALPHA+BETA*Q(1)+XK14A*Q(1)*Q(2)+XK14B*Q(1)*Q(3)
     *+2*XK15*Q(1)*Q(1)
            AA(2,4)=-GAMMA-XK9*W2*Q(1)+DELTA*Q(2)-XK12B*X14*Q(3)
     *+2*XK13A*Q(2)*Q(2)+XK13B*Q(2)*Q(3)+XK14A*Q(1)*Q(2)
            AA(3,4)=EPS*Q(3)-XK12A*Q(2)+XK13B*Q(2)*Q(3)+XK14B*Q(1)*Q(3)
C           STEP 14
C           SOLVES THE N X N LINEAR SYSTEM J(Q) Y = -F(Q)

              DISC=AA(1,1)*AA(2,2)*AA(3,3)+AA(1,3)*AA(2,1)*AA(3,2)
     *       +AA(1,2)*AA(2,3)*AA(3,1)-AA(1,3)*AA(2,2)*AA(3,1)
     *         -AA(1,2)*AA(2,1)*AA(3,3)-AA(3,2)*AA(2,3)*AA(1,1)

              DI1=AA(1,4)*AA(2,2)*AA(3,3)+AA(1,3)*AA(2,4)*AA(3,2)
     *       +AA(1,2)*AA(2,3)*AA(3,4)-AA(1,3)*AA(2,2)*AA(3,4)
     *         -AA(1,2)*AA(2,4)*AA(3,3)-AA(3,2)*AA(2,3)*AA(1,4)
```

```
            DI2=AA(1,1)*AA(2,4)*AA(3,3)+AA(1,3)*AA(2,1)*AA(3,4)
     *     +AA(1,4)*AA(2,3)*AA(3,1)-AA(1,3)*AA(2,4)*AA(3,1)
     *       -AA(1,4)*AA(2,1)*AA(3,3)-AA(3,4)*AA(2,3)*AA(1,1)

            DI3=AA(1,1)*AA(2,2)*AA(3,4)+AA(1,4)*AA(2,1)*AA(3,2)
     *     +AA(1,2)*AA(2,4)*AA(3,1)-AA(1,4)*AA(2,2)*AA(3,1)
     *       -AA(1,2)*AA(2,1)*AA(3,4)-AA(3,2)*AA(2,4)*AA(1,1)

            Y(1)=DI1/DISC
            Y(2)=DI2/DISC
            Y(3)=DI3/DISC

C           STEPS 15 AND 16
            R=0.
      DO 20 L=1,3
      IF (ABS(Y(L)/Q(L)).GT.R) R=ABS(Y(L)/Q(L))
20    CONTINUE
            Q(1)=Q(1)+Y(1)*XM
          Q(2)=Q(2)+Y(2)*XM
          Q(3)=Q(3)+Y(3)*XM
C     WRITE(OUP,*) '2',Q1,Q2,Q3,Q(1),Q(2),Q(3)
      IF (Q(L).LT.0) Q(L)=1d-40

      Q1 = Q(1)
      Q2 = Q(2)
      Q3 = Q(3)
C     WRITE(OUP,*) '4',Q1,Q2,Q3,Q(1),Q(2),Q(3)

      IF (R.LT.TOL) THEN
C                   PROCESS IS COMPLETE
C               WRITE(OUP,4)
                GOTO 70
            END IF


C           STEP 17
            K=K+1
C     WRITE(OUP,*) 'OUTPUT NEWTON'
C     WRITE(OUP,*) K,X7,R,Y(1),Y(2),Y(3),Q(1),Q(2),Q(3)
C     WRITE(OUP,*) AA(1,1),AA(1,2),AA(1,3),AA(1,4)
C     WRITE(OUP,*) AA(2,1),AA(2,2),AA(2,3),AA(2,4)
C     WRITE(OUP,*) AA(3,1),AA(3,2),AA(3,3),AA(3,4)
C     WRITE(OUP,*) DISC,DI1,DI2,DI3

      GOTO 100

70       CONTINUE
         Z11=H*F1(T,W1,W2,Q1,Q2,Q3,X7,X9,X10,X11,X12,X13)
         Z12=H*F2(T,W1,W2,Q1,Q2,Q3)
         Z13=H*F3(T,W3,Q1)
C        STEP 6
         Z21=H*F1(T+H/2,W1+Z11/2,W2+Z12/2,Q1,Q2,Q3,X7,X9,X10,X11,
     *X12,X13)
         Z22=H*F2(T+H/2,W1+Z11/2,W2+Z12/2,Q1,Q2,Q3)
         Z23=H*F3(T+H/2,W3+Z13/2,Q1)
C        STEP 7
         Z31=H*F1(T+H/2,W1+Z21/2,W2+Z22/2,Q1,Q2,Q3,X7,X9,X10,X11,
     *X12,X13)
         Z32=H*F2(T+H/2,W1+Z21/2,W2+Z22/2,Q1,Q2,Q3)
         Z33=H*F3(T+H/2,W3+Z23/2,Q1)
```

```
C        STEP 8
         Z41=H*F1(T+H,W1+Z31,W2+Z32,Q1,Q2,Q3,X7,X9,X10,X11,X12,
      *X13)
         Z42=H*F2(T+H,W1+Z31,W2+Z32,Q1,Q2,Q3)
         Z43=H*F3(T+H,W3+Z33,Q1)
C        STEP 9
         W1=W1+(Z11+2*Z21+2*Z31+Z41)/6
         W2=W2+(Z12+2*Z22+2*Z32+Z42)/6
         W3=W3+(Z13+2*Z23+2*Z33+Z43)/6

C     WRITE(OUP,*) '3',Q1,Q2,Q3,Q(1),Q(2),Q(3)


C        STEP 10
         T=A+I*H

C        STEP 19
         NJ1=NJ1+1
         IF(NJ1.LT.NJUMP) GOTO 110
         NJ1=0
         WRITE(OUP,1) T,W1,W2,W3,Q(1),Q(2),Q(3),X6,X7,X9,X10,X11,X12,
      *X13,X14
c     WRITE(OUP,*) F1(T,X1,X2,Q1,Q2,Q3,X7,X9,X10,X11,X12,X13),
c     *F2(T,X1,X2,Q1,Q2,Q3)
110      CONTINUE
         GOTO 400
C     STEP 18
C     DIVERGENCE
200   WRITE(OUP,5) NN
C     STEP 20
400   CLOSE(UNIT=5)
      CLOSE(UNIT=OUP)
      IF(OUP.NE.6) CLOSE(UNIT=6)
      STOP
1     FORMAT(16(1X,E12.6))
2     FORMAT(5(1X,E12.6))
3     FORMAT(1X,'ITER.=',1X,I2,1X,'APPROX. SOL.
IS',1X,3(1X,E15.8),/,1X,
     *'APPROX. ERROR IS',1X,E15.8)
4     FORMAT(1X,'SUCCESS WITHIN TOLERANCE 1.0E-4')
5     FORMAT(1X,'DIVERGENCE - STOPPED AFTER ITER.',1X,I2)
      END
```

Appendix A.3 Fortran Code for Chlorinated Compounds

```
C*********************************************************************
*
C
*
C   RUNGE-KUTTA FOR SYSTEMS OF DIFFERENTIAL EQUATIONS ALGORITHM 5.7
*
C
*
C*********************************************************************
*
C
C
C
C     TO APPROXIMATE THE SOLUTION OF THE MTH-ORDER SYSTEM OF FIRST-
C     ORDER INITIAL-VALUE PROBLEMS
C              UJ' = FJ(T,U1,U2,...,UM), J=1,2,...,M
C           A <= T <= B, UJ(A)=ALPHAJ, J=1,2,...,M
C     AT (N+1) EQUALLY SPACED NUMBERS IN THE INTERVAL [A,B].
C
C     INPUT ENDPOINTS A,B; NUMBER OF EQUATIONS M; INTIAL
C           CONDITIONS ALPHA1,...,ALPHAM; INTEGER N.
C
C     OUTPUT APPROXIMATIONS WJ TO UJ(T) AT THE (N+1) VALUES OF T.
C
      DOUBLE PRECISION, DIMENSION(3,4) :: AA
      DOUBLE PRECISION, DIMENSION(3) :: Y
      DOUBLE PRECISION, DIMENSION(3) :: Q
      CHARACTER NAME1*30,BB*1
      INTEGER OUP,FLAG
      LOGICAL OK

      DOUBLE PRECISION X1,X2,X6,X7,X9,X10,X11,X12,X13,X14,X15
      DOUBLE PRECISION XK6,XK7,XK8,XK9,XK10A,XK10B,XK11A,XK11B,XK12A
      DOUBLE PRECISION
XK12B,XK13A,XK13B,XK14A,XK14B,XK15,XK20,XK21,XK22
      DOUBLE PRECISION
W1,W2,W3,W4,W5,TOL,ALPHA,BETA,GAMMA,DELTA,EPS,R,U
      DOUBLE PRECISION XK23,XK24,XK25,AFE,BFE,CFE,DFE,DISC,DI1,DI2,DI3
      DOUBLE PRECISION Z11,Z12,Z13,Z14,Z15,Z21,Z22,Z23,Z24,Z25,Z31,Z32,
      *Z33,Z34,Z35,Z41,Z42,Z43,Z44,Z45


C     CHANGE FUNCTION F1 THROUGH F5 FOR A NEW PROBLEM
C     NOTE: THIS VERSION TO BE USED FOR CHLORINATED COMPOUNDS.
C           IN THIS MODEL, CT REACTS ONLY WITH O2 AND PCE ONLY WITH OH.
C           Chloride is a conservative specie.
C     F1=Fe2+, F2=H2O2, F3=PCE, F4=Cl-, F5=CT
      F1(T,X1,X2,Q1,Q2,Q3,X7,X9,X10,X11,X12,X13) = 2.7d-03*(X12+
      *X13)-63.d0*X1*X2-3.2d08*X1*Q1-1.2d06*X1*Q2-1.0d07*X1*Q3+
     *1.0d03*(X7+X9+X10+2*X11)*Q2+5.0d07*(X7+X9+X10+2*X11)*Q3
      F2(T,X1,X2,Q1,Q2,Q3) = -63d0*X1*X2-3.3d7*X2*Q1+
      *8.3d5*Q2*Q2+9.7d7*Q3*Q2+5.2d9*Q1*Q1
      F3(T,W3,Q1)= -XK20*W3*Q1
      F4(T,W3,Q1,W5,Q3)= 4*XK20*W3*Q1+4*XK23*W5*Q3
      F5(T,W5,Q3)= -XK23*W5*Q3
```

```
      OPEN(UNIT=5,FILE='CON',ACCESS='SEQUENTIAL')
      OPEN(UNIT=6,FILE='CON',ACCESS='SEQUENTIAL')
C     DEFINE FUNCTIONS F1,...,FM
      WRITE(6,*) 'This is the Runge-Kutta Method for systems with m=2.'
      WRITE(6,*) 'Remember to modify the function according to the
rxns'
      WRITE(6,*) 'Enter Y or N '
      WRITE(6,*) ' '
      READ(5,*)  BB
      IF(( BB .EQ. 'Y' ) .OR. ( BB .EQ. 'y' )) THEN
         OK = .FALSE.
10       IF (OK) GOTO 11
            WRITE(6,*) 'Input left and right endpoints separated by'
            WRITE(6,*) 'blank'
            WRITE(6,*) ' '
            READ(5,*) A, B
            IF (A.GE.B) THEN
               WRITE(6,*) 'Left endpoint must be less'
               WRITE(6,*) 'than right endpoint'
            ELSE
               OK = .TRUE.
            ENDIF
         GOTO 10
11       OK = .FALSE.
c         WRITE(6,*) 'Input the TWO initial conditions.'
c        WRITE(6,*) ' '
c         READ(5,*) W1, W2
12       IF (OK) GOTO 13
            WRITE(6,*) 'Input a positive integer for the number'
            WRITE(6,*) 'of subintervals '
            WRITE(6,*) ' '
            READ(5,*) N
            IF ( N .LE. 0 ) THEN
              WRITE(6,*) 'Must be positive integer '
            ELSE
              OK = .TRUE.
            ENDIF
         GOTO 12
13       CONTINUE
      ELSE
         WRITE(6,*) 'The program will end so that the functions'
         WRITE(6,*) 'F1-F5 can be created '
         OK = .FALSE.
      ENDIF
      IF(.NOT.OK) GOTO 400
      WRITE(6,*) 'Select output destination: '
      WRITE(6,*) '1. Screen '
      WRITE(6,*) '2. Text file '
      WRITE(6,*) 'Enter 1 or 2 '
      WRITE(6,*) ' '
      READ(5,*) FLAG
      IF ( FLAG .EQ. 2 ) THEN
         WRITE(6,*) 'Input the file name in the form - '
         WRITE(6,*) 'drive:name.ext'
         WRITE(6,*) 'with the name contained within quotes'
         WRITE(6,*) 'as example:   ''A:OUTPUT.DTA'' '
         WRITE(6,*) ' '
         READ(5,*) NAME1
         OUP = 3
         OPEN(UNIT=OUP,FILE=NAME1,STATUS='NEW')
```

```
      ELSE
         OUP = 6
      ENDIF
      WRITE(OUP,*) 'RUNGE-KUTTA AND NEWTON METHODS FOR SYSTEMS'
      WRITE(OUP,6)
6     FORMAT(5X,'T(i)',9X,'W1(i)',8X,'W2(i)',8X,'W3(i)',8X,'W5',8X,
     *'Q1(i)',8X,'Q2(i)',8X,'Q3(i)',8X,'X6(i)',8X,'X7(i)',8X,'X9(i)',
     *8X,'X10(i)',8X,'X11(i)',8X,'X12(i)',8X,'X13(i)',8X,'X14(i)')
C     STEP 1
      H=(B-A)/N
      T=A
C     STEP 2 INITIAL CONDITIONS
      TOL=1.d-5
      NN=10000
      Q1=1.d-40
      Q2=1.d-40
      Q3=1.d-40
      Q(1)=Q1
      Q(2)=Q2
      Q(3)=Q3
C     W1=FE2+,W2=H2O2,W3=PCE,W4=Cl-,W5=CT,X15=SO4
      W1=1.d-40
      W2=1.1d-01
      W3=8.9d-05
      W4=0.d0
      W5=0.d0
      X15=0.d0
C     REACTION RATE CONSTANTS FROM GALLARD AND DE LAAT 1999
      XK6=2.7d-3
      XK7=63.d0
      XK8=3.2d08
      XK9=3.3d07
      XK10A=1.2d06
      XK10B=1.d07
      XK11A=1.d3
      XK11B=5.d07
      XK12A=1.58d05
      XK12B=1.d10
      XK13A=8.3d05
      XK13B=9.7d07
      XK14A=0.71d10
      XK14B=1.01d10
      XK15=5.2d09
C     OH RXNS W/PCE,Cl,SO4
      XK20=2.d09
      XK21=3.d09
      XK22=3.5d05
C     O2 RNXS W/CT,Cl,SO4
      XK23=3.8d03
      XK24=140.d0
      XK25=0.d0
C     IRON SPECIES. INITIAL CONDITIONS CALCULATED WITH EXCELL SOLVER
      X6=9.00d-05
      X7=6.75d-05
      X9=1.9573d-05
      X10=5.1431d-07
      X11=3.6444d-08
      X12=2.30157d-06
      X13=4.30616d-08
      X14=1.0000d-02
      NJUMP=10000
```

```
      XM=1
      U=1
C     STEP 3
      WRITE(OUP,1) T,W1,W2,W3,W5,Q1,Q2,Q3,X6,X7,X9,X10,X11,X12,X13,X14
C     STEP 4
      NJ1=0

C     WRITE(OUP,*) '1',Q1,Q2,Q3,Q(1),Q(2),Q(3)

      DO 110 I=1,N
C        STEP 5


         ALPHA=W1*W2*XK7
         BETA=XK8*W1+XK9*W2+XK20*W3+XK21*W4+XK22*X15
         GAMMA=XK6*(X12+X13)
         DELTA=XK10A*W1+XK11A*(X7+X9+X10+2*X11)+XK12A

EPS=XK10B*W1+XK11B*(X7+X9+X10+2*X11)+XK12B*X14+XK23*W5+XK24*W4+
      *XK25*X15

C        QUADRATIC EQN TO SOLVE FOR FE3+
         AFE=2*.8d-3/(X14**2)
         BFE=1+2.9d-3/X14+7.62d-7/(X14**2)+3.1d-3*W2/X14+
      *2.0d-4*2.9d-3*W2/(X14**2)
         CFE=W1-X6
         DFE=BFE**2-4*AFE*CFE
2200     IF(DFE.GT.0) GOTO 2100
         WRITE(oup,*) 'WARNING: quadratic eqn is negative'
2100     X7=(-BFE+SQRT(DFE))/(2*AFE)
         IF(X7.LT.0) X7=0
         X9=2.9d-03*X7/X14
         IF(X9.LT.0) X9=0
         X10=7.62d-07*X7/(X14**2)
         IF(X10.LT.0) X10=0
         X11=8.0d-04*(X7**2)/(X14**2)
         IF(X11.LT.0) X11=0
         X12=3.1d-03*X7*W2/X14
         IF(X12.LT.0) X12=0
         X13=2.0d-04*2.9d-03*W2*X7/(X14**2)
         IF(X13.LT.0) X13=0
         X6=W1+X7+X9+X10+2*X11+X12+X13
         IF(X6.LT.0) X6=0


C        STEP 11
         K=1
C        STEP 12
100      IF (K.GT.NN) GOTO 200
C          STEP13
C          COMPUTE J(Q)
           AA(1,1)=-BETA-XK14A*Q(2)-XK14B*Q(3)-4*XK15*Q(1)
           AA(1,2)=-XK14A*Q(1)
           AA(1,3)=-XK14B*Q(1)
           AA(2,1)=XK9*W2-XK14A*Q(2)
           AA(2,2)=-DELTA-4*XK13A*Q(2)-XK13B*Q(3)-XK14A*Q(1)
           AA(2,3)=XK12B*X14-XK13B*Q(2)
           AA(3,1)=-XK14B*Q(3)
           AA(3,2)=XK12A-XK13B*Q(3)
           AA(3,3)=-EPS-XK13B*Q(2)-XK14B*Q(1)
```

```
C           COMPUTE -F(Q)
            AA(1,4)=-ALPHA+BETA*Q(1)+XK14A*Q(1)*Q(2)+XK14B*Q(1)*Q(3)
     *+2*XK15*Q(1)*Q(1)
            AA(2,4)=-GAMMA-XK9*W2*Q(1)+DELTA*Q(2)-XK12B*X14*Q(3)
     *+2*XK13A*Q(2)*Q(2)+XK13B*Q(2)*Q(3)+XK14A*Q(1)*Q(2)
            AA(3,4)=EPS*Q(3)-XK12A*Q(2)+XK13B*Q(2)*Q(3)+XK14B*Q(1)*Q(3)
C           STEP 14
C           SOLVES THE N X N LINEAR SYSTEM J(Q) Y = -F(Q)

             DISC=AA(1,1)*AA(2,2)*AA(3,3)+AA(1,3)*AA(2,1)*AA(3,2)
     *     +AA(1,2)*AA(2,3)*AA(3,1)-AA(1,3)*AA(2,2)*AA(3,1)
     *       -AA(1,2)*AA(2,1)*AA(3,3)-AA(3,2)*AA(2,3)*AA(1,1)

             DI1=AA(1,4)*AA(2,2)*AA(3,3)+AA(1,3)*AA(2,4)*AA(3,2)
     *     +AA(1,2)*AA(2,3)*AA(3,4)-AA(1,3)*AA(2,2)*AA(3,4)
     *       -AA(1,2)*AA(2,4)*AA(3,3)-AA(3,2)*AA(2,3)*AA(1,4)

             DI2=AA(1,1)*AA(2,4)*AA(3,3)+AA(1,3)*AA(2,1)*AA(3,4)
     *     +AA(1,4)*AA(2,3)*AA(3,1)-AA(1,3)*AA(2,4)*AA(3,1)
     *       -AA(1,4)*AA(2,1)*AA(3,3)-AA(3,4)*AA(2,3)*AA(1,1)

             DI3=AA(1,1)*AA(2,2)*AA(3,4)+AA(1,4)*AA(2,1)*AA(3,2)
     *     +AA(1,2)*AA(2,4)*AA(3,1)-AA(1,4)*AA(2,2)*AA(3,1)
     *       -AA(1,2)*AA(2,1)*AA(3,4)-AA(3,2)*AA(2,4)*AA(1,1)

             Y(1)=DI1/DISC
             Y(2)=DI2/DISC
             Y(3)=DI3/DISC

C           STEPS 15 AND 16
            R=0.
       DO 20 L=1,3
       IF (ABS(Y(L)/Q(L)).GT.R) R=ABS(Y(L)/Q(L))
20     CONTINUE
             Q(1)=Q(1)+Y(1)*XM
           Q(2)=Q(2)+Y(2)*XM
           Q(3)=Q(3)+Y(3)*XM
C      WRITE(OUP,*) '2',Q1,Q2,Q3,Q(1),Q(2),Q(3)
       IF (Q(L).LT.0) Q(L)=1d-40

       Q1 = Q(1)
       Q2 = Q(2)
       Q3 = Q(3)
C      WRITE(OUP,*) '4',Q1,Q2,Q3,Q(1),Q(2),Q(3)

       IF (R.LT.TOL) THEN
C                    PROCESS IS COMPLETE
C                 WRITE(OUP,4)
                  GOTO 70
            END IF


C           STEP 17
            K=K+1
C      WRITE(OUP,*) 'OUTPUT NEWTON'
C      WRITE(OUP,*) K,X7,R,Y(1),Y(2),Y(3),Q(1),Q(2),Q(3)
C      WRITE(OUP,*) AA(1,1),AA(1,2),AA(1,3),AA(1,4)
C      WRITE(OUP,*) AA(2,1),AA(2,2),AA(2,3),AA(2,4)
C      WRITE(OUP,*) AA(3,1),AA(3,2),AA(3,3),AA(3,4)
C      WRITE(OUP,*) DISC,DI1,DI2,DI3
```

```
      GOTO 100

70       CONTINUE
         Z11=H*F1(T,W1,W2,Q1,Q2,Q3,X7,X9,X10,X11,X12,X13)
         Z12=H*F2(T,W1,W2,Q1,Q2,Q3)
         Z13=H*F3(T,W3,Q1)
         Z14=H*F4(T,W3,Q1,W5,Q3)
         Z15=H*F5(T,W5,Q3)
C        STEP 6
         Z21=H*F1(T+H/2,W1+Z11/2,W2+Z12/2,Q1,Q2,Q3,X7,X9,X10,X11,
     *X12,X13)
         Z22=H*F2(T+H/2,W1+Z11/2,W2+Z12/2,Q1,Q2,Q3)
         Z23=H*F3(T+H/2,W3+Z13/2,Q1)
         Z24=H*F4(T+H/2,W3+Z13/2,Q1,W5+Z15/2,Q3)
         Z25=H*F5(T+H/2,W5+Z15/2,Q3)
C        STEP 7
         Z31=H*F1(T+H/2,W1+Z21/2,W2+Z22/2,Q1,Q2,Q3,X7,X9,X10,X11,
     *X12,X13)
         Z32=H*F2(T+H/2,W1+Z21/2,W2+Z22/2,Q1,Q2,Q3)
         Z33=H*F3(T+H/2,W3+Z23/2,Q1)
         Z34=H*F4(T+H/2,W3+Z23/2,Q1,W5+Z25/2,Q3)
         Z35=H*F5(T+H/2,W5+Z25/2,Q3)
C        STEP 8
         Z41=H*F1(T+H,W1+Z31,W2+Z32,Q1,Q2,Q3,X7,X9,X10,X11,X12,
     *X13)
         Z42=H*F2(T+H,W1+Z31,W2+Z32,Q1,Q2,Q3)
         Z43=H*F3(T+H,W3+Z33,Q1)
         Z44=H*F4(T+H,W3+Z33,Q1,W5+Z35,Q3)
         Z45=H*F5(T+H,W5+Z35,Q3)
C        STEP 9
         W1=W1+(Z11+2*Z21+2*Z31+Z41)/6
         W2=W2+(Z12+2*Z22+2*Z32+Z42)/6
         W3=W3+(Z13+2*Z23+2*Z33+Z43)/6
         W4=W4+(Z14+2*Z24+2*Z34+Z44)/6
         W5=W5+(Z15+2*Z25+2*Z35+Z45)/6

C     WRITE(OUP,*) '3',Q1,Q2,Q3,Q(1),Q(2),Q(3)


C        STEP 10
         T=A+I*H

C        STEP 19
         NJ1=NJ1+1
         IF(NJ1.LT.NJUMP) GOTO 110
         NJ1=0
         WRITE(OUP,1)
T,W1,W2,W3,W5,Q(1),Q(2),Q(3),X6,X7,X9,X10,X11,X12,
     *X13,X14
c     WRITE(OUP,*) F1(T,X1,X2,Q1,Q2,Q3,X7,X9,X10,X11,X12,X13),
c     *F2(T,X1,X2,Q1,Q2,Q3)
110      CONTINUE
         GOTO 400
C    .STEP 18
C     DIVERGENCE
200   WRITE(OUP,5) NN
C     STEP 20
```

```
400   CLOSE(UNIT=5)
      CLOSE(UNIT=OUP)
      IF(OUP.NE.6) CLOSE(UNIT=6)
      STOP
1     FORMAT(16(1X,E12.6))
2     FORMAT(5(1X,E12.6))
3     FORMAT(1X,'ITER.=',1X,I2,1X,'APPROX. SOL.
IS',1X,3(1X,E15.8),/,1X,
     *'APPROX. ERROR IS',1X,E15.8)
4     FORMAT(1X,'SUCCESS WITHIN TOLERANCE 1.0E-4')
5     FORMAT(1X,'DIVERGENCE - STOPPED AFTER ITER.',1X,I2)
      END
```

Appendix B. Comparing Costs of Carbon Disposal vs. (Fenton) Carbon Regeneration

The economic analysis conducted here was designed to compare alternative carbon replacement/regeneration strategies in processes using activated carbon for contaminant adsorption. In scenario #1, spent carbon is replaced with new activated carbon, and the waste carbon is disposed of as a hazardous waste. Scenario #2 differs in that carbon is periodically regenerated, or at least partially regenerated using Fenton's reagents to destroy the adsorbed contaminants. The economic analysis was carried out by comparing costs that are unique to each scenario on both a present worth and an annual cost basis. Most of the costs for activated carbon adsorption for a gas-phase streams derived from SVE (the basic scheme for both scenarios) are common to the alternatives compared. As such they are omitted from the analysis. These include energy costs for the SVE system, capital costs for the carbon adsorption unit, initial carbon costs and some maintenance and other labor activities. A description of the costs that are unique to each alternative follows:

	Scenario #1	Scenario #2
Carbon costs	GAC replacement cost GAC cost = \$1.60/lb Disposal cost = \$0.48/lb plus transportation to UT \$3000 for 8316 lbs GAC plus \$28/ton UT disposal tax	5% loss/regeneration cycle GAC cost = \$1.60/lb No disposal costs
H_2O_2 consumption	Not Applicable	\$0.345/lb H_2O_2 plus transportation from Houston \$3.50/mi, 1067 miles
Incremental capital for chemical dosing/storage	Not Applicable	Dosing pumps, H_2O_2 storage tanks

Source: Disposal cost (email correspondence with Clean Harbors Environmental, 2004).

The scenarios were built in part on the basis of field experience in this project (H_2O_2 dosing and time to recovery) and in part based on engineering rules of thumb or professional judgment. Cost comparisons were carried out for carbon recovery when (i) PCE and (ii) Methylene chloride were the target contaminants. The behaviors of these compounds during carbon regeneration were diametrically opposite. PCE provides a challenging recovery problem, presumably because of its affinity for the carbon surface and consequent slow desorption rate. Carbon recovery following Methylene chloride breakthrough is remarkably fast, probably due to its low affinity for the carbon surface. Other assumptions or data used to support the economic comparison follow:

- bulk GAC density = 0.5 kg/L
- gas-flow rates during SVE = 10, 100 cfm (2 distinct analyses)
- equilibrium is assumed to exist among gas, liquid and solid phases at breakthrough during SVE
- T = 25°C

- The concentration of contaminant (PCE or MC) in the gas treated by SVE is 100 ppmv
- GAC column diameter = 1 m
- The mass of carbon in the column is irrelevant since we will calculate carbon wastage rates for each scenario investigated
- The pump efficiency during recirculation of Fenton's reagents is 0.70
- The discount generator is 0.08
- Equipment for H_2O_2 dosing and storage has a service life of 20 years
- All GAC costs are in year 2000 dollars and all other costs are current

Calculations:

Estimating time to breakthrough:

At a MC-gas phase concentration of 100 ppm, the concentration in the liquid can be calculated using Henry's law. From La Grega et al., (2001),

H=exp(A-B/T) where A = 6.65 and B=3.82x10^3

then the Henry's law constant can be calculated at a T = 25°C (298 K)

$$\boldsymbol{H} = \exp\left(6.65 - \frac{3.82\boldsymbol{x}10^3}{298}\right) = 2.09\boldsymbol{x}10^{-3}\,\boldsymbol{atm}\cdot\boldsymbol{m}^3/\boldsymbol{mol} = 2.1\boldsymbol{atm}/\boldsymbol{M}$$

$$\boldsymbol{C}_{\boldsymbol{L,MC}} = \frac{\boldsymbol{C}_{\boldsymbol{g,MC}}}{\boldsymbol{H}} = \frac{100\boldsymbol{x}10^{-6}\,\boldsymbol{atm}}{2.1\boldsymbol{atm}/\boldsymbol{M}} \times \frac{85\boldsymbol{g}}{\boldsymbol{mol}} \times \frac{1000\boldsymbol{mg}}{\boldsymbol{g}} = 4.05\boldsymbol{mgMC}/\boldsymbol{L}$$

At saturation, the concentration of MC in equilibrium with the solid is

$$\boldsymbol{C}_{\boldsymbol{S,MC}} = \boldsymbol{K}\boldsymbol{C}_{\boldsymbol{eq}}^{\,1/\boldsymbol{n}} = 0.069(\boldsymbol{mg}/\boldsymbol{g})(\boldsymbol{L}/\boldsymbol{mg})^1 \times (4.05\boldsymbol{mg}/\boldsymbol{L})^1 = 0.280\boldsymbol{mgMC}/\boldsymbol{gGAC}$$

where K and 1/n are the Freundlich parameters for MC and the URV-MOD1 GAC. The concentration of PCE in the solid is 250 mg/g (from the field data).

The carbon wastage rate at Q_{air} = 10 cfm,

$$\dot{\boldsymbol{m}}_{\boldsymbol{c}}\,\boldsymbol{C}_{\boldsymbol{s}} = \boldsymbol{Q}_{\boldsymbol{air}}\boldsymbol{C}_{\boldsymbol{air}} = \frac{10\,\boldsymbol{ft}^3}{\min} \times \frac{7.5\boldsymbol{gal}}{\boldsymbol{ft}^3} \times \frac{3.78\boldsymbol{L}}{\boldsymbol{gal}} \times \frac{1\boldsymbol{mol}}{24.465\boldsymbol{L}} \times \frac{1}{10^4} = 11.6\boldsymbol{x}10^{-4}\,\boldsymbol{mol}/\min$$

so,
$$\dot{\boldsymbol{m}}_{\boldsymbol{c}} = \frac{\frac{11.6\boldsymbol{x}10^{-4}\boldsymbol{mol}}{\min} \times \frac{165.83\boldsymbol{x}10^3\boldsymbol{mgPCE}}{\boldsymbol{mol}}}{250\boldsymbol{mgPCE}/\boldsymbol{gGAC}} = 0.769\boldsymbol{gGAC}/\min$$

$$\dot{\boldsymbol{m}}_{\boldsymbol{c}} = 0.769\boldsymbol{gGAC}/\min = 439\boldsymbol{lbsGAC}/6\boldsymbol{months} = 878\boldsymbol{lbs}/\boldsymbol{yr}$$

At a gas flowrate of 10 cfm, the carbon wastage rate for PCE-loaded GAC is nearly 900lbs/yr and for MC is

$$\dot{m}_c = \frac{\frac{11.6x10^{-4}\,mol}{\min} \times \frac{85x10^{3}\,mgMC}{mol}}{0.280\,mgMC/gGAC} = 356\,gGAC/\min$$

$$\dot{m}_c = 356\,gGAC/\min = 202981\,lbsGAC/6\,months = 405{,}961\,lbs/yr$$

The carbon wastage rate at Q_{air} = 100 cfm,

$$\dot{m}_{c,PCE} = 7.69\,gGAC/\min = 4385\,lbsGAC/6\,months = 8770\,lbs/yr$$

$$\dot{m}_{c,MC} = 3518\,gGAC/\min = 2{,}005{,}979\,lbsGAC/6\,months = 4{,}011{,}958\,lbs/yr$$

Up to this point, all calculations are common to both option 1 and 2 (See the following table).

Properties and GAC Wastage Rate for Methylene Chloride and PCE

Compound	Form.	Initial Conc. (ppm)	H (atm/M)	C_s (mg/g) = $KC_{eq}^{1/n}$	GAC wastage rate (lbs /yr)	
					Q_{air} =10 cfm	Q_{air} =100 cfm
Methylene Chloride (MC)	CH_2Cl_2	100	2.1	0.280	405,961	4,011,958
Perchloroethylene (PCE)	C_2Cl_4			250	878	8770

Note: MC Henry's law constant calculated with the parameters A = 6.65, B=3.82x10^3 and T = 25°C.
The PCE concentration in the solid is measured from field data.

For option 2, it is necessary to perform additional calculations to find out the cost of regeneration via Fenton's reaction.

Annual Cost for H_2O_2 - Option 2

SVE+TCE (aqueous phase) and MC (aqueous phase) loaded GAC-Field data

Target Comp.	$C_{s,i}$ (mg/g)	%Target degraded	GAC (g)	mass degraded (g)	H_2O_2 added (L)	Regeneration period (hrs) 7L reservoir
PCE	270	50	78 (0.17lbs)	10.5	1.5	48
MC	79	86	100 (0.22lbs)	6.8	0.30	2

Note: For PCE, H_2O_2 additions (50%) to 7-L reservoir: 150 mLs at time 0, 1,2,4,6,23,25,27,29,48 hrs. Annual hydrogen peroxide cost is for 2 regenerations/yr (assumes 50% regeneration for PCE). For MC, H_2O_2 additions (50%) to 7-L reservoir: 150 mLs at time 0,1,2,3,4,5,6 hrs. Analysis uses (2)-150 mL H_2O_2 additions as they are sufficient to degrade 86% of MC in 2 hrs.
Source: Field data (see section Field-Scale Regeneration Trials in final report).

The H_2O_2 Cost is \$0.34/lb (\$0.90/L)- US. Peroxide

$$\frac{\$0.34}{\boldsymbol{lb}} \times \frac{2.2\boldsymbol{lbs}}{1\boldsymbol{kg}} \times \frac{1.2\boldsymbol{kg}}{\boldsymbol{L}} = \$0.90/\boldsymbol{L}$$

In the field experiments, 1.5 L H_2O_2 were added to a 7-L reservoir to regenerate 78 g GAC-loaded with PCE (50% in 48 hrs). For MC, 0.3 L H_2O_2 were added to regenerate 100 g GAC (86% in 2 hrs).

$$78\boldsymbol{gGAC} \times \frac{1\boldsymbol{kg}}{1000\boldsymbol{g}} \times \frac{2.2\boldsymbol{lbs}}{1\boldsymbol{kg}} = 0.17\boldsymbol{lbsGAC} \qquad \text{for PCE}$$

$$100\boldsymbol{gGAC} \times \frac{1\boldsymbol{kg}}{1000\boldsymbol{g}} \times \frac{2.2\boldsymbol{lbs}}{1\boldsymbol{kg}} = 0.22\boldsymbol{lbsGAC} \qquad \text{for MC}$$

If 1000 lbs of GAC will be regenerated at a time, the H_2O_2 utilization (lbs) per pound of carbon for PCE-loaded GAC is

$$1.5\boldsymbol{LH_2O_2} \times \left(\frac{1000\boldsymbol{lbs}}{0.17\boldsymbol{lbs}}\right) = 8824\boldsymbol{LH_2O_2} \times \frac{1.2\boldsymbol{kgH_2O_2}}{\boldsymbol{LH_2O_2}} \times \frac{2.2\boldsymbol{lbsH_2O_2}}{\boldsymbol{kgH_2O_2}} = 23{,}295\boldsymbol{lbsH_2O_2}$$

23,295 lbs H_2O_2 to regenerate 1000 lbs GAC

$$\frac{23{,}295\,\boldsymbol{lbsH_2O_2}}{1000\,\boldsymbol{lbsGAC}} = \frac{23.3\,\boldsymbol{lbsH_2O_2}\,/\,\boldsymbol{lbsGAC}}{0.5} = \frac{46.6\,\boldsymbol{lbsH_2O_2}}{\boldsymbol{lbsGAC}}$$ for PCE-loaded GAC

and for MC,

$$0.30\,\boldsymbol{LH_2O_2} \times \left(\frac{1000\,\boldsymbol{lbs}}{0.22\,\boldsymbol{lbs}}\right) = 1364\,\boldsymbol{LH_2O_2} \times \frac{1.2\,\boldsymbol{kgH_2O_2}}{\boldsymbol{LH_2O_2}} \times \frac{2.2\,\boldsymbol{lbsH_2O_2}}{\boldsymbol{kgH_2O_2}} = 3600\,\boldsymbol{lbsH_2O_2}$$

3600 lbs H_2O_2 to regenerate 1000 lbs GAC,

$$\frac{3600\,\boldsymbol{lbsH_2O_2}}{1000\,\boldsymbol{lbsGAC}} = \frac{3.6\,\boldsymbol{lbsH_2O_2}\,/\,\boldsymbol{lbsGAC}}{0.85} = \frac{4.2\,\boldsymbol{lbsH_2O_2}}{\boldsymbol{lbsGAC}}$$ for MC-loaded GAC

Given the carbon wastage rate for PCE and MC (calculated above), the annual cost of H_2O_2 can be calculated for PCE at 10 and 100 cfm respectively,

$$\frac{46.6\,\boldsymbol{lbsH_2O_2}}{\boldsymbol{lbsGAC}} \times \frac{878\,\boldsymbol{lbsGAC}}{\boldsymbol{yr}} = \frac{40{,}915\,\boldsymbol{lbsH_2O_2}}{\boldsymbol{yr}} \times \frac{\$0.345}{\boldsymbol{lbH_2O_2}} = \$14{,}116\,/\,\boldsymbol{yr}$$

$$\frac{46.6\,\boldsymbol{lbsH_2O_2}}{\boldsymbol{lbsGAC}} \times \frac{8770\,\boldsymbol{lbsGAC}}{\boldsymbol{yr}} = \frac{408{,}682\,\boldsymbol{lbsH_2O_2}}{\boldsymbol{yr}} \times \frac{\$0.345}{\boldsymbol{lbH_2O_2}} = \$140{,}995\,/\,\boldsymbol{yr}$$

The annual cost of H_2O_2 for MC at 10 and 100 cfm

$$\frac{4.2\,\boldsymbol{lbsH_2O_2}}{\boldsymbol{lbsGAC}} \times \frac{405{,}961\,\boldsymbol{lbsGAC}}{\boldsymbol{yr}} = \frac{1{,}705{,}036\,\boldsymbol{lbsH_2O_2}}{\boldsymbol{yr}} \times \frac{\$0.345}{\boldsymbol{lbH_2O_2}} = \$588{,}237\,/\,\boldsymbol{yr}$$

$$\frac{4.2\,\boldsymbol{lbsH_2O_2}}{\boldsymbol{lbsGAC}} \times \frac{4{,}011{,}958\,\boldsymbol{lbsGAC}}{\boldsymbol{yr}} = \frac{16{,}850{,}224\,\boldsymbol{lbsH_2O_2}}{\boldsymbol{yr}} \times \frac{\$0.345}{\boldsymbol{lbH_2O_2}} = \$5{,}813{,}327\,/\,\boldsymbol{yr}$$

The H_2O_2 transportation cost is $3.50/mile -US Peroxide (1067 miles from Houston, TX to Tucson, AZ)

The cost of H_2O_2 depends on the requirements (e.g., H_2O_2 strength and grade, volume delivered per year, packaging, and distance to the production plant, etc.). Within the U.S., the list price for 50% Technical Grade, delivered in full tank trucks with a 40,000 lbs capacity, and shipment from the nearest production plant, is as follows:

Product: $0.345 per lb-50% (FOB Houston, TX)

Freight: $3.50 per mile (regardless of delivery volume)

Total H_2O_2 cost summary

Comp.	Annual H_2O_2 Cost ($/yr) $2m^3$ reservoir ($0.345/lb H_2O_2)		Transportation Cost ($/yr) ($3850/trip) 40,000 lbs truck load		Total H_2O_2 Cost ($/yr)	
	Q_{air} =10 cfm	Q_{air} =100 cfm	Q_{air} =10 cfm	Q_{air} =100 cfm	Q_{air} =10 cfm	Q_{air} =100 cfm
PCE	14,116 (40,915lbs H_2O_2 /yr)	140,995 (408,682 lbs H_2O_2/yr)	3,850	38,500	17,966	179,495
MC	588,237 (1.7Mlbs H_2O_2/yr)	5,813,327 (16.8M lbs H_2O_2/yr)	163,625	1,617,000	751,862	7,430,327

GAC Costs ($/yr) – Comparison

GAC Purchase Cost = $1.60/lb based on annual usage rate (Adams and Clark, 1989)

Cost index 1989 = 355

Cost index 2000 = 395.7

GAC disposal cost ($/yr) = $0.48/lb

Plus disposal transportation cost ($/yr) = $3000/8316 lbs GAC

Plus UT tax ($/yr) = $28/1000 kg = $12.73/1000lbs

Calculation of GAC cost – Option 1

Compound	GAC Purchase Cost ($/yr) – as of 2000		GAC Disposal Cost ($/yr)		Total GAC Cost ($/yr)	
	Q_{air} =10 cfm	Q_{air} =100 cfm	Q_{air} =10 cfm	Q_{air} =100 cfm	Q_{air} =10 cfm	Q_{air} =100 cfm
MC	0.72M	7.2M	0.35M	3.4M	1.1M	11M
PCE	1,566	15,641	749	7,485	2,315	23,126

Note: Costs of GAC include purchase ($1.60/lbs) and disposal (disposal + transportation + tax).

Calculation of GAC Cost – Option 2

Compound	GAC Cost ($/yr), ($1.60/lb) – 1989 (2000)		Total H_2O_2 Cost for GAC regeneration ($/yr)		Total GAC Cost ($/yr) as of 2000	
	Q_{air} =10 cfm	Q_{air} =100 cfm	Q_{air} =10 cfm	Q_{air} =100 cfm	Q_{air} =10 cfm	Q_{air} =100 cfm
PCE	140 (156)	1,403 (1,564)	17,966	179,495	18,122	180,898
MC	38,208 (42,588)	376,471 (419,633)	0.75M	7.4M	792,588	7,819,633

Note: Option 2 assumes 5% GAC loss/regeneration event. GAC Disposal Cost is $0/yr.

Additional GAC Cost for Option 2

Compound	Option 1 GAC Cost ($/yr), ($2.60/lb)		Option 2 GAC Cost ($/yr) ($H_2O_2$ + GAC Costs)		Option 2 Additional GAC Cost ($/yr)	
	Q_{air} =10 cfm	Q_{air} =100 cfm	Q_{air} =10 cfm	Q_{air} =100 cfm	Q_{air} =10 cfm	Q_{air} =100 cfm
PCE	2,545	25,416	18,122	180,898	15,577	155,482
MC	1.1M	11.1M	792,588	7,819,633	-307,412	-3,280,367

Note: Negative numbers indicate savings by using option 2.

Labor Costs ($/yr) - Comparison

Labor costs are comparable for both systems assuming breakthrough time and regeneration occur at the same time. Since, methylene chloride can be degraded almost completely (86%) in-place, then the capacity of the GAC is a 100% for both systems. Hence, regeneration and breakthrough times coincide for both systems. For PCE on the other hand, the GAC capacity is only 50% after regeneration. Thus, GAC regeneration events occur twice as often as the breakthrough times. Consequently, the labor costs are double for option 2 (In-place GAC regeneration).

Labor Cost - Option 1 (Assumes 8 hr/GAC replacement event)

Compound	GAC Replacement Events/yr		Labor Cost $/yr, ($40.00/hr)	
	Q_{air} =10 cfm	Q_{air} =100 cfm	Q_{air} =10 cfm	Q_{air} =100 cfm
PCE, 100% GAC capacity	1	9	320	2880
MC, 0.28 mg/g	406	4000	129,920	1.3M

Labor Cost -Option 2 (Assumes 8 hr/GAC regeneration event)

Compound	Regeneration Events/yr		Labor Cost $/yr, ($40.00/hr)	
	Q_{air} =10 cfm	Q_{air} =100 cfm	Q_{air} =10 cfm	Q_{air} =100 cfm
PCE, 50% GAC capacity	2	18	640	5,760
MC, 0.28 mg/g	406	4000	129,920	1.3M

Additional Labor Cost – Option 2

Compound	Regeneration Events/yr		Labor Cost $/yr, ($40.00/hr)	
	Q_{air} =10 cfm	Q_{air} =100 cfm	Q_{air} =10 cfm	Q_{air} =100 cfm
PCE, 50% GAC capacity	1	9	320	2,880

Pump Selection and Process Energy Cost Calculations

Assuming that 1000 lbs of GAC will be regenerated at a time,

$\rho_{GAC} = 0.5$ g/cm^3

Then, Volume/regeneration is 0.9 m^3 ≈ 1 m^3

Storage tank estimation is 2 m^3

Detention time estimation is 10 min

Q = 0.1 m^3/min = 100 L/min = 26.5 gpm

Assuming a GAC column diameter of 1 m, the pump pressure head is:

$V_{GAC\ bed} = 0.9$ m^3

$A_{GAC\ bed} = \Pi r^2 = \Pi(0.5m)^2 = 0.79$ m^2

$h_{GAC\ bed} = V/A = 0.9$ m^3/0.79 m^2 = 1.15 m

$d_{GAC\ bed} = 1$ m (h:d = 2.5:1)

Then, $h_{column} = 2.5$ m

$h_{column} = 2.5$ m (8.2 ft) = 3.55 psi (1 foot head = 0.433527502 psi)

Based on the pump requirements of flowrate (26.5 gpm) and pressure head (3.55 psi),

Air-Powered Double Diaphragm Pump (Positive Displacement Pump)
High-Flow Double Diaphragm Pump with Air Filter Regulator

Max GPM	Max psi	Wetted parts	Price, $
44	120	PP/Teflon PTFE	935

Source: Cole Parmer Catalog n(p.1562).

Pump Power requirements,

$P_{theoretical} = Q_l \rho_l g h$ where

Q_l = 30 gpm (1.89×10^{-3} gps),

ρ_l =998 kg/m^3,

g = 9.8 m/s^2 and

h(m) = height + 50% due to head loss = 2.5 m x 1.5 = 3.75 m

$$P_{theoretical} = Q_l \rho_l g h = \left(\frac{1.89 \times 10^{-3} m^3}{\min}\right) \times \left(\frac{998 kg}{m^3}\right) \times \left(\frac{9.8 m}{s^2}\right) \times 3.75 m = 69.3 W$$

$$P_{actual} = P_{theoretical} / n$$

where n is the efficiency of the pump (assume n=0.7)

$$P_{actual} = 69.3 W / 0.7 = 99 W$$

$$PowerCost(\$) = P_{actual}(kW) \times \frac{\$0.11}{kw - hr} \times \frac{hrs}{year}$$

The pump usage (hr/year) depends on the regeneration events (see table below). For example, for the PCE-loaded GAC regeneration at 10 cfm air flowrate:

$$\frac{regenerationtime(hrs)}{year} = \left(48 hrs \times \frac{1000 lbs}{0.17 lbs}\right) \times (2 regenerations / yr) = 564{,}706 hrs / yr$$

$$PowerCost(\$) = 99 \times 10^{-3} kW \times \frac{\$0.11}{kw - hr} \times \frac{564{,}706 hrs}{year} = \$6{,}149 / yr$$

Additional Process Energy Cost – Option 2
Pump requirements for regeneration events

Target	Time/regen (hrs) – 0.2 lbs GAC	Time/regen (hrs)- 1000 lbs GAC	Regen/year		Hrs/year		Power Cost, $	
			10cfm	100cfm	10cfm	100cfm	10cfm	100cfm
PCE 0.17lbsGAC	48	282,353	2	18	564,706	5,082,354	6,150	55,347
MC 0.22lbsGAC	2	9,091	406	4000	3,690,946	36,364,000	40,194	396,004

Note: the regeneration time (hrs) and the number of regenerations required per year were calculated above.

Additional Capital Cost – Option 2

2 Chemical storage tanks[1], 2 m^3	1,014
2 Positive Displacement Pumps[2]	2,000
Incremental Labor (10% capital cost)	3,077
Additional Capital Cost, $	6,091

Note: Capital Cost for 2 GAC columns is $30,772.
Source: [1]www.watertanks.com, [2]Eng. estimate.

Summary Annual Costs – Option 2 (In-place GAC Regeneration)

PCE, Q_{air} = 10 cfm, Cs=250 mg/g

Energy	6,150
Labor	320
GAC	18,122
O & M, $/yr	24,592
Present Worth (n=20 years, i=8%), $	241,448
Total Cost, $	247,539
Annual Cost, $	25,212

Note: Additional capital is $6,091.

PCE, Q_{air} = 100 cfm, Cs=250 mg/g

Energy	55,347
Labor	2,880
GAC	180,898
O & M, $/yr	239,125
Present Worth (n=20 years, i=8%), $	2,347,764
Total Cost, $	2,353,855
Annual Cost, $	239,745

Note: Additional capital is $6,091.

MC, Q_{air} = 10 cfm, Cs=0.28mg/g

Energy	40,194
Labor	0
GAC	792,588
O & M, $/yr	832,782
Present Worth (n=20 years, i=8%), $	8,176,376
Total Cost, $	8,182,467
Annual Cost, $	833,402

Note: Additional capital is $6,091.

MC, Q_{air} = 100 cfm, Cs=0.28mg/g

Energy	396,004
Labor	0
GAC	7,819,633
O & M, $/yr	8,215,637
Present Worth (n=20 years, i=8%), $	80,662,335
Total Cost, $	80,668,426
Annual Cost, $	8,216,257

Note: Additional capital is $6,091.

Summary annual costs – Option 1 (GAC replacement/disposal)

Compound	Total GAC Cost ($/yr) as of 2000	
	Q_{air} =10 cfm	Q_{air} =100 cfm
PCE	2,315	23,126
MC	1.1M	11M

Note: Costs of GAC include purchase ($1.60/lbs) and disposal costs.

The annual cost analysis provided the following summary results (incremental cost only, or costs unique to the alternative).

SVE Flow	Target Contaminants	
	PCE	MC
10 cfm	#1: $2,315 #2: $25,212	#1: $1.1M #2: $0.83M
100 cfm	#1: $23,126 #2: $239,745	#1: $11 M #2: $8.2M

Note: Option 1: GAC cost = $1.60/lb + disposal costs (disposal, transportation and UT tax). Option 2: GAC cost = $1.60/lb (no disposal), H_2O_2 cost (purchase and transportation), additional process energy, labor, and capital (dosing pumps, chemical storage tanks).

Fraction of H_2O_2 of the Total Cost for Option 2

The following table shows the estimate of the fraction of total cost that arises from H_2O_2 in our scenario #2:

Compound	Total H_2O_2 Cost for GAC regeneration ($/yr)		Total Annual Cost ($/yr)		Fraction of H_2O_2 Cost for GAC regeneration ($/yr)	
	Q_{air} =10 cfm	Q_{air} =100 cfm	Q_{air} =10 cfm	Q_{air} =100 cfm	Q_{air} =10 cfm	Q_{air} =100 cfm
PCE	17,966	179,495	25,212	239,745	71%	75%
MC	0.75M	7.4M	0.83M	8.2M	90%	90%

Note: All values were obtained from previous tables.

Some references for GAC costs:

Clark, Robert M. 1989. Granular Activated Carbon: Design, Operation and Cost. Lewis Publishers.

Activated carbon costs range from $1.40 to $2 per pound ($2,800 to $4,000 per ton) (U.S. EPA 1998). U.S. EPA. 1998. "Technical Bulletin: Zeolite, A Versatile Air Pollutant Adsorber." EPA 456/F-98-004. Office of Air Quality, Clean Air Technology Center. July.

Carbon cost is $2 to $3 per pound. http://www.frtr.gov/matrix2/section4/4-61.html
DOE, 1994. ***Technology Catalogue***, First Edition. February.

EPA, 1991. ***Granular Activated Carbon Treatment, Engineering Bulletin***, EPA, OERR, Washington, DC, EPA/540/2-91/024.

LaGrega, M., Buckingham, P., Evans, J. and Environmental Resources Management (2001). ***Hazardous Waste Management***, 2nd edition. San Francisco: McGraw Hill.

EPA
United States
Environmental Protection
Agency

PRESORTED STANDARD
POSTAGE & FEES PAID
EPA
PERMIT NO. G-35

Office of Research and Development (8101R)
Washington, DC 20460

Official Business
Penalty for Private Use
$300

Recycled/Recyclable
Printed with vegetable-based ink on
paper that contains a minimum of
50% post-consumer fiber content
processed chlorine free